Application of synchronized harmonic measurements

APPLICATION OF SYNCHRONIZED HARMONIC MEASUREMENTS

MODELLING, WIDE-AREA HARMONIC MEASUREMENTS AND MEASUREMENT UNCERTAINTIES

PROEFSCHRIFT

ter verkrijging van de graad van doctor aan de Technische Universiteit Eindhoven, op gezag van de Rector Magnificus prof. dr. ir. F.P.T. Baaijens, voor een commissie aangewezen door het College voor Promoties, in het openbaar te verdedigen op vrijdag 4 december 2020 om 11:00 uur

door

Stanislav Babaev

geboren te Grozny, Rusland

Dit proefschrift is goedgekeurd door de promotoren en de samenstelling van de promotiecommissie is als volgt:

voorzitter:	Prof. dr. ir. P.M.J. van den Hof
promotor:	Prof. dr. ir. J.F.G. Cobben
copromotor:	Dr. V. Cuk
leden:	Prof. dr. ir. M. Bollen (Luleå University of Technology)
	Prof. dr. ir. J. Desmet (Universiteit Gent)
	Prof. dr. ir. P. van der Wielen
	Prof. dr. ing. G. Pemen
adviseur:	Dr. H. van den Brom (VSL)

Het onderzoek of ontwerp dat in dit proefschrift wordt beschreven is uitgevoerd in overeenstemming met de TU/e Gedragscode Wetenschapsbeoefening.

Science can and should give people
a happy existence in the future.

I.I. Mechnikov

CONTENTS

SUMMARY

Harmonic emission evaluation has been known as a complex problem for many decades. Fluctuating nature of harmonics, high level of diversity and additional implications which arouse with interconnection of renewable generation require improvement of the existing assessment and measurement methods. The closely linked problem is determination of the origin of harmonic distortion in case when multiple sources of harmonics are connected to the network. The system-wide studies of harmonic propagation phenomena and emission assessment present challenges for researchers and engineers. In essence, the broad term 'propagation' includes several specific harmonic-related mechanisms among which are: harmonic interaction, phase angle diversity and cancellation, harmonic attenuation and impact of system and load impedance. In this thesis it has been shown that the application of synchronized multi-point distributed measurement system is a suitable technique for investigating the harmonic propagation in low voltage and medium voltage electrical networks.

In order to establish a foundation for the various applications of synchronized measurement infrastructure for harmonic monitoring the requirements for such system need to be defined. In this research work the impact of a time synchronization error on measured harmonic magnitudes and phase angles has been studied experimentally. Through applying a correlation technique based on Fast Fourier Transform the quantification of time error translated to magnitude and angle measurements has been given. Based on these experiments, literature review and comparative studies a minimum time accuracy leading to meaningful harmonic measurements has been proposed.

Medium and high voltage power networks frequently have only limited number of measurement devices, especially for the purpose of power quality monitoring. This often leads to the necessity of calculating or estimating voltages or currents based on the harmonic models of power system components. These models in turn are the source of the uncertainty which needs to be considered not only in calculations but also for harmonic simulations. With provision of field measurements by enabling Phasor Measurement Units infrastructure an indication of the uncertainty of single π model of a 50 kV underground cable has been estimated. To accomplish this task a current transducer output needed to be corrected for the certain ratio and phase angle bias at different harmonic frequencies.

For low voltage distribution systems underground cables are the bottleneck for accurate emission evaluation due to the lack of representative data on their impedance at frequencies higher than fundamental. In this thesis a novel non-invasive method for measuring harmonic impedance has been proposed. The measurements were recorded synchronously at both ends of the cable and impedance was estimated in a complex form as a transfer function based on the notion of linear time invariant system. In addition an uncertainty of the measurement system has been evaluated with assigning confidence intervals to estimated harmonic impedance.

An impact of supply voltage on harmonic current injections of various power electronics based loads has been investigated. New models of these harmonic loads have been derived based on the measurements. The models accurately describe response of the harmonic current phase angle to the angle of background voltage at the corresponding frequency. To demonstrate the applicability of derived models they have further been used in harmonic simulations of a low voltage distribution feeder. The modelling of the feeder and simulation conditions were focused on overcoming typical assumptions used in previous simulation studies.
At last, a wide-area harmonic measurement campaign has been executed in the low voltage and medium voltage grid characterized by high level of flexibility and control. Synchronized waveform recorders with high accuracy were placed at various nodes of the network. Based on these synchronized data voltage and current harmonics have been analyzed and conclusions were drawn on transfer of distortions, harmonic interaction and cancellation phenomena.

1

INTRODUCTION

An efficient network harmonic observability serves as the instrument for identifying and mitigating voltage distortion in power grids. Over the past years, primarily due to the paradigm of sustainable development, electrical technologies have seen a remarkable advancement. Curiously enough, whilst this technical progress without any doubts facilitates the reduction of a harmful anthropogenic impact on our planet, it shifts the conventional operation of electrical networks towards more complicated scenarios. One of the inevitable consequences of this process of transition is an increasing fraction of power quality issues manifesting themselves in voltage and current distortions. In our attempt to respond to the influence of these changes on power quality in electrical grids new methods of harmonic monitoring should be adopted. Rather than relying mainly on conventional measurement techniques broadly described in various technical recommendations and standards, the changes in engineering perception of the problem are required. That being said, complex processes ongoing in modern powers networks and future smart grids would require not only rapid development of fundamental technologies, but merely the change in a mindset of the main actor involved therein – a human. For existence of innovations cannot reveal its full potential without the conscious acceptance by the end user.

1.1. HARMONIC OBSERVABILITY

RELEVANCE, accuracy and reliability are amongst crucial parameters describing some representative set of data. When these data are meant to be used in critical applications the requirements for data quality are stringent. Since secure, reliable and efficient operation of modern power systems is a binding motive to satisfy the demands of contemporary society, the significance of data acquired by electrical measurement equipment is undoubtedly paramount. When the focus of a measurement campaign is voltage and current harmonics – components which are "integrated" within accustomed power frequency waveform yet distinguished by frequencies at multiples of fundamental, specific requirements shall be met. On the one hand, the very existence of these

requirements owes to the dynamic nature of frequency components which are present in modern power grids. On the other, an additional factor to account for is the sporadic response of power system components, also including an instrumentation chain when exposed to current and voltage distortions. To take into consideration the statement of harmonic fluctuations it is suggested (and widely accepted) to make use of aggregation intervals over longer periods of time. Such the aggregations of measurement data are mathematically approachable when operating with magnitudes of measurands but demonstrate ambiguity with respect to phase angles. Nevertheless, even prior to reckoning on any algorithms original data shall be acquired given physical constraints of the measurement equipment – the measurement errors. The statement of uncertainty is what makes findings plausible and relevant. Whilst at first glance, quantifying accuracy requirements for voltages and currents at power frequency seems valid, it becomes apparent that this is the *necessary* condition for measuring components at higher frequencies. Yet bringing into the statements the condition of *sufficiency* – by estimating uncertainties for frequencies other than fundamental, is what could take into consideration abrupt effects of frequency-dependence of the instrumentation chain. In other words, the ability of the measurement system to meet these *necessary and sufficient* conditions is the first essential link in the chain known as *observability*. The term observability conveys the idea of describing the complete system behavior while utilizing outputs of this system. Particularly for voltage and current harmonic components this would mean identifying values of the dynamically changing variables across the distributed system. Such an approach without any doubts would demand the shift in conventional harmonic distortion assessment and measurement techniques.

1.2. RESEARCH OBJECTIVES

The main objectives of this research can be formulated as follows:

- *To enable application of synchronized Power Quality measurements for various purposes.*

While the first objective is aimed to facilitate the transition towards complete harmonic observability, it is also intent on promoting renewed perception of analyzing power quality phenomena. Diverse details are included in this goal rendering the scope of the problem wider than merely metrology. Prior to setting up requirements for such measurement infrastructure, the most significant issues regarding the phenomena in question shall be determined and carefully investigated. Having in spotlight voltage and current distortions, a close link between peculiarities of metrological systems and nature of evolving power quality disturbances should be established.

- *To develop models of harmonic sources and components serving as input to advanced power quality studies.*

When the foremost goal is to acquire a deeper understanding of the underlying processes leading to or being a consequence of a power quality disturbance, an inevitability of mathematical interpretations is prominent. Moreover, if we were to connect these two objectives with each other, a genuine synergy would occur. This synergy allows to

enhance a grasp of the necessity in pattern change with respect to metrological implications applicable to harmonic measurements. The change which could be possible by providing meaningful validation of potential disturbance processes.

1.3. RESEARCH MOTIVATION

FOR power system analysis (not specifically power quality) synchronized measurements have already been proposed as the method for resolving several engineering tasks such as stability assessment, fault location, distribution state estimation, and event detection [1–3]. For these purposes, phasor measurement units (PMU) based infrastructure proved to be an efficient solution. Synchronized phasors reported by each PMU must comply with synchronization accuracy requirement of not worse than ±31.7 μs [4] which is satisfactory for most of the applications sought by power system engineers. On the other hand, while carrying out power quality analysis and taking into consideration complex phenomena of harmonic interaction between background voltage harmonic distortion and harmonic current injections of the nonlinear sources [5–7], strict prerequisites in terms of an accuracy of the measurement system shall be satisfied. This also holds for the time synchronization accuracy, for it is essential to accurately process not only magnitudes of harmonic components but also their phase angles. As it was proved by the authors of [8, 9] the well-known effect of harmonic cancellation is what eventually governed by the diversity of phase angles of different harmonic-producing sources. All the same, it appears from these studies that evaluation of harmonic current and voltage components requires an improvement over the existing practices. The grid measurement techniques which rely on time synchronization can provide the conventional power quality assessment with such an improvement. The configuration of this type of measurement infrastructure can moreover allow for a time correlation between voltage harmonic distortion and harmonic current injections at different locations. Additionally, distributed harmonic measurement systems can be used for the estimation and evaluation of electrical parameters of power system components, particularly impedance of the underground cables.

1.4. RESEARCH APPROACH

ULTIMATELY this research work is built on three key parts, each of these contributing coherently to the subsequent parts.

1. **Metrology.** Whilst being focused on investigations about novel measurement infrastructures recording voltage and current harmonics in time-synchronized manner across distributed systems, this block of studies offers also extensive examinations of accuracy of measurements. Not less important is survey on signal processing methods, involving both conventional broadly used and more advanced techniques. This major part required theoretical studies, comparison methods, and laboratory and field measurement experiments;

2. **Power system components.** The concept of observability calls for knowledge on control vectors. For the purpose of distortion analysis in power grids this implies awareness of the impedance values of major components – underground cables,

overhead lines and power transformers. On the one hand, it is crucial to understand how these components determine and drive the harmonic behavior of the entire system. On the other, it is advantageous to have instruments for estimating parameters of the network components when the data are not available. By employing data acquired both from laboratory and real power systems, we demonstrate how judgement on the correctness of models can be made; how estimation techniques can resolve the lack of information on true values of required control vectors; how in general conclusions on transfer of voltage distortions can be deduced. By means of respective computer simulations we study, validate and test hypotheses which were written for experimental work we performed;

3. **Harmonic producing sources.** Without doubts, accurate models of harmonic producing sources are essential for studying their impact on voltage distortion levels. Such models should allow to represent harmonic current injections of the device in question when fluctuating voltage harmonics are supplied to its terminals. This insinuates that modelling procedure eventually shall provide mathematical derivation of harmonic phase angle response to various supply conditions. Curiously enough, while such models in first place are truly designed to perform computer simulation studies, they can also contribute to our understanding of harmonic processes in the fully observable system. This research task is a combination of laboratory-performed measurements, mathematical modelling and computer simulations.

1.5. THE MEAN4SG PROJECT

MEAN4SG — Metrology Excellence Academic Network for Smart Grids is a European initiative within Horizon 2020 framework aiming to address research challenges for smart grids metrology. This project is a platform for the interdisciplinary research and transfer of knowledge and experiences between different parties. In attempt to deal with the shortage of highly-skilled professionals in the field of power systems metrology and relying on the support of International Electrotechnical Commission, eleven early-stage scientists were admitted to the program. The researchers were provided with the opportunity to create knowledge in various subjects: power quality, smart grid modelling and management, advanced monitoring with phasor measurement units and smart cable diagnosis. It is expected that outcomes of this European Union action will push forward the smart grid concept and sustainable development.

1.6. THIS THESIS

THE research objectives are addressed in the main six chapters of this thesis. The chapters are organized as follows.

Chapter 2: Time Synchronization – Requirements and Advantages

In this chapter the concept of distributed measurement systems is introduced. Such systems feature measurement instruments which are typically synchronized to the external or internal time source. On applying these devices for the purpose of capturing high frequency components the certain requirements shall be met. Through investigating exist-

ing synchronization protocols and evaluating state-of-the-art a gap in the requirements for time synchronization accuracy applicable to harmonic measurements is identified. By adjusting the parameters of specifically designed laboratory setup the impact of synchronization error on measured harmonic magnitudes and phase angles is studied. To demonstrate the advantages of distributed measurement system a wavelet-based algorithm is proposed for harmonic analysis.

Chapter 3: Uncertainty of Harmonic Modelling

Elaborating further on synchronized spectrum measurements, a field experiment at medium voltage (MV) level enabling phasor measurement unit (PMU) infrastructure is established. The significance of evaluating uncertainty associated with conventional power system component models is discussed. It is demonstrated that at frequencies higher than fundamental inaccuracy of the models becomes substantial. Whilst PMU brings the system to observable state, it is proven in this chapter that a field instrumentation chain consisting of current and voltage transducers gives rise to the additional source of the uncertainty naturally caused by frequency dependence of these devices.

Chapter 4: Harmonic Impedance of a Low Voltage Cable

In low voltage (LV) distribution systems the impact of power system components on voltage distortion is likewise necessary to evaluate. It is stressed in this chapter that erroneous information on cable harmonic impedance values leads to incorrect conclusions about power quality issues. More often than not, the data on cable impedance are not available or in some cases difficult to retrieve. By engaging time-synchronized waveform recorders installed at the laboratory a method for estimating harmonic impedance of LV underground cable is developed. The uncertainty of estimated harmonic impedance is evaluated based on metrological characterization of the utilized measurement system.

Chapter 5: Modelling of Non-linear Sources

To strengthen methods of voltage and current distortion analysis in electrical networks, relevant models of harmonic-producing sources can be incorporated into the computer simulations. Frequency-domain measurement-based models are favorable because of the relatively low complexity, fast performance and moderate amount of initial input data needed to accomplish the modelling. However, when the ultimate goal of such models is to represent harmonic behavior of a load in the presence of fluctuating voltage distortion at its terminals, the computational burden and the model accuracy are among determinative requirements to consider. In this chapter it is explained how the LV models characterized by low complexity can be mathematically derived from measurement routines by applying novel methods of circular statistics.

Chapter 6: Case Study: Distribution System Modelling

To further develop an understanding of harmonic processes the frequency-domain models developed in previous chapter are used in a computer simulation of low voltage distribution feeder. The renewed technique for distribution system modelling implicates that typical assumptions used in conventional simulations' methods shall be dealt with. In this technique the complete consideration is given to the interaction between background harmonic voltages and emitted harmonic currents of non-linear devices. That is, over the course of time the diversity between phase-corrected non-linear injections is evaluated whilst their impact on voltage distortion along distribution feeder is calculated given uncertainties of frequency-dependent impedance.

Chapter 7: Wide-area Harmonic Measurements
In the book finale the quintessence of knowledge creation as the outcome of this research project is shared. A highly accurate distributed measurement system is used to synchronously record voltage and current waveforms in the power grid featuring unprecedented controlability and flexibility. The dynamic interaction of harmonic-producing sources with the medium and low voltage electrical networks is studied and profound conclusions on transfer of voltage distortions between various parts of the distribution network are drawn.

REFERENCES

[1] F. Aminifar, M. Shahidehpour, M. Fotuhi-Firuzabad, and S. Kamalinia, *Power system dynamic state estimation with synchronized phasor measurements,* IEEE Transactions on Instrumentation and Measurement **63**, 352 (2014).

[2] A. Von Meier, E. Stewart, A. McEachern, M. Andersen, and L. Mehrmanesh, *Precision Micro-Synchrophasors for Distribution Systems: A Summary of Applications,* IEEE Transactions on Smart Grid **8**, 2926 (2017).

[3] J. Yang, W. Li, T. Chen, W. Xu, and M. Wu, *Online estimation and application of power grid impedance matrices based on synchronised phasor measurements,* IET Generation, Transmission & Distribution **4**, 1052 (2010).

[4] *IEEE Standard for Synchrophasor Measurements for Power Systems* (C37.118.1-2011, 2011).

[5] J. E. Caicedo, A. A. Romero, H. C. Zini, R. Langella, J. Meyer, and N. R. Watson, *Impact of reference conditions on the frequency coupling matrix of a plug-in electric vehicle charger,* Proceedings of International Conference on Harmonics and Quality of Power, ICHQP , 1 (2018).

[6] J. Meyer, S. Muller, P. Schegner, S. Z. Djokic, A. J. Collin, and X. Xu, *Comparison of methods for modelling electric vehicle chargers for harmonic studies,* in *2016 Power Systems Computation Conference (PSCC)* (IEEE, 2016) pp. 1–7.

[7] S. Müller, J. Meyer, and P. Schegner, *Characterization of Small Photovoltaic Inverters for Harmonic Modeling,* in *ICHQP* (IEEE, 2014) pp. 659–663.

[8] J. Meyer, A. M. Blanco, M. Domagk, and P. Schegner, *Assessment of Prevailing Harmonic Current Emission in Public Low-Voltage Networks,* IEEE Transactions on Power Delivery **32**, 962 (2017).

[9] V. Cuk, J. F. G. Cobben, W. L. Kling, and P. F. Ribeiro, *Analysis of harmonic current summation based on field measurements,* IET Generation, Transmission & Distribution **7**, 1391 (2013).

2

TIME SYNCHRONIZATION — REQUIREMENTS AND ADVANTAGES

The ongoing transition from the conventional centralized power grid to the new type of electrical system involving distributed generation poses new requirements on the measurements of electrical quantities and observability of the power system. This is due to the desire to manage new decentralized networks embracing bi-directional power flows instead of the "fit and forget" policy. The process of integrating renewable generation into distribution networks together with increasing amount of non-linear loads brings also new complications for power quality monitoring, particularly harmonic distortions. The new measurement approach featuring synchronization of waveform recorders distributed across power networks brings superior performance over conventional harmonic monitoring techniques. Nevertheless, many peculiarities associated with new measurement infrastructures shall be carefully studied and considered. In this chapter, after having investigated the influence of a time synchronization error on harmonic measurements and defined the requirements we demonstrate an advantage of the distributed measurement system through a case study.

2.1. SURVEY ON TIME SYNCHRONIZATION: APPLICATIONS

SINCE the time when first Phasor Measurement Units (PMU) were introduced into power grids, various applications of these devices have been sought and eventually implemented. It is interesting to mention, that the original idea to utilize PMU-based infrastructure for state estimation in transmission systems did not impose high accuracy requirements to the measurement chain. It was related to the performance of developed state estimation algorithms which were actually meant to deal with the uncertainty of redundant measurements in high voltage networks. In this sense it is different from the state estimation in distribution systems where significant amount of network nodes typically lacks measurement equipment which creates scarcity of representative data. For the latter, understanding complex power flows would contribute to better active man-

agement of distributed generators. As it was shown by authors of [1] this application surely demanded strict accuracy levels of the instrumentation chain.

Further, in order to evaluate power system response to a certain event it is necessary to compare data recorded at different points of the grid precisely at the same moment of time when event occurs. An ability of PMUs to accurately estimate phasors at geographically separated locations is strongly dependent on time synchronization accuracy which is stipulated by [2]. This accuracy must be not worse than ± 31.7 μs for 50 Hz power frequency in order to maintain Total Vector Error (TVE) lower than 1% and phase angle difference not higher than 0.573°. With relation to that fact, the authors of [3] demonstrated the influence of asynchronization and the complete instrumentation chain on the phase displacement. All the same, in [4] authors demonstrated that combined instrumentation channel error together with timing error imposed by standard can make TVE larger than 1%. Consequently, it has been proposed to keep time-synchronization accuracy at sub-microsecond level for the majority of power system applications.

When considering monitoring of various power quality phenomena among which are voltage and current distortions, the synchronized measurement infrastructure can equip power quality experts with unprecedented tools. Additionally, where conventional PQ recorders might provide ambiguous results - synchronized data can conveniently support the assessment of a PQ problem. As it was shown in [5] the dynamic interaction between different harmonic sources might jeopardize harmonic emission assessment when implemented truly in accordance with [6]. Specifically, it has been demonstrated that within a power network with several distorting loads a certain source of harmonics may be regarded as both injecting and absorbing harmonics, which makes the general summation law impractical for evaluating harmonic emission. By using synchronized PQ recorders, the authors have separated the current emissions of distributed generators from other harmonic loads and used them as input for accurate emission assessment.

Precisely as for other applications the quality of resolving harmonic phase angles between distributed recorders relies upon accuracy of time synchronization. In [7] it was pointed out that a time error leading to X degrees of phase displacement at fundamental frequency translated to the X*n degrees at harmonic frequency, where n is a harmonic order. We shall, therefore, focus on methodologies which allow us to characterize the impact of time synchronization error on the measurements of frequency components.

In [8] several techniques on assessing the synchronization time delay have been examined with respect to the synchronization protocol IEEE 1588. Naturally, these techniques in belong in three different categories: evaluating time stamps of both sent and received message; comparing common sinusoidal signal sent to each measurement node; comparing signal generated at each measurement node.

Perhaps, the most prevalent synchronization technology for power system measurements is commonly built on GPS. Theoretically, GPS time source provides the highest possible accuracy of $\pm$ 100 ns among other synchronization strategies [9], [10]. However, the performance of this method is extremely dependent on the quality of GPS signal. This might be impaired due to certain atmospheric conditions or obscuring an antenna itself. Curiously enough, it is absolutely not straightforward to quantify how certain time error can impact measurement estimates of frequency components at multiple locations. As an example, in [11] authors deduced amplitude and phase differences

for harmonic synchrophasors assuming ideal case of direct link connection between devices. The more realistic case with two devices having connected to GPS time source was tested against complete loss of one or both timing sources. All the same, the conclusions were deduced only with respect to TVE corresponding to power frequency. The latter compliance tests of PMUs are in line with what is stated in standard [2] only with respect to power frequency. If the goal, however, is to engage extra functionality not covered in this standard, for instance to utilize harmonic synchrophasors, it is important to understand that all measurements are bound not to zero crossings of the signals, but instead to the absolute time. Therefore, this technical detail raises the question about direct influence of time error on potential estimates of voltage and current phasors at harmonic frequencies.

For aggregated power quality measurements, as per standard [12], it is possible (but not very common) to choose for synchronization of power quality recorders (not PMU), should this be deemed beneficial for aggregation of measurement intervals of class A instruments. Thereby the recommendation is to keep time-clock uncertainty of ±20 ms. As each measurement typically begins at zero crossing of the fundamental component of voltage at a certain location of the grid, the variation of fundamental phase angle across the grid renders an additional error for multi-point harmonic measurements when performed in accordance with the recommendation of [12]. This, in turn, hinders the capability of such devices to provide accurate output beyond what is stipulated by standard for the aggregated harmonic output.

2.2. QUALITY OF SYNCHRONIZATION AND ITS IMPACT ON HARMONIC MEASUREMENTS

To investigate how various time errors can influence acquisition of frequency components at distributed locations we shall rely upon flexible measurement setup with known and quantifiable synchronization accuracy. Let us first look at the Figure 2.1 which comprises two NI cRIO waveform recorders with their input voltage channels connected to real-time simulator OPAL-RT. Within this setup the OPAL-RT is used for generating coded time-sequence based on Inter-Range Instrumentation Group (IRIG-B) protocol. This protocol is widely accepted for distribution of clock signals across various control and monitoring devices at electrical substations. As IRIG-B protocol requires decoding upon acquisition of this signal by a receiver, it is preferable to execute decoding algorithm on the hardware with deterministic capabilities. We shall perform it therefore directly on the FPGA of the two cRIO devices. The hardware limitations and the decoding algorithm introduce to the measurement system ±12.5 μs of uncertainty in time. Additional source of the error arises from the minimum step size of the mathematical solver of OPAL-RT which equals to 10 μs. Thus, on combining these two, we may conclude that for this setup the best achievable accuracy of the synchronization is ±22.5 μs.

We then supply voltage signal simultaneously to the both acquisition devices triggered by IRIG-B time source. The fundamental frequency of the signal is characterized by negligible deviation since we make use of the programmable voltage source. We then impose set of stationary voltage harmonics on top of the fundamental achieving "clipped" shape of the output waveform.

To compare harmonic content measured by each of the devices we first estimate power spectral densities of the acquired signals. As the next step these estimates are used as an input to Magnitude Squared Coherence (MSC) function which provides a meaningful measure of the similarities between magnitudes of frequency components of the signals. The MSC can be calculated as follows:

$$C_{xy}(f) = \frac{|P_{xy}(f)|^2}{P_{xx}(f)P_{yy}(f)} \tag{2.1}$$

where P_{xx} and P_{yy} are power spectral densities and P_{xy} is cross power spectral density. The Magnitude Squared Coherence is a dimensionless quantity and values close to 1 would indicate that magnitudes of the one signal strongly correlated with the magnitudes of another.

On the other hand, a phase angle between frequency components of two signals can be evaluated also from cross power spectral density. However, for this electrical quantity we make use of estimates of cross power spectral density calculated with averaged periodogram technique [13]. The periodogram is the Fourier transform of the aperiodic correlation of the windowed data sequence and it provides a good balance between the frequency resolution and variance while eliminating a noise. In general case, it can be calculated as follows:

$$P_{xx}(\omega) = \sum_{-\infty}^{\infty} c_{vv}[m]e^{-j\omega m} \tag{2.2}$$

where

$$c_{vv}[m] = \sum_{n=0}^{L-1} x[n]w[n]x[n+m]w[n+m] \tag{2.3}$$

and L is a length of the signal, $x[n]$ is a given signal and $w[n]$ is a window sequence.

We then introduce user-controlled time errors of 100 μs and 1 ms into the generated IRIG-B sequence and evaluate their impact on measured magnitudes and phase angles of frequency components.

2.2.1. ESTIMATES OF HARMONIC MAGNITUDES

We first present MSC values as per equation 2.1 for central bins of odd harmonic orders from 1 through 15. Based on the information presented in Table 2.1 we can conclude that in the majority of cases the MSC deviates from 1 only slightly. This implies high level of correlation between harmonic magnitudes of two voltage signals regardless of the time error.

But how does the picture look like for adjacent spectral components? In Figure 2.2 we may notice that the magnitude correlation near central odd frequency bins becomes lower, especially for the harmonic orders higher than 11. In turn, and as the Figure 2.3 proves, if the time delay is increased further to 1 ms, the magnitudes of adjacent spectral lines become extremely uncorrelated even for harmonics of low orders. This observation brings the discussion over the procedure recommended by the standard IEC 61000-4-7 for harmonic grouping. The grouping method advocates the Parseval's relation which postulates the equality between signal power in the time domain and signal power in the frequency domain. Non-ideal measurement conditions and algorithms contribute

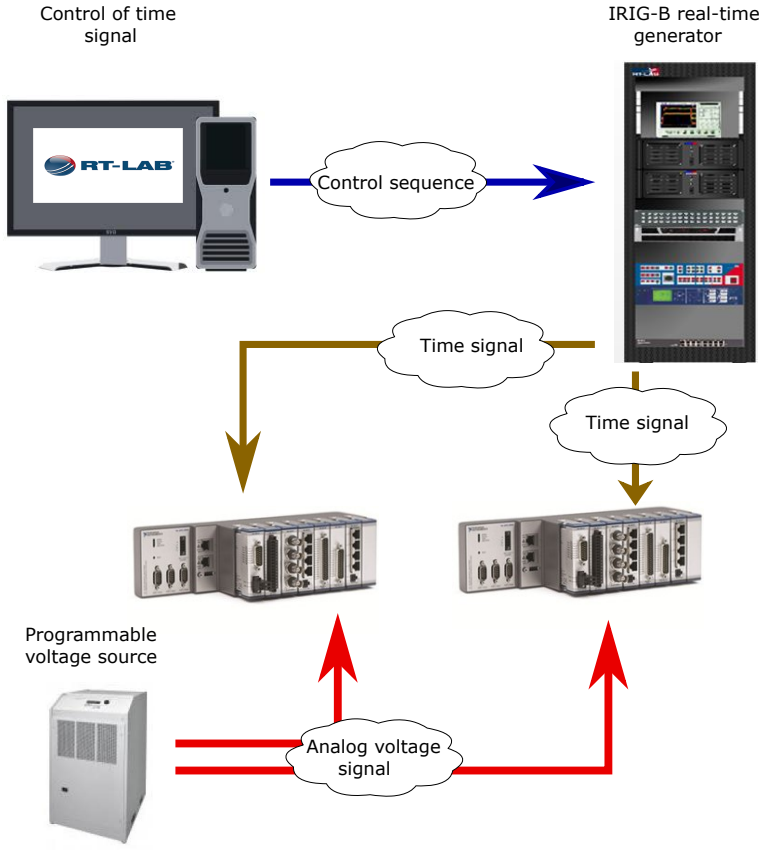

Figure 2.1: Synchronized measurement structure.

Table 2.1: Impact of synchronization error on harmonic magnitudes.

h	**Magnitude Squared Coherence**		
	22.5 μs	100 μs	1 ms
1	1.0000	1.0000	1.0000
3	0.9998	0.9998	0.9998
5	0.9995	0.9995	0.9995
7	0.9990	0.9990	0.9988
9	0.9983	0.9984	0.9985
11	0.9975	0.9974	0.9953
13	0.9965	0.9966	0.9963
15	0.9955	0.9952	0.9938

to a fact that components of a signal are not strict multiple of the fundamental - rather they are "spread" to adjacent spectral lines considering 5 Hz frequency distance (for 50 Hz power frequency). In theory the grouping method accounts for the fluctuations and possible spectral leakage by ensuring that the total power is evaluated upholding Parseval's statement. This is done by taking into consideration not only integer multiples of main harmonic orders but rather all adjacent spectral lines with "central" bin frequency therefore comprising the average power. Consequently, in non-ideal conditions when substantial time synchronization error is present and spectral leakage is inherent the grouping will not restore the loss of frequency content. That being said, the desired accurate preservation of signal power will render meaningless as there will exist significant differences between two measured signals. Figures 2.2 and 2.3 confirm that final harmonic indices are subject to an error due to susceptibility of frequency components around the main odd orders to the time synchronization error.

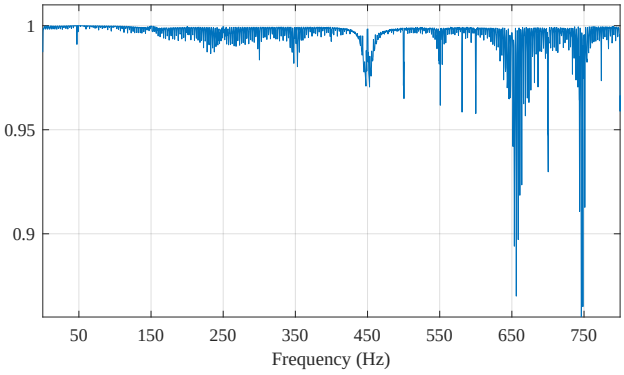

Figure 2.2: Magnitude Squared Coherence function — synchronization accuracy 100 μs.

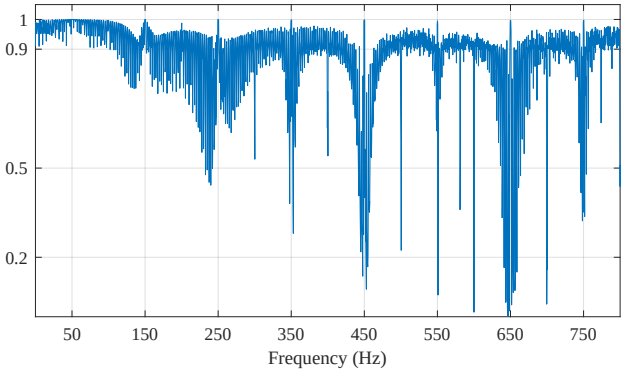

Figure 2.3: Magnitude Squared Coherence function — synchronization accuracy 1 ms.

2.2.2. MEASUREMENT OF HARMONIC PHASE ANGLE

In comparison with magnitudes, harmonic phase angles are strongly susceptible to the imperfections of a time source. Any whatever small angle difference between two measured signals at fundamental frequency will translate to larger values at higher harmonic orders. An example of this dependence is demonstrated in Figure 2.4. With no additional delay introduced we observe that with the initial uncertainty of ±22.5 μs the difference between angles at 15th harmonic order equals to 2.2422°. Additionally, an increase of relative angles demonstrates nearly linear trend with the increasing frequencies. We further look at the case with the time error of 100 μs. From the Figure 2.5 we understand that even angle difference of 2.0315° at fundamental frequency will correspond to 30.5803° at 750 Hz. Finally, to prove that phase lag between estimated harmonic components of the same signal becomes significant when time error is no more within sub-millisecond range, we show in Figure 2.6 cross power phase angles measured synchronously with time error of 1 ms between two waveform recorders.

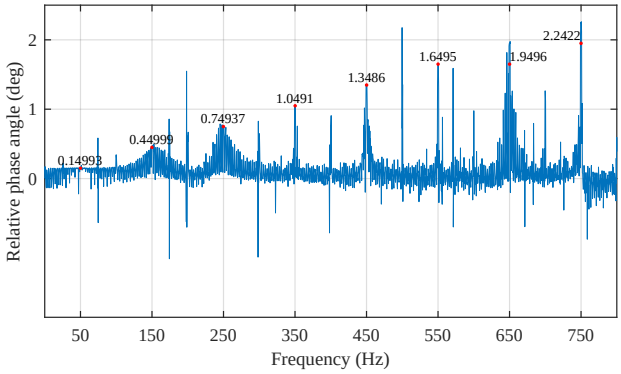

Figure 2.4: Phase angles between two signals for synchronization accuracy of ±22.5 μs.

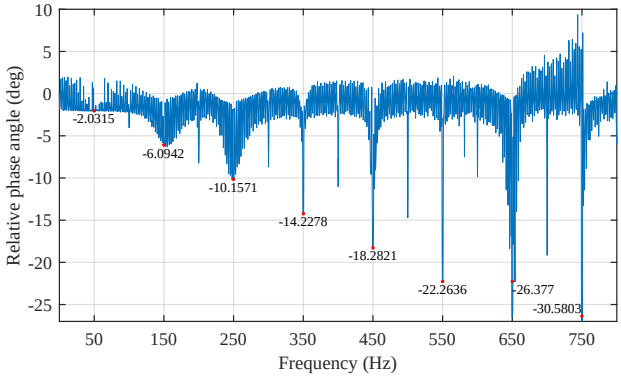

Figure 2.5: Phase angles between two signals for synchronization accuracy in the range of 100 μs.

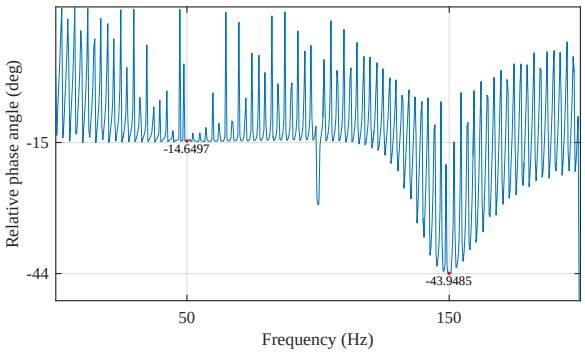

Figure 2.6: Phase angles between two signals for synchronization accuracy in the range of 1 ms.

2.3. CASE STUDY: WAVELET ANALYSIS BASED ON SYNCHRONIZED DATA

THE wavelet transforms have been introduced to power systems experts as a powerful tool for the analysis of harmonic distortions already some time ago. Unlike the Fast Fourier Transform (FFT), wavelets provide time-frequency information of the analyzed signal. This valuable time information allows to assess the evolution of harmonic components in power systems over the course of time [14–17]. Wavelets are localized waves which decay to zero after finite amount of time. A continuous wavelet transform (CWT) involves application of basis functions $w_{jk}(t)$ which are rescaled (or dilated) j times and translated (or shifted) k times. This process is recursive in its nature and produces basic feature of wavelets - multi-resolution, allowing to separate an input signal into different scales of resolution. The multi-resolution provides short times with high frequencies and long time with low frequencies. The time-scale plane can then be transformed to time-frequency plane depending on sampling frequency. For the analysis of power system harmonics the resulting accuracy of this multi-resolution is dependant on the choice of mother wavelet $w(t)$ [18].

Considering these unique features of this signal processing method with relation to harmonic time analysis, distributed waveform recorders which are synchronized to the precision time source can provide us with additional power quality assessment tools. To demonstrate the advantage of the synchronized measurement infrastructure we have set a laboratory experiment with a low voltage distribution feeder. In Figure 2.7 the distributed data acquisition system consists of National Instruments cRIO chassis with all channels being synchronized. Taking into account time error requirements investigated for harmonic measurement in the previous section, the synchronization across the system was performed connecting all the chassis via digital line with master clock generated on one of the devices. This ensured time error of no more than 200 ns. Furthermore, we recorded synchronously current waveforms of 3 kW photovoltaic inverter operating under the emulated irradiance level of 1000 W/m^2 and 11 kW induction motor powered by variable speed drive (VSD). Additionally, we have acquired voltages and currents at the point of common coupling (PCC). With this feeder being energized by the public grid

with total harmonic distortion (THD) of 3% we then process recorded waveforms with analytic Morlet continuous wavelet transform [19].

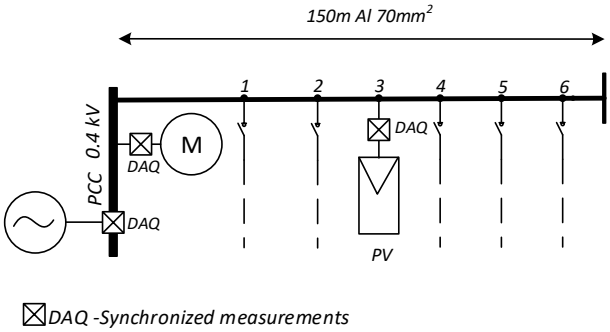

Figure 2.7: Low voltage feeder with distributed waveform recorders.

Aiming to demonstrate the correlation between time-varying harmonic injections of a particular load and its influence on harmonic voltage at different point of the network we provide graphical visualizations of CWT. We first estimate wavelet cross-power spectrum of different electrical quantities to obtain distribution of powers of two signals. These cross-powers in turn can be used as an input to Magnitude Squared Coherence (MSC). In combination with continuous wavelet transform the correlation between signals features additionally a valuable information in the time-frequency plane allowing us to analyze non-stationary fluctuating frequency components. This enhanced MSC function is mathematically a dimensionless value, however, it technically represents a portion of the output signal power which is generated by the input at the corresponding frequency [20].

The results of such an analysis are conveniently represented in the form of a scalogram. For the test setup depicted in Figure 2.7 we present three scalograms of correlated spectra of voltages and currents. The information in Figures 2.8, 2.9 and 2.10 shall be read as follows: values close to zero over specific frequency range denote that powers of the harmonics are not correlated at that certain time (blue color), whilst values close to the unity suggest that harmonic powers are correlated (yellow color). Different to MSC functions derived from FFT, the wavelet counterpart ensures that phase lag information is also preserved. The phase lag between the signals is shown by the black arrows over the areas with high correlation.

It is visible that correlated spectrum of individual current of VSD depicted in Figure 2.9 contains similar components which are present in the correlated pair of combined current and voltage at PCC (Figure 2.8). For this case the largest values of correlation coefficients correspond to the frequencies 250 Hz and 550 Hz. Therefore, we can conclude that the powers at these harmonic frequencies are produced by VSD. On contrary, by examining wavelet coherence between U_{PCC} and I_{PV} (Figure 2.10) we observe different spectral content at frequencies between 250 Hz and 550 Hz. These are only visible in Figure 2.8 as a set of coherent spectral lines. To conclude, the employment of synchronized waveform recorders combined with advanced signal processing methods can facilitate power quality analysis in distribution networks.

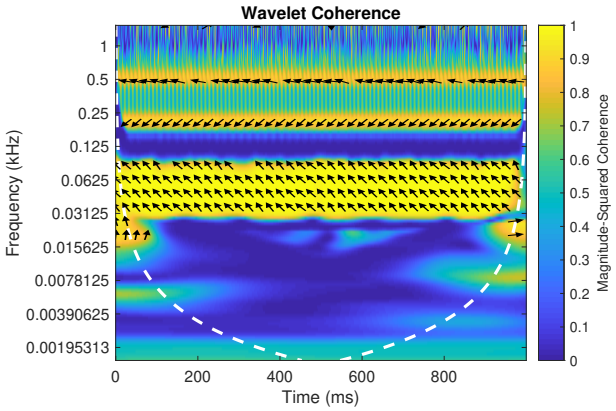

Figure 2.8: Wavelet Magnitude Squared Coherence between U_{PCC} and I_{PCC}.

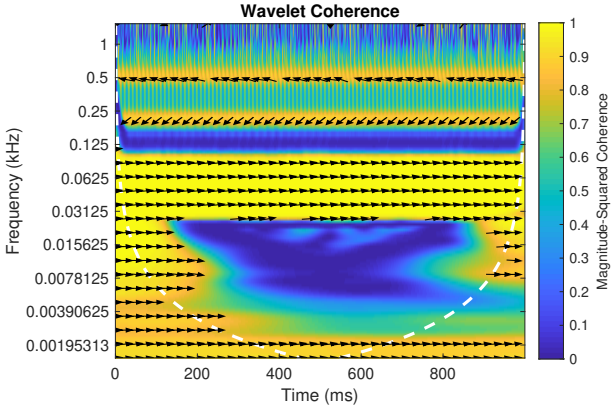

Figure 2.9: Wavelet Magnitude Squared Coherence between U_{PCC} and I_{VSD}.

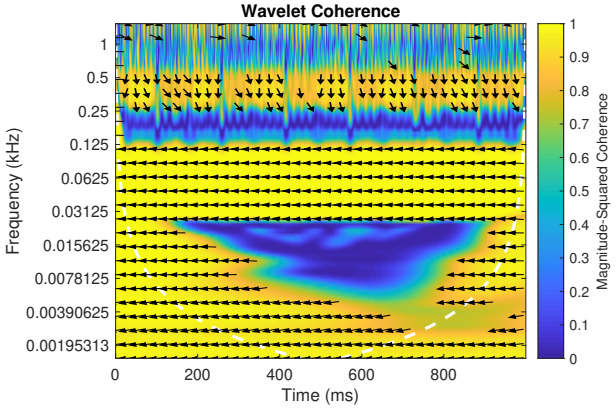

Figure 2.10: Wavelet Magnitude Squared Coherence between U_{PCC} and I_{PV}.

2.4. CONCLUSION

ACCORDING to the commonly accepted and recommended practise for harmonic emission evaluation initial data are gathered by conventional single point measurement equipment. The valuable harmonic phase angle information is typically suppressed, thus making it challenging to accurately deduce conclusions about emissions of a certain harmonic source. Synchronized measurement infrastructure can in turn broaden the instrument portfolio of power quality experts and bring new opportunities for advanced emission analysis methods. Nevertheless, upon installing new measurement devices a time synchronization error shall be carefully accounted for, for harmonic distortion in modern power systems is characterised by fast dynamic nature and typically non-stationarity. Keeping synchronization accuracy at sub-millisecond level might compromise plausibility of harmonic measurements and an appropriate balance between complexity (cost) of the system and its performance shall be sought. In that sense, it can be reasonable to impose a maximum phase angle difference of 0.573° at 40^{th} order of harmonics, but not for fundamental frequency as it is currently accepted for PMU measurements. This will require time synchronization accuracy of minimum ± 500 ns. Such a level of accuracy might be achieved with GPS time source, or in the laboratory conditions by connecting several acquisition devices via digital line.

REFERENCES

[1] A. Venturi, P. Clarkson, A. Forbes, E. Davidson, A. J. Roscoe, G. M. Burt, X. S. Yang, and P. S. Wright, *The role of accurate measurements within smartgrids,* IEEE PES Innovative Smart Grid Technologies Conference Europe , 1 (2011).

[2] *IEEE Standard for Synchrophasor Measurements for Power Systems* (C37.118.1-2011, 2011).

[3] A. Mingotti, L. Peretto, and R. Tinarelli, *Accuracy Evaluation of an Equivalent Synchronization Method for Assessing the Time Reference in Power Networks,* IEEE Transactions on Instrumentation and Measurement **67**, 600 (2018).

[4] R. S. Singh, H. Hooshyar, and L. Vanfretti, *Laboratory test set-up for the assessment of PMU time synchronization requirements,* 2015 IEEE Eindhoven PowerTech, PowerTech 2015 (2015), 10.1109/PTC.2015.7232731.

[5] B. Peterson, J. Rens, J. Meyer, G. Botha, and J. Desmet, *Evaluation of Harmonic Distortion from Multiple Renewable Sources at a Distribution Substation,* IEEE International Workshop on Applied Measurements for Power Systems (AMPS) Proceedings , 37 (2017).

[6] *Electromagnetic compatibility (EMC) - Part 3-6: Limits - Assesment of emission limits for the connection of distorting installations to MV, HV and EHV power systems* (IEC 61000-3-6, 2008).

[7] B. Dickerson, *Applications of synchronised power quality measurements,* Arbiter Systems white paper , 0.

[8] D. Grimaldi and F. Lamonaca, *Measurement techniques to assess the time synchronization in Distributed Systems,* 16th IMEKO TC4 Int. Symp.: Exploring New Frontiers of Instrum. and Methods for Electrical and Electronic Measurements; 13th TC21 Int. Workshop on ADC Modelling and Testing - Joint Session, Proc. , 480 (2008).

[9] M. Eroglu S., Toprak S., Urgan O, MD, Ozge E. Onur, MD, Arzu Denizbasi, MD, Haldun Akoglu, MD, Cigdem Ozpolat, MD, Ebru Akoglu, *Harmonic monitoring system via GPS-synchronized measurement-update and new developments,* Saudi Med J **33**, 3 (2012), arXiv:arXiv:1011.1669v3 .

[10] a. Carta, N. Locci, and C. Muscas, *GPS-based System for the Measurement of Synchronized Harmonic Phasors,* 2007 IEEE Instrumentation & Measurement Technology Conference IMTC 2007 **58**, 1 (2007).

[11] M. Lixia, C. Muscas, and S. Sulis, *Application of IEEE 1588 to the measurement of synchrophasors in electric power systems,* IEEE International Symposium on Precision Clock Synchronization for Measurement, Control and Communication, ISPCS '09 - Proceedings , 142 (2009).

[12] *Electromagnetic compatibility (EMC) - Part 4-30: Testing and measurement techniques - Power quality measurement methods* (IEC 61000-4-30, 2015).

[13] A. V. Oppenheim, R. W. Schaffer, and J. R. Buck, *Discrete-Time Signal Processing,* 2nd ed. (1998).

[14] J. Barros and R. I. Diego, *Analysis of harmonics in power systems using the wavelet-packet transform,* IEEE Transactions on Instrumentation and Measurement **57**, 63 (2008).

[15] R. I. Diego and J. Barros, *Global method for time-frequency analysis of harmonic distortion in power systems using the wavelet packet transform,* Electric Power Systems Research **79**, 1226 (2009).

[16] J. Barros, R. I. Diego, and M. De Apraiz, *Applications of wavelet transforms in electric power quality: Harmonic distortion,* 2011 IEEE International Workshop on Applied Measurements for Power Systems, AMPS 2011 - Proceedings , 13 (2011).

[17] J. Barros, R. I. Diego, and M. De Apraiz, *A discussion of new requirements for measurement of harmonic distortion in modern power supply systems,* IEEE Transactions on Instrumentation and Measurement **62**, 2129 (2013).

[18] J. Bruna and J. J. Melero, *Selection of the Most Suitable Decomposition Filter for the Measurement of Fluctuating Harmonics,* IEEE Transactions on Instrumentation and Measurement **65**, 2587 (2016).

[19] S.-j. Huang and C.-t. Hsieh, *Visualizing time-varying power system harmonics using a Morlet wavelet transform approach,* Electric Power Systems Research **58**, 81 (2001).

[20] L. White and B. Boashash, *Cross Spectral Analysis of Nonstationary Processes,* IEEE Transactions on information theory **36**, 830 (1990).

3

UNCERTAINTY OF HARMONIC MODELLING

One of the important aspects in the control of power quality disturbances in electrical networks is network observability. To be able to predict the emission and propagation of disturbances, network operators install power quality monitors in a subset of substations, depending on the needs and regulatory requirements – for instance when a representative sample is needed to benchmark the quality of supply in the network. The main reason to limit the number of monitoring points is the price, both in terms of equipment and installation efforts. An additional restriction in power quality monitoring is the number of channels per measurement device. Typically, voltages at substation busbars need to be monitored for regulatory purposes, while currents are not obligatory and are installed per needs, where the choice is sometimes made between a number of incoming and outgoing feeders in the substation. In power quality assessment it is not uncommon practise to calculate variables based on the limited measurements and specifically chosen models. The latest developments in research in addition also allow for various state estimation techniques. In either case, the awareness of the uncertainty associated with the chosen model is of paramount importance since it gives an indication about plausibility of the results. Moreover, the aforementioned statement holds for models used in the simulation studies.

3.1. SINGLE π MODEL OF A MEDIUM VOLTAGE CABLE

To characterize the propagation of power quality phenomena, disturbance levels at non-monitored locations feeders often need to be estimated, which requires modelling based on limited measurements and network parameters. Whilst the modelling of predominantly linear network elements such as transformers, cables, lines and generators is mature knowledge [1–5], the validity of these models in field operation conditions can be compromised. This is mainly due to the fact that deviations in performance of these models from theoretical frequency dependence are rarely verified practically, with

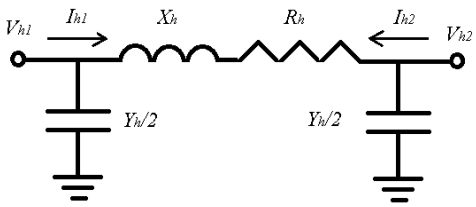

Figure 3.1: Single π harmonic model of a cable.

few of these tested in laboratory conditions. It seems logical to generalize these deviations, however, this task is challenging due to several factors, for example uncertainty of cable length, conductivity of surrounding soil and complex behaviour of resistance and reactance when exposed to different frequencies.

To sum up, the accuracy of harmonic modelling shall be quantified given the presence of aforementioned factors. One of the most frequently employed models by power quality experts is the model of a medium voltage underground cable. In a majority of study cases it is opted for the lumped impedance model — or in other words single π model. For low-frequency spectra studies it is often chosen for because of its relative simplicity and minimum amount of initial data required for the modelling [4]. The parameters and variables of this model are shown in Figure 3.1

In this model, X_h is the total inductive reactance of the cable, R_h is the resistance, and Y_h is the admittance, all for the observed harmonic order h. The variables which can be either measured or calculated are the harmonic voltages and currents at both ends of the cable – V_{h1}, V_{h2}, I_{h1} and I_{h2}. With known cable parameters and three out of four variables measured, the fourth variable (in this case current) can be calculated as:

$$I_{h1} = \frac{Y_h}{2}(V_{h1} + V_{h2}) - I_{h2} \tag{3.1}$$

From equation 3.1 we can infer that involved electrical variables correspond to geographically separated locations. To be able to utilize this equation (and hence the model itself) the measurands need to be synchronized in time with the ability to resolve phase angle information. When the fourth variable has been calculated it can be in turn compared with its measured value — a reference, and conclusion about difference between them can drawn. From this equation it becomes clear that for calculating the unknown current value the cable model parameters are limited to shunt capacitance which is provided per unit length. Thus, within single π model the source of uncertainty translated to the cable parameters can be attributed to the frequency dependence of capacitance and cable length. Assuming that all measurands are assigned with quantifiable uncertainty, the uncertainty of the cable model can be indicated.

3.2. MEASUREMENT INFRASTRUCTURE

THE synchronization of conventional power quality meters is uncommon practice. However, a number of manufacturers of phasor measurement units offers nowadays

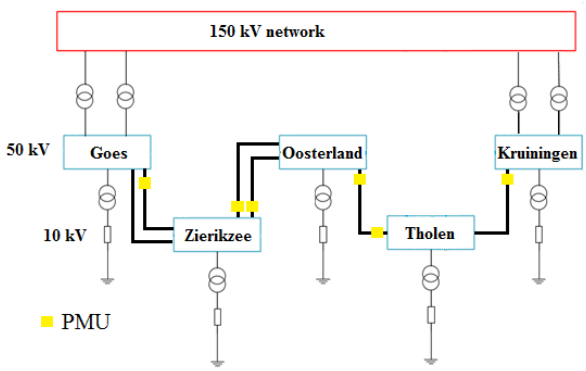

Figure 3.2: Topology of 50 kV ring network.

the functionality of synchronized spectra measurements. In certain cases it is possible already today to obtain such field data on a large scale. An example of the 50 kV network featuring PMU infrastructure is shown in Figure 3.2.

This network is operated by Dutch company Enduris located in Zeeland.Overall, there are six synchronized PMUs installed at five substations. Next to the functionality of reporting voltage and current phasors in accordance with [6] these devices are equipped with power quality functionality allowing among others for reporting every second harmonic voltage and current phasors [7]. In order to be able to derive worthwhile conclusions over uncertainty of the lumped impedance model while applying equation 3.1, we have to rely on at least one current transducer with highest possible accuracy class acting as a reference [8]. From the network shown in Figure 3.2 such a requirement was possible to meet at the substation Oosterland where at one end of the underground cable the accuracy class of current transducer equals to 0.1 for power frequency. For conclusive comparisons we shall closely investigate this cable leading to substation Tholen with another PMU connected to current transducer with accuracy class of 1. With approximate cable length of 15 km and maximum studied frequency of harmonic voltages and currents equaled to 550 Hz, the choice of single section π model is justifiable. The criteria is based on the evaluation of proportion of a line length to the wavelength of the frequency of interest. Typically, for nominal π models it is required that the length of a line does not exceed quarter of the calculated wavelength [9]. The low order harmonics in this network have significant excitation level and lead therefore to lesser sensitivity issues. However, one of the aspects affecting accuracy of measurements in medium and high voltage grids is the utilization of the voltage and current transformers. The impact of these instrument transformers on the measurements performed at power frequency is well described in the literature and standards [10]. The problem is, however, amplified at frequencies higher than fundamental with these transducers demonstrating different behavior. We must, therefore, focus on reducing uncertainty arising from the current and voltage instrumentation transformers at harmonic frequencies.

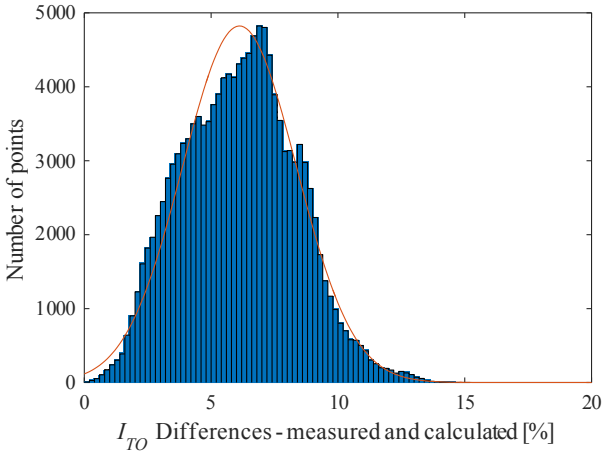

Figure 3.3: Histogram of differences for the 5th harmonic of the current.

3.2.1. CORRECTION FACTORS

Upon applying equation 3.1 on measured data at fundamental frequency we observe that difference between calculated and measured reference currents are limited to 2% for the majority of data samples. Looking further at currents at 5th harmonic order we notice that the difference between calculated and measured values are further increased to approximately 6%. A convenient way to demonstrate this fact is by plotting a histogram of values presented in Figure 3.3.

At this stage we can assume that such a difference in observed results between fundamental and harmonic frequency is dictated by uncertainty arising from current transducers. By fixing one side of instrumentation chain as reference we reduce the uncertainty of another by calculation and application of correction factors. The calculation process of these correction factors is based on a step-wise incorporation of magnitude and phase angle biases to the measured values. This is a perturbation procedure aiming to find an optimum value of biases leading to the minimum difference between measured and calculated harmonic current phasors. Every subsequent perturbation applied to the set of harmonic phasors is followed by computation of the new estimated difference between measured and calculated currents for the end of the cable with low accuracy current transducer. The mean values of these differences based on the fitted probability distribution function are then collected in the form of the curve where the minimum of the function corresponds to the calculated magnitude or phase angle correction factors. Such curves are shown in Figure 3.4 and Figure 3.5 reflecting ratio and phase errors, respectively.

From these figures we can conclude that sensitivity of harmonic measurements to phase displacement errors of the current transducer is larger in comparison with impact of ratio error. It is, however, to note that influence of both biases are non-negligible nevertheless and in general, the variation of final result is significant.

As we mentioned early, the one side of measurement chain containing current transducer with high accuracy shall be fixed as reference and we are bound to impose the

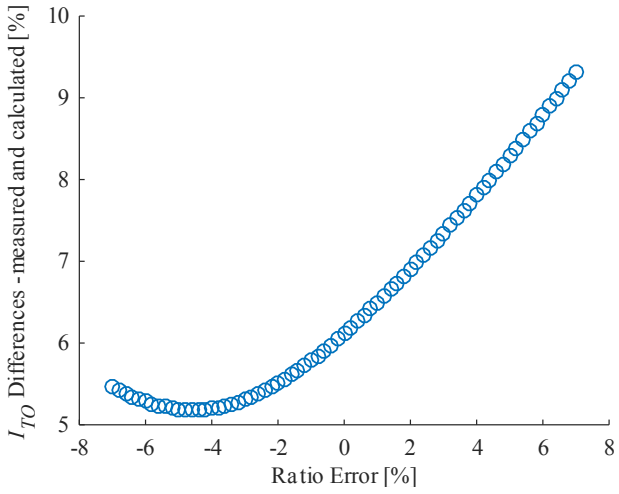

Figure 3.4: Estimated ratio bias of current transducer at 5th harmonic order.

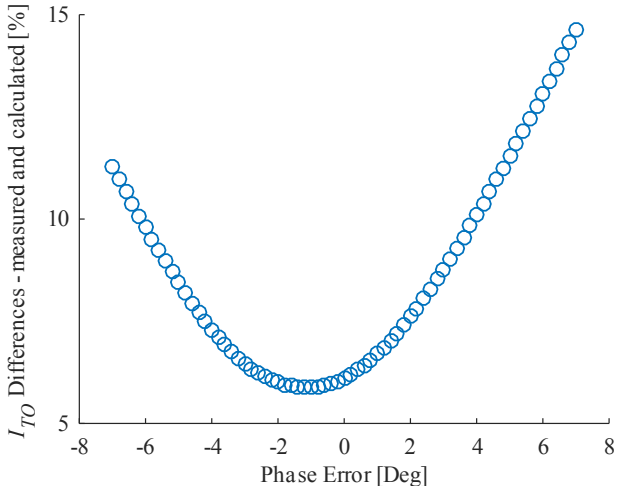

Figure 3.5: Estimated phase angle bias of current transducer at 5th harmonic order.

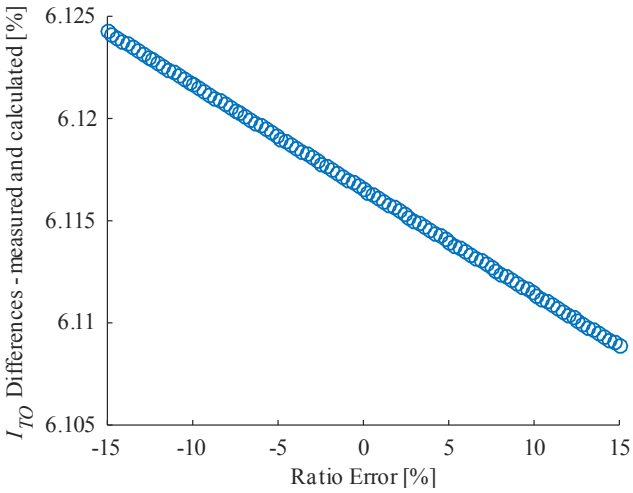

Figure 3.6: Estimated ratio bias of voltage transducer at 5th harmonic order.

same condition on voltage measurements. At substation Oosterland the accuracy class of voltage transducer at power frequency is 0.5 whilst at substation Tholen it equals to 1. Thus, this necessary condition is satisfied. But what is the actual impact of voltage transducer on the harmonic measurements with regards to the considered model? To answer this question we perform the same procedure of correction factor estimation, but this time for voltage transducers. In Figures 3.6 and 3.7 the dependencies between estimated current differences and biases applied to the measured voltage are shown. As it can be seen, even upon applying the ratio and phase biases of a wider range, the impact of this operation does not lead to the significant changes at the output. We can, therefore, infer that in this particular case the sensitivity of measurements to the deviations in ratio and phase associated with the voltage transducer are either not significant or alternatively not found by the executed correction factor algorithm. It is why in this chapter we will not consider impact of voltage transducers any further. However, it is known that especially in high voltage systems voltage transducers can be a bottleneck in performing emission assessment for various frequencies and even might have and internal resonance at certain frequency range.

3.3. MODEL UNCERTAINTY

HAVING estimated required correction coefficients for all considered harmonic frequencies we can now incorporate these corrections into the Equation 3.1 and get the final value of model uncertainty. Figure 3.8 is characterized by mean value of the differences of approximately 4.95%. We notice that the correction method has contributed to the improvement of the result with more than 1% at 5th harmonic order.

For 7th harmonic order since the corrected measurements show significant deviations from raw harmonic current phasors we present data in the form of probability den-

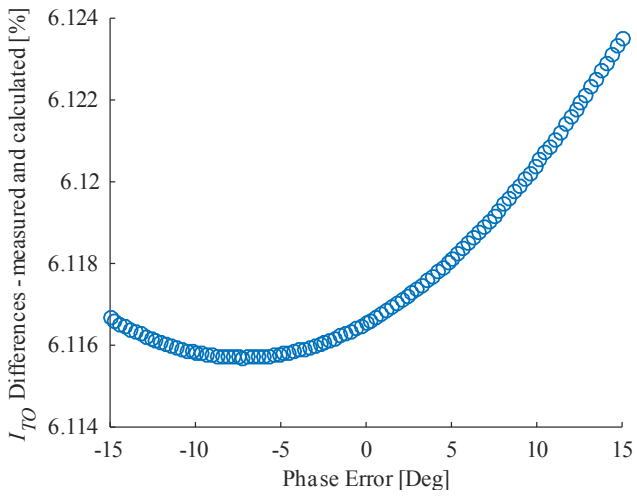

Figure 3.7: Estimated phase angle bias of voltage transducer at 5th harmonic order.

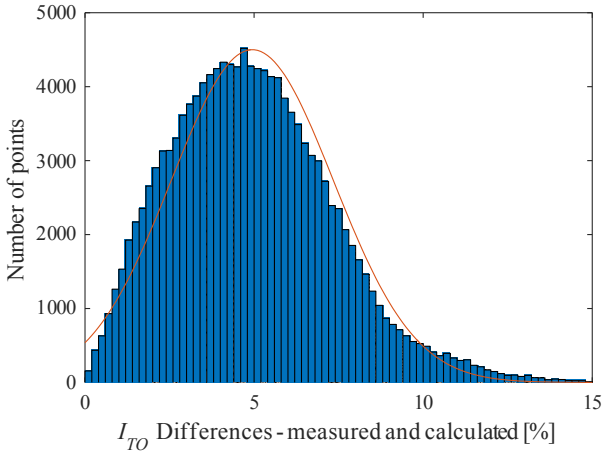

Figure 3.8: Histogram of differences after correction for 5th harmonic of the current.

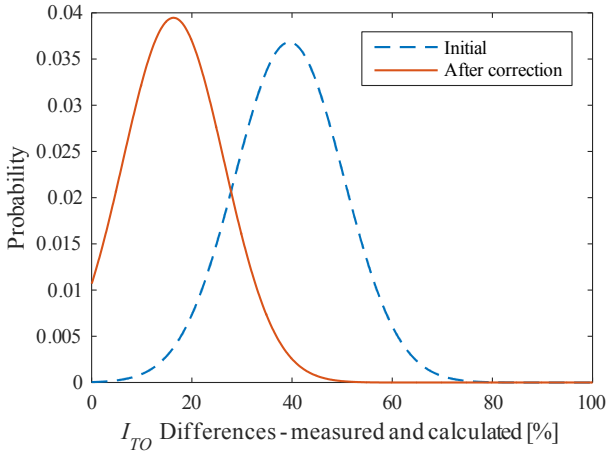

Figure 3.9: Probability density functions of initial and corrected values of current for 7th harmonic.

Table 3.1: Single π model uncertainty based on corrected measurements for selective harmonics.

h	**Ratio error**	**Phase error**	**I relative error initial**	**I relative error corrected**
#	%	deg	%	%
5	-4.6	-1.2	6.12	4.95
7	-35.3	-16.4	39.46	11.54
11	-79	16.3	80.47	10.05

sity curves in order to emphasize the differences. Figure 3.9 shows plots of probability density functions for harmonic current differences between reference values and model-based calculations. It is visible that these differences become larger with increasing harmonic frequencies. At these higher frequencies the measurement accuracy plays crucial part with correction coefficients eliminating not only uncertainty associated with the current transducer but also uncertainty arising from the whole instrumentation chain including control cables.

With this straightforward mathematical operations we at last arrive to the final values of uncertainty attributed to the single π model at several harmonic frequencies. We present these results along with required magnitude and and phase angle correction factors in Table 3.1. The remaining relative error of current included in this table gives an indication of the uncertainty introduced by single π harmonic model of the cable. Based on the presented results we may conclude that starting from 7th harmonic order the uncertainty of studied cable model becomes significant - but so do the errors at the output of current transducer.

3.4. CONCLUSION

THE single π model of underground cable is without any doubts attractive for harmonic propagation studies due to its clarity and simplicity. In this chapter we demon-

strated by means of practical experiments and simple calculations that even upon studying harmonics of low-frequency order and having a cable or relatively short length, the model gives rise to the non-negligible uncertainty. Since there exist more complex models providing higher accuracy levels and requiring larger computational efforts - an example here is the equivalent π model of a cable derived from the equations describing wave propagation [9], it is our sole understanding that in every particular model-based study a great deal of attention shall be given to uncertainty of instrumentation chain. The uncertainty of current transducers is found to be significant confirming that their broad frequency response is not known. The absence of awareness about this fact can lead to deceptive results of harmonic emission assessment. We, thus, conclude that calibration of measurement transformers and likewise their characterization for harmonic frequencies must be integral part of model-based harmonic emission assessment for medium and high voltage electrical networks.

REFERENCES

[1] Task Force on Harmonics Modeling and Simulation, *Modeling and simulation of the propagation of harmonics in electric power networks. I. Concepts, models, and simulation techniques,* IEEE Transactions on Power Delivery **11**, 452 (1996).

[2] A. A. Girgis and R. B. McManis, *Frequency Domain Techniques for Modeling Distibution or Transmission Networks Using Capacitor Switcbing Induced Transients,* **4**, 1882 (1989).

[3] Y. Zhu and J. V. Milanovic, *Automatic Identification of Power System Load Models Based on Field Measurements,* IEEE Transactions on Power Systems **33**, 3162 (2018).

[4] P. Ribeiro, *Guidelines On Distribution System And Load Representation For Harmonic Studies,* ICHPS V International Conference on Harmonics in Power Systems. , 272 (1992).

[5] M. McGranaghan, R. Dugan, J. King, and W. Jewell, *Distribution Feeder Harmonic Study Methodology,* IEEE Transactions on Power Apparatus and Systems **PAS-103**, 3663 (1984).

[6] *IEEE Standard for Synchrophasor Measurements for Power Systems* (C37.118.1-2011, 2011).

[7] B. Dickerson, *Applications of synchronised power quality measurements,* Arbiter Systems white paper , 0.

[8] V. Milojevic, *Algorithm for estimation of transmission line parameters,* , 1 (2015).

[9] J. Arrillaga and N. Watson, *Power system harmonics* (John Wiley & Sons, Ltd, Chichester, England, 2003) p. 391.

[10] A. Mingotti, L. Peretto, and R. Tinarelli, *Accuracy Evaluation of an Equivalent Synchronization Method for Assessing the Time Reference in Power Networks,* IEEE Transactions on Instrumentation and Measurement **67**, 600 (2018).

4

HARMONIC IMPEDANCE OF A LOW VOLTAGE CABLE

Incorrect values of cable harmonic impedance can lead to wrong conclusions when assessing impact of current distortion on the power network. A simple theoretical derivation of resistance and reactance for harmonic frequencies often is not sufficient as it neglects type and cross-section of cables as well as their configuration and actual installation pattern. In some cases if cable design data are available, it is possible to obtain estimates of impedance through application of certain modelling techniques. Often, these data are difficult to acquire and approximation of impedance values remains uncertain. Therefore, accurate measurements of resistance and reactance at different frequencies are required. Moreover, in order to take into account all the deciding factors including cable laying, its configuration, neutral grounding strategy and given the asymmetrical distribution of the eddy currents, the impedance measurement shall be performed on-site on already installed cables. In this chapter the focus is on low voltage distribution systems, though the fundamental principles discussed in here can be considered and applied for medium voltage level.

4.1. LINE IMPEDANCE IN A NUTSHELL

THE harmonic impedance of cables and transmission lines plays critical role in harmonic analysis. Accurate impedance at all frequencies of interest is necessary for evaluation of harmonic emission levels, identification of potential resonance problems and design of adequate mitigation measures. It is known that cable impedance under non-sinusoidal conditions can deviate significantly from theoretical values derived from 50 Hz resistance and reactance. Among factors influencing impedance at high frequencies are skin and proximity effects with the latter requiring ample modelling. The analytical expressions and Finite Element methods presented in literature demonstrate that it is the proximity effect which is responsible for unique harmonic behavior of cables. As authors of [1] pointed out in their investigation on subsea power transmission cable, the

proximity effect in multi-conductor cables leads to a drastic increase of both resistance and reactance with raising frequencies. The results of this paper were confirmed in [2] with additional regard to the asymmetrical distribution of eddy currents in a three-core submarine cable.

Fundamentally, the harmonic behavior of the subsea cables is different from underground ones. In [3] authors provided a thorough survey on existing modelling strategies of underground low-voltage distribution cables. It was proved that sufficient discrepancies in results can occur at harmonic frequencies when employing models with different complexity levels. Moreover, another important observation concerned the impact of the ground path on zero-sequence resistance, which can be altered sufficiently depending on the grounding strategy. Further, the measurements performed on disconnected low voltage cables by utilization of external signal generator revealed additional impact of cable configuration and installation practice on final harmonic impedance values [4], [5]. Additionally, a steel wire armor has been accounted as responsible for extra increase of cable resistance due to eddy current losses.

Several papers address the issue of determining parameters of lines at fundamental frequency without putting them out of service. The most recent state-of-the-art focuses on state estimation techniques involving synchronized phasor data. Among others are contributions [6–9] which presented methodology for estimating line parameters for high voltage transmission systems with provision of phasor measurement units (PMUs). Further, a method applicable to distribution system level was proposed in [10]. In this research work authors determined the parameters of medium voltage feeders considering uncertainties associated with transducer errors.

It can be concluded that modelling of cables constitutes mature knowledge given different cable technologies (and voltage levels). From the viewpoint of practical applicability, especially in low voltage distribution systems, often simplified models are taken for calculations. The reasons could stretch from the lack of representative input data for modelling to trivial absence of time of experts performing modelling and calculations.

It seems, consequently, plausible to work on measurement-based methods aiming to resolve resistance and reactance values of low voltage cables at different frequencies in presence of fluctuating harmonics in the system.

4.2. ESTIMATION ALGORITHM

IN laboratory environment we have developed a non-invasive procedure for estimating parameters of the low voltage cable. The procedure subsequently does not require an external source of harmonic excitation and thus it does not introduce additional disturbances to the system. It employs natural variations of harmonic currents and voltages and due to the availability of synchronized data ensures the integrity of impedance angle.

4.2.1. CIRCUIT THEORY

The fundamental idea behind the calculation of cable harmonic impedance is utilization of natural excitation of the system provided by operation of non-linear loads. Thus, the

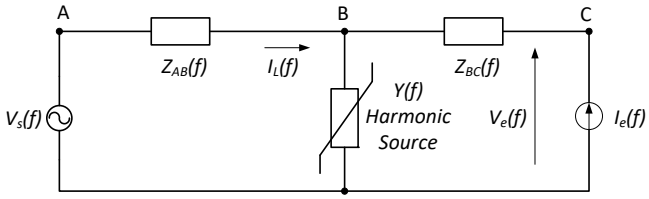

Figure 4.1: Equivalent circuit.

following equation is sufficient:

$$Z(f) = \frac{V_1(f) - V_2(f)}{I(f)} \tag{4.1}$$

where $V_1(f)$ and $V_2(f)$ are voltages measured at the beginning and end of the cable, respectively, and $I(f)$ is a line current measured at the sending end of the cable. For low-voltage systems it is reasonable to assume that current difference between sending and receiving end of the cable is negligible. This follows from the fact that capacitance of LV cables is typically low, thus ensuring that capacitive (or charging) currents do not affect phase angle values. It is evident from equation 4.1 that for correct calculation of the line harmonic voltage drop and subsequently estimation of the impedance, all the values must be recorded synchronously.

The cable impedance can be estimated within certain degree of accuracy when particular non-linear load provides sufficient harmonic excitation levels. These harmonic currents in turn cause line voltage drop at different frequencies. The impedance is estimated up to the point of connection of dominant harmonic producing source, that is, for obtaining the value which corresponds to the full length of the cable, the load must be connected at the end of it.

This idea is illustrated in Figure 4.1, where a dominant harmonic source represented by complex admittance $Y(f)$ is connected to the point B after the impedance section $Z_{AB}(f)$. Given the source voltage $V_s(f)$ and voltage at the end of the cable $V_e(f)$, the goal of the proposed methodology is to estimate the value of $Z_{AB}(f)$ over which the harmonic voltage drop occurred during the operation of dominant harmonic load $Y(f)$. At the same time, the critical part is to filter out uncorrelated noise and impact of another harmonic producing loads $I_e(f)$.

4.2.2. SIGNAL PROCESSING

One of the main issues for accurate estimation of harmonic impedance with non-invasive methods is voltage background harmonics. These background harmonic components introduce an error in final estimated value of the impedance. Due to the fast dynamic nature of background distortion the elimination of their impact is a non-trivial task. When the harmonic impedance of the cable is of concern, another origin of error is the combined effect of simultaneous operation of all the other loads connected along the feeder.

The level of excitation provided by this loads can be quite low, yet reasonably enough to act as a source of noise. In these conditions in order to ensure the robust performance of the algorithm a continuous assessment of the impedance over the range of frequencies shall be executed. For this purpose, and as it was already given in chapter 2, power spectra estimators derived from periodograms can be used. The basic concept of periodogram calculation is to establish a correlation estimate of the signal and after that apply Fourier transform. The correlation sequence in general representation:

$$c_{vv}[m] = \sum_{n=0}^{L-1} x[n]\,w[n]\,x[n+m]\,w[n+m] \tag{4.2}$$

where L is a length of the signal, $x[n]$ is a given signal and $w[n]$ is a window sequence. Thus, both pure windowed sequence of a signal and its shifted version are used in estimation procedure.

The fundamental property of the periodogram estimate is the increase of variance with the frequency when the length of a window m approaches a signal length L. On the other hand, obtaining smooth estimate of the power spectrum requires decreasing the length of the signal and number of Discrete Fourier Transform (DFT) points, which leads to poor frequency resolution. For balancing these factors Welch [11] suggested to reduce random variations of the estimate by breaking the signal into several independent periodograms and then averaging their output. According to Welch the equation 4.3 for auto-correlated power spectrum can be written as follows:

$$P_{xx}(\omega) = \sum_{-\infty}^{\infty} c_{vv}[m]e^{-j\omega m} \tag{4.3}$$

This type of signal processing algorithm is best suitable for working with noisy signals, for any uncorrelated noise can be removed from the system. At the same time, the important features of the input and output are conveniently represented by averages.

In order to apply the described algorithm for harmonic impedance estimation the notion of Linear Time Invariant (LTI) system is used. The attributes of that system are such that it is fully described by its impulse response. This impulse response in turn can be utilized to calculate the output of the system due to any input occurred. The following general equation 4.4 is applied:

$$y[n] = x[n]h[n] \tag{4.4}$$

where $y[n]$ is the output of the system, $x[n]$ is the input and $h[n]$ is the impulse response. Further, the concept of LTI system implies that output $y[n]$ is expressed by means of all the samples of impulse response and input sequences, which are linearly superimposed and shifted accordingly in time. This feature provides a foundation for continuous assessment of harmonic impedance [12]. The impulse response $h(\omega)$ is then can be estimated as:

$$h(\omega) = \frac{P_{xy}(\omega)}{P_{xx}(\omega)} \tag{4.5}$$

where $P_{xy}(\omega)$ is cross-correlated power spectrum of line voltage drop and line current and $P_{xx}(\omega)$ is auto-correlated power spectrum of current. The output of the equation 4.5 is equivalent to the impedance values calculated at different frequencies.

Welch averaged periodogram may be also considered as a tool allowing to mitigate the severity of spectral leakage phenomenon. The algorithm is characterised by a number of variable parameters, whose values can be determined experimentally. These essential parameters were tuned according to the following logic:

- The cable under the study and one non-linear load were energized by the external power source providing stable voltage with constant frequency of 50 Hz without background distortion;
- Resistance and reactance values were extracted for selective frequencies by applying proposed algorithm;
- Aforementioned steps were performed after substituting the external power source with a public grid which is characterized by deviating power frequency and a certain background distortion;
- The parameters of the algorithm were established by analyzing differences in impedance results between the two cases with an assumption that the case with sinusoidal power source with stable frequency was considered as the reference.

Consequently, based on 25 kHz sampling frequency, the 1-cycle Hamming window and 500 DFT points were used. Moreover, 10-second segments of a signal were further broken to 500 independent periodograms with 10% overlap. In that manner, the impact of spectral leakage was reduced and smooth averaged output was obtained.

4.3. MEASUREMENTS IN THE PRESENCE OF UNCERTAINTY

To achieve accurate impedance estimation of a low voltage cable at harmonic frequencies a system characterized by high accuracy levels shall be utilized. This holds not only for time synchronization error, but rather for the whole instrumentation chain in question. However, since the best technical characteristics of the equipment are always bound to the increased cost, in selective cases it might seem only reasonable to be aware of the combined uncertainty associated with the system. That is, by characterizing the performance of the measurement system and by assigning confidence intervals to derived values (in this case impedance) the awareness of plausibility of final results can be achieved. In the following sections we will discuss this in details.

4.3.1. FEEDER CONFIGURATION

The established power network infrastructure includes low-voltage power source and underground low voltage 70 mm^2 Al feeder with approximate length of 150 m. Overall, there are six connection points along the cable realized with 16 mm^2 Cu of 30 m length each. These connections act as conventional “households” and different types of loads can be connected thereto. This configuration represents a part of a typical low voltage network in the urban environment.

At the end of the feeder we connected a programmable load California Instruments 3091LD which acts as an emulator of large power electronics-based load. This load provides necessary harmonic current injections. Additionally, two identical solar inverters

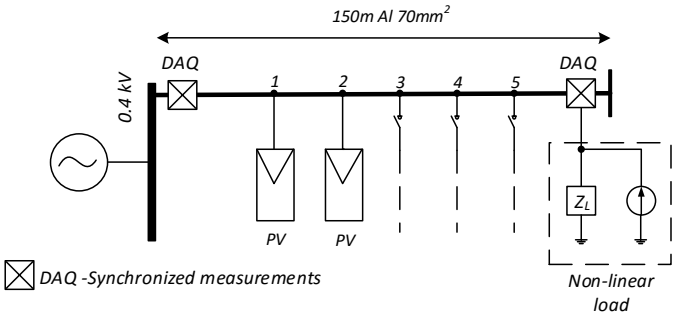

Figure 4.2: Experimental setup.

4

Mastervolt Soladin 3000 Web are connected towards the beginning of the feeder. These inverters are supplied by Solar Power Simulator TerraSAS ETS, which can emulate operation of the solar power plant under different irradiation levels. The purpose of the inverters is to provide small current distortions and therefore to act as a source of additional noise in the system. These solar inverters operate with rated THD level less than 3%, therefore ensuring only little impact on harmonic voltage drop. The one-line configuration of the setup with measurement points is depicted in Figure 4.2.

4.3.2. SYNCHRONIZED WAVEFORM RECORDING

The distributed fast data acquisition system consists of two National Instruments cRIO-9038 chassis. Voltage and current waveforms are recorded at 25 kHz sampling frequency with all the samples synchronized across all channels and chassis to the precision time source. The clock signal is generated on a field-programmable gate array (FPGA) of the master device and then distributed via high-speed digital interface to the slave device. The digital modules used for this procedure are NI-9401. It is essential that both of the acquisition devices are triggered synchronously at the start of the data recording. The accuracy of time synchronization is at the range of 200 ns.

Voltage signals are measured directly at both ends of the cable whereas line current is provided by rogowsky coil type PEM LFR 03/3. The chassis are equipped with input voltage NI-9225 and current NI-9234 measurement cards with 24-bits analog-to-digital converters (ADC) based on delta-sigma technology. This implies that output of ADC is characterized by unequal amount of samples produced from one cycle to another. Thus, a resampling algorithm is utilized as a part of developed synchronization software package. Further, the voltage cards contain three differential input channels with channel-to-channel isolation excluding the possibility of ground loop influence. In contrast, all four input channels of current measurement cards are referenced to the chassis ground through resistor. In order to avoid possible impact of ground loops we connected the chassis to the common ground. For the impedance estimation only current of one phase is sufficient to measure. This measurement is set at the beginning of the cable.

The recorded data are stored directly on the hard drive of each measurement device, therefore eliminating all potential delays associated with transfer of data via Ethernet or

Table 4.1: Equipment specifications.

Component	Gain error, %	Offset error, %	Noise, mV
Voltage card	±0.05	±0.008	2
Current card	±0.05	±0.006	0.05
Current probe	±0.3	±0.05	3

other means of communication.

4.3.3. EVALUATION OF MEASUREMENT UNCERTAINTY

We have evaluated measurement uncertainty based on the metrological specifications of a measurement equipment. A Type B uncertainty is calculated according to Guide to the expression of uncertainty in measurement [13] recommendations. Typical calibration values for each component of the measurement chain are given in Table 4.1. The anti-alias bandwidth of voltage and current cards is 22 kHz and reported values for current probes are valid for frequency range from 0.45 Hz to 20 kHz.

Firstly, a standard uncertainty associated with each component of voltage and current measurements is evaluated. Further, a combined standard uncertainty for current is computed through application of summation in quadrature:

$$u_c(I) = \sqrt{u_1(I)^2 + u_2(I)^2} \tag{4.6}$$

where $u_1(I)$ and $u_2(I)$ are standard uncertainties of input current card and current probe, respectively.

The uncertainty of the impedance estimation involves correlated input quantities, therefore, the degree of correlation shall be estimated with correlation coefficient according to:

$$r(V,I) = \frac{u_c(I)\delta_V}{u_c(V)\delta_I} \tag{4.7}$$

where $u_c(I)$ and $u_c(V)$ are combined standard uncertainties of current and voltage measurements, respectively and δ_I, δ_V are current perturbation and associated voltage drop, respectively. The combined standard uncertainty for correlated input quantities is given as:

$$\begin{aligned} u_c(Z) = {} & c_V^2 u_c^2(V) + c_I^2 u_c^2(I) \\ & + 2u_c(V)u_c(I)r(V,I)c_V c_I \end{aligned} \tag{4.8}$$

Where c_V and c_I are sensitivity coefficients. The sensitivity coefficients are calculated as follows:

$$c_V = \frac{\partial Z}{\partial V} \tag{4.9}$$

$$c_I = \frac{\partial Z}{\partial I} \tag{4.10}$$

The correlation coefficient in equation 4.7 is frequency dependent and therefore its value will be increasing with increased frequency due to higher value of impedance. Further, the second term of equation 4.8 takes negative sign and thus, the final uncertainty is

Table 4.2: Uncertainty budget.

Quantity	Standard uncertainty $u(x_i)$	Probability	Expanded uncertainty k factor = 2
Minimum excitation, I = 9.05 A			
V	70 mV	normal	140 mV
I	2.9 mV	normal	5.8 mV
Z	7.7 $m\Omega$	normal	15.4 $m\Omega$
Medium excitation, I = 10.84 A			
V	70 mV	normal	140 mV
I	3.3 mV	normal	6.6 mV
Z	5.9 $m\Omega$	normal	11.8 $m\Omega$
Maximum excitation, I = 13.38 A			
V	70 mV	normal	140 mV
I	3.6 mV	normal	7.2 mV
Z	5.2 $m\Omega$	normal	10.4 $m\Omega$

expected to decrease with higher order of harmonics, provided that voltage and current readings are above the uncertainty level of the measurement system. The estimated uncertainty budget for different excitation levels at power frequency is presented in Table 4.2.

4.3.4. REFERENCE MEASUREMENTS

Low voltage cable systems are characterized by higher values of resistive component of the impedance which leads to low X/R ratio at power frequency. In laboratory conditions this fact presents exceptional opportunity to perform highly accurate measurements for the sole purpose of deriving reference value of cable resistance. This can be served as a reference for all subsequent experiments with harmonic impedance measurements. One of the most efficient methods of obtaining reference resistance is through direct current injections. We have connected a DC source to the studied feeder and provided controlled excitation from 1 A to 10 A and current measurements with calibrated accuracy 0.5% + 2 digits. The DC current was drawn by precision current measurement shunts with calibrated resistances of 10 $m\Omega$ and 100 $m\Omega$ which were connected to the last household (Figure 4.2). We have installed two identical digital multimeters Agilent 34401A at the beginning of the feeder and at the last connection point to measure value of the voltage drop across the DC resistance. These multimeters are characterized by 0.0030% gain error and 0.0005% offset error as per data provided by the manufacturer.

We repeated measurements 13 times for different current levels while calculating resistance after each subsequent step. The majority of results has fallen between boundaries of 0.0934 Ω and 0.0936 Ω. Based on this, we have taken 0.0935 Ω as the reference. On the other hand, the reactance at fundamental frequency was calculated based on the layout and data sheet specifications. The value of 0.023 Ω was accepted as reference reactance.

Table 4.3: Load operating scenarios[1].

#	1	2	3	4	5	6	7	8	9
I_1, A	13.0	10.8	11.7	12.8	11.3	12.6	13.0	9.0	13.9
P_1, kW	2.9	2.5	2.6	2.9	2.6	2.9	3.0	2.0	3.0

[1] constant power load with crest factor of current 1.8 and THD_i=44%

4.4. IMPEDANCE UNDER SINUSOIDAL SUPPLY CONDITION

To evaluate stability of the non-invasive impedance estimation methodology we first energize our distribution feeder by means of a programmable power source. By performing this experiment we make sure that supply frequency is fixed at 50 Hz with minimal deviations. The harmonic excitation is only provided by 3-phase balanced nonlinear load connected to the household #6, which corresponds to the connection point at the end of the feeder and no background voltage distortion present in the system. By adjusting crest factor of the load we provide harmonic current excitation to the system. The respective load settings are presented for 9 different test stages in Table 4.3. As an example, Figure 4.3 and Figure 4.4 show pattern of the harmonic load current together with associated voltage distortion at the sending end of a cable for 7th and 13th harmonic orders, respectively. The overshoots are due to imperfections in the control of load bank during rapid change of load demand.

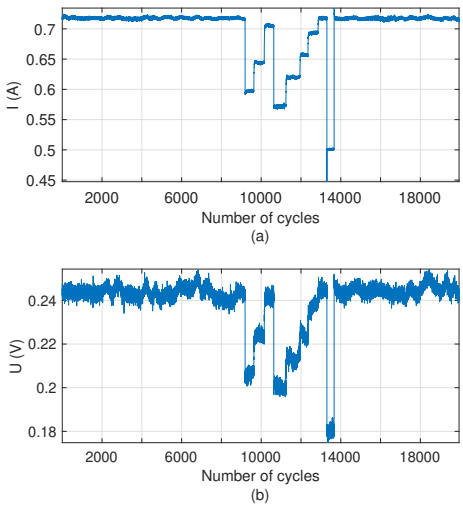

Figure 4.3: 7^{th} harmonic 1-cycle RMS values: **(a)** Load current; **(b)** Voltage at the beginning of cable.

The visual analysis of these graphs confirms that lower harmonic current values at higher harmonic orders contribute to a larger voltage distortion due to increased value of the impedance. Additionally, a valuable information can be extracted from the graph demonstrating cable voltage drops at different harmonic frequencies (Figure 4.5). The recorded voltage drop values for 5th and 11th harmonic components are significantly

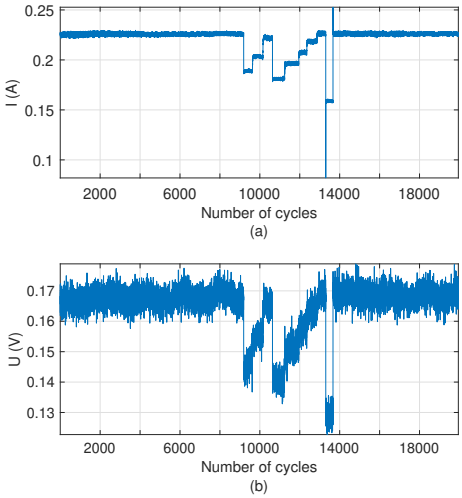

Figure 4.4: 13^{th} harmonic 1-cycle RMS values: **(a)** Load current; **(b)** Voltage at the beginning of cable.

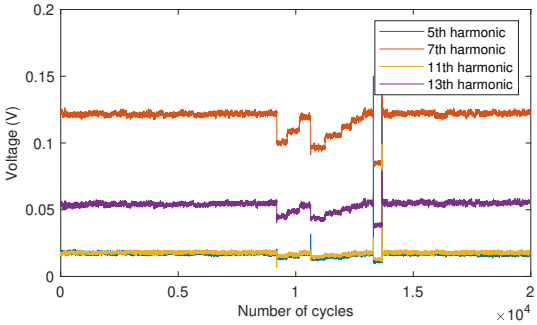

Figure 4.5: Voltage drop at different frequencies.

smaller than corresponding values of 7th and 13th and are close to the uncertainty level of voltage acquisition cards. As the next step, these components shall be excluded from impedance estimation algorithm.

While applying estimation algorithm to the acquired data we observed that the outcome was significantly impacted by the value of phase angle between voltage drop ΔV and corresponding current I at different frequencies. We conveniently demonstrate selective angle distributions in the form of histogram charts in Figure 4.6 and Figure 4.7 for 7th and 11th harmonic orders, respectively. For 11th harmonic it is to notice that associated voltage drop is caused by imaginary component only. This practically means that an insufficient harmonic excitation by the real part of current will lead to very high uncertainty values for resistance estimates.

Since three-phase balanced non-linear load could inject among others zero-sequence harmonics, an uneven voltage drop over zero-sequence impedance is expected. This phenomenon is related to the fact that zero-sequence components tend to add in neu-

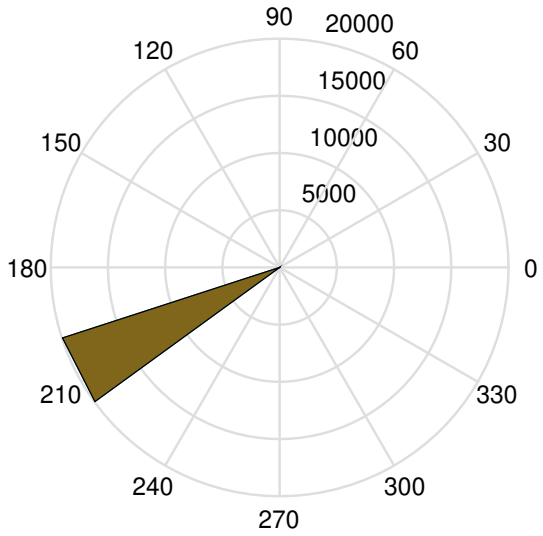

Figure 4.6: Angle between ΔV and I at 7^{th} harmonic.

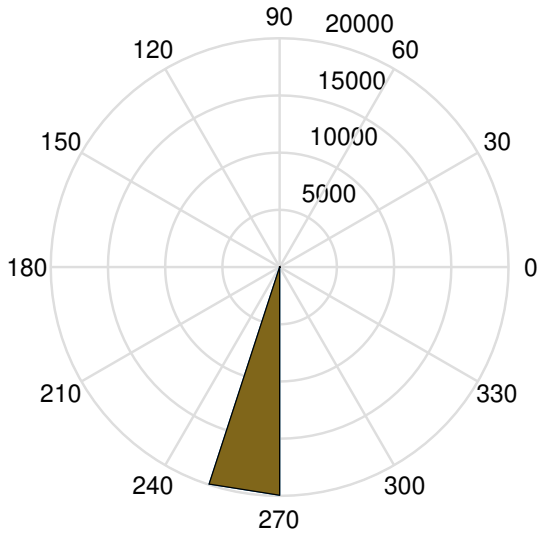

Figure 4.7: Angle between ΔV and I at 11^{th} harmonic.

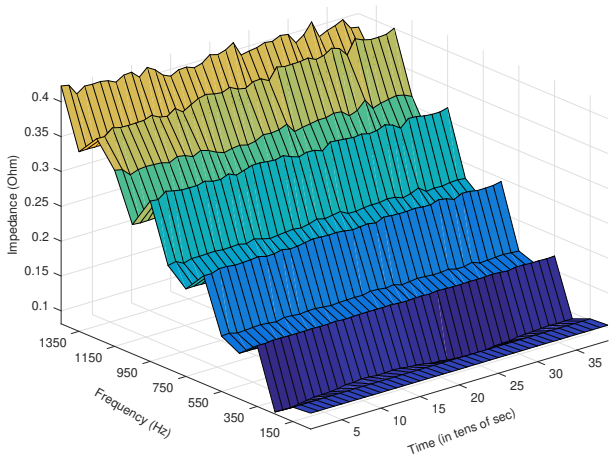

Figure 4.8: Magnitudes of cable impedance values at different frequencies.

tral wire. In theory, these components are expected to be exactly three times of the corresponding phase value. However, in practical situation due to the leakage effect to the ground the magnitude of current in neutral wire can demonstrate some deviations from anticipated value. Another influencing factor is that typically all three phases are not perfectly balanced at all frequencies so zero-sequence components do not necessarily correspond to triple harmonic orders. In order to complement the impedance method it is suggested to use neutral wire measurement for compensation of zero-sequence currents.

In Figure 4.8 we present estimated magnitudes of cable impedance for several harmonic orders in the form of 3-d plot reflecting both time and frequency scales. This graph is meant to demonstrate features of continuous online assessment of harmonic impedance. It can be inferred for this plot that estimates of impedance are stable over the course of time.

Finally, in Table 4.4 we include estimated impedance for harmonic orders from 1 to 19 along with standard uncertainties and harmonic current values. From this table it can be inferred that the magnitude of estimated fundamental impedance is close to the reference value of 0.0963 Ω. The difference between two values is 7.9 $m\Omega$ which is within the evaluated expanded uncertainty for 95% of values (coverage factor k = 2). The main difference lies in the reactive part of impedance and this is due to the initially low X/R ratio which requires higher excitation levels in imaginary part of current. As it can be seen, the harmonic impedance estimates demonstrate consistent increasing behavior and rising levels of standard uncertainty with decreasing excitation level.

In addition, the consistency of impedance estimates over the course of time can be further checked by evaluating vector plots of harmonic impedance. These plots for some of the frequencies are presented in Figure 4.9 and Figure 4.10. Each figure contains 40 estimates of complex impedance values and each value corresponds to 10 seconds period, over which averaged periodogram was calculated. From these graphs it can be inferred

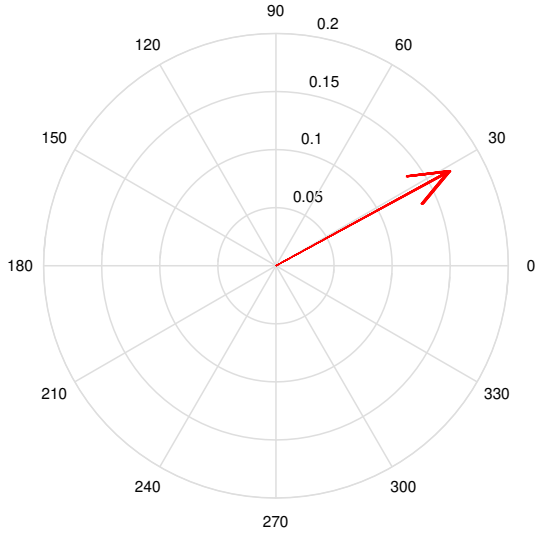

Figure 4.9: 7^{th} harmonic impedance.

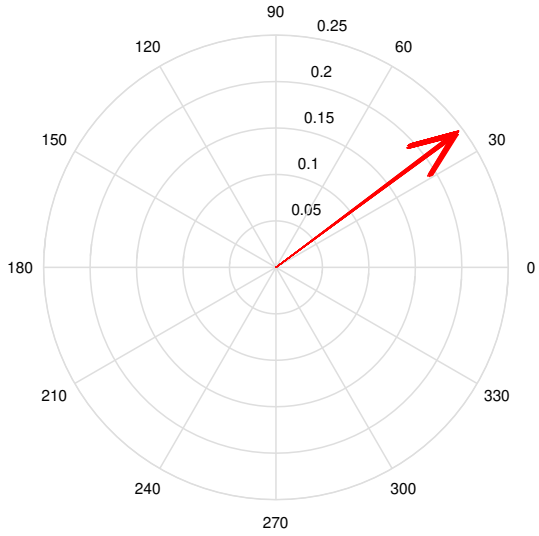

Figure 4.10: 13^{th} harmonic impedance.

Table 4.4: Complex impedance estimates.

h	$R + iX$	$\|Z\|$	Standard uncertainty	I
#	Ω	Ω	$m\Omega$	A
1	0.1037 + 0.0097i	0.1042	7.7	9.05
3	0.0953 + 0.0363i	0.1020	3.8	3.93
7	0.1478 + 0.0814i	0.1687	25.5	0.5
9	0.0982 + 0.1092i	0.1469	62.1	0.25
13	0.1894 + 0.1417i	0.2365	82.3	0.16
15	0.1050 + 0.1783i	0.2069	442.4	0.04
19	0.2418 + 0.1964i	0.3115	274.5	0.06

that variation of impedance estimates is negligible.

4.5. IMPACT OF BACKGROUND DISTORTION

WHILST experiments with ideal sinusoidal power source and minimum deviation of supply frequency constitute conditions which are perfect for evaluating performance of online impedance estimation, we shall also focus on scenarios resembling practical operation of distribution feeder. To do so, we energize it with the public grid with THD equal to 1.7% with dominating 5th and 7th harmonics. Later, we put into operation two identical solar power inverters connected the households #1 and #2. We then apply a slow ramp irradiation profile ensuring common DC input for both inverters. The current injected by one of the inverters is shown in Figure 4.11. The fundamental current measured at the sending end of the cable is shown in Figure 4.12.

The solar inverters introduce variations into measured current. At the same time fluctuations of voltages at harmonic frequencies are resulted from harmonic interaction with background voltage distortion. These patterns are reflected in Figure 4.13 and Figure 4.14 for 5th and 11th harmonic orders, respectively.

After collecting all the required waveforms we perform continuous harmonic impedance

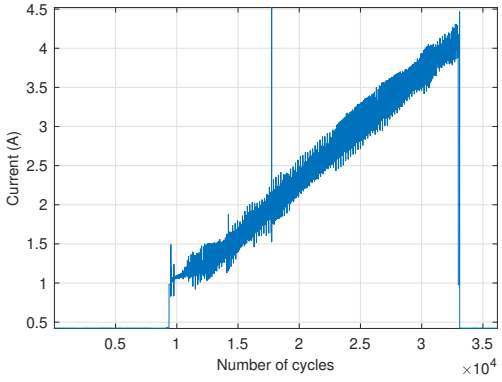

Figure 4.11: Inverter fundamental output current.

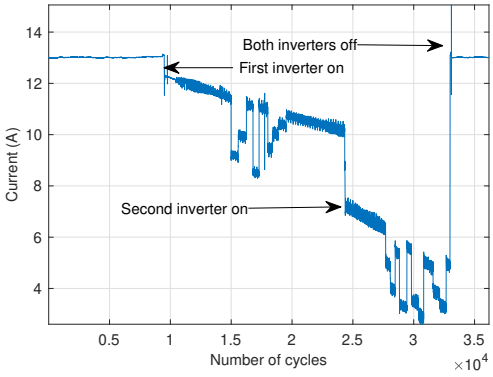

Figure 4.12: Fundamental line current.

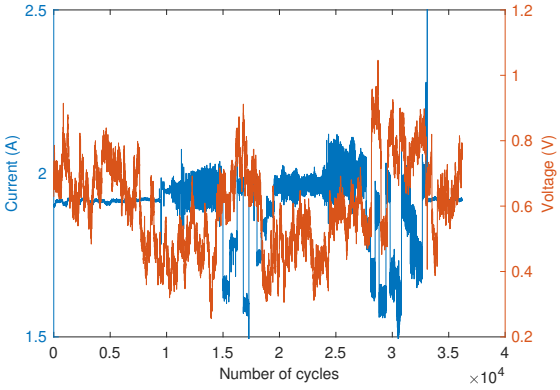

Figure 4.13: 5^{th} harmonic voltage and current (1-cycle RMS).

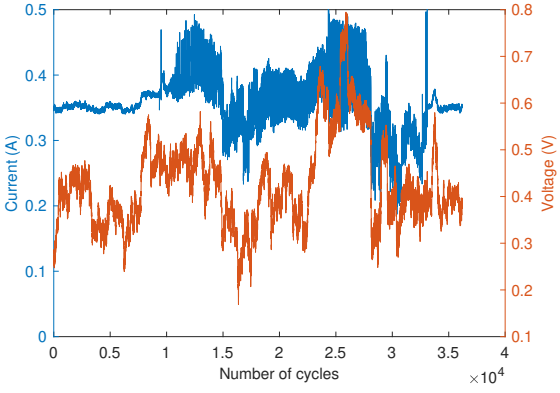

Figure 4.14: 11^{th} harmonic voltage and current (1-cycle RMS).

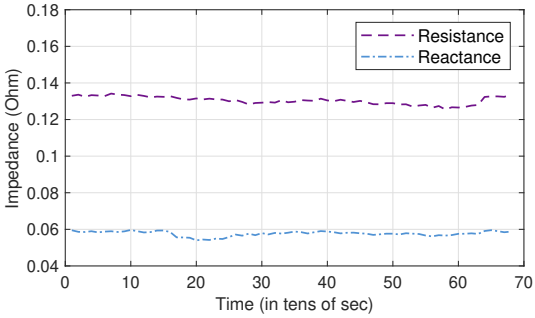

Figure 4.15: 5^{th} harmonic resistance and reactance.

assessment. For this case we split complex impedance into resistive and reacitve parts. Figure 4.15 illustrates the outcome of the cable 5th harmonic impedance estimation. The calculated difference between extreme points is no more than 10 $m\Omega$ for R and X which indicates that substantial part of the noise introduced by background voltage distortion and solar power was filtered out, whereas the operation of a dominant harmonic source fully contributed to the determination of cable impedance.

All the same, the impact of noise becomes more pronounced at higher harmonic orders characterized by lower excitation levels. We look at the 11th harmonic resistance and reactance estimates which are plotted against different modes of operation in Figure 4.16 and Figure 4.17 in the form of box plots over 100 seconds observation time. The upper and lower bounds of the boxes correspond to 75th percentile and 25th percentile, respectively and red lines indicate median values. The following modes of operation are considered:

1. NL – only non-linear load operating;
2. 1 PV – first solar inverter switched on;
3. LD – changes in load demand;
4. 2 PVs - second solar inverter switched on and both are now in operation;
5. LD (2) – changes in load demand

From Figure 4.16 we can deduce that operation of photovoltaic inverters introduces variation into resistance estimates. However, this variation reduces during fast changes of load demand indicating that estimate can be improved in noisy environment with low excitation levels. One of the possible reasons of improvement is increased correlation between current of dominant harmonic source and its contribution to the voltage distortion. According to the results, the difference between two extreme median values of resistance estimates is no more than 20 $m\Omega$.

As for the reactance estimates, we can conclude based on Figure 4.17 that variance of estimates minimal during first phase of step changes in load demand indicating an accurate estimate with median value of 0.11 Ω (indicative uncertainties are presented

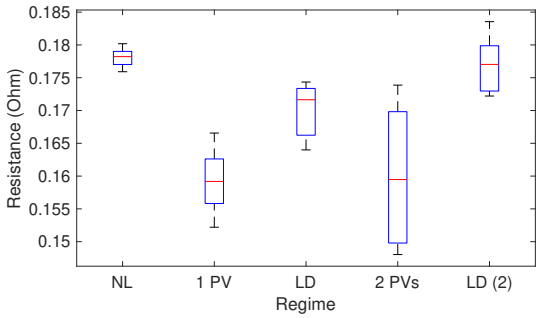

Figure 4.16: Resistance at 11^{th} harmonic.

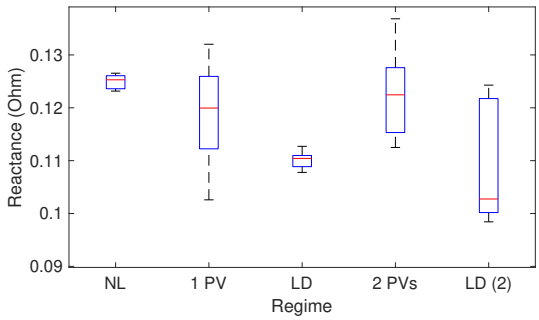

Figure 4.17: Reactance at 11^{th} harmonic.

in Table 4.4). In contrast, the largest deviations in reactance values correspond to the second phase of load step changes. The underlying reason is insufficient excitation of reactive component of the cable during this particular regime of operation. Finally, for this case we demonstrate the absolute values of impedance magnitude in Figure 4.18. We can conclude, therefore, that proposed online procedure for continuous cable harmonic impedance evaluation is characterized by stable performance in presence of the uncorrelated noise.

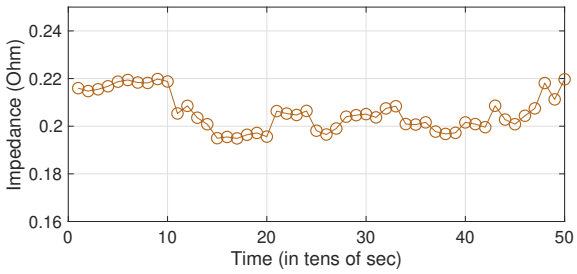

Figure 4.18: Magnitudes of 11^{th} harmonic impedance.

4.6. CONCLUSION

In this chapter we put our focus on discussion over the important parameter in distortion analysis - harmonic impedance of underground cable in low voltage distribution systems. A parameter whose importance is typically overlooked due to a number of factors. It goes without saying that amount of low voltage cable systems comprising assets of modern distribution systems operators is strikingly large. On one side, keeping technical details over each cable including its precise length and power frequency impedance values seems reasonable, but not always feasible. On the other, the availability of technical specifications for harmonic frequencies definitely constitutes a gap. We consider it important to not only propose new methods for efficient estimation of such quantities for frequencies other than fundamental, but to merely raise a situational awareness of all experts involved in distribution systems power quality analysis. Therefore, in the line of this duty, and as the main contribution of this chapter, we demonstrated one of the ways to measure harmonic impedance of the cable.

Undoubtedly, while utilizing synchronized measurement infrastructure for harmonic impedance estimation, characterization of uncertainty of instrumentation chain must be of paramount importance. Whilst time synchronization error must be kept at submicrosecond level, meaningful confidence intervals should be assigned to every estimated impedance value at each harmonic order. If the aim is to estimate one in a non-invasive manner, then it is needed to provide a way of differentiating contributions of dominant distortion source from any other fluctuations, including uncorrelated noise. The data proves also that treating harmonic systems at low voltage level as linear time invariant is justified and may be used as basis for many an algorithm. In this chapter the output of the developed algorithm is a transfer function which describes frequency response of LTI system. This transfer function contains real and imaginary components at different frequencies which correspond to harmonic impedance values. Lastly, calculation of final impulse response of the system is based on the injections of dominant harmonic source.

REFERENCES

[1] C. H. Chien and R. W. G. Bucknall, *Harmonic Calculations of Proximity Effect on Impedance Characteristics in Subsea Power Transmission Cables,* IEEE Transactions on Power Delivery **24**, 2150 (2009).

[2] A. Pagnetti, A. Xemard, F. Paladian, and C. A. Nucci, *An improved method for the calculation of the internal impedances of solid and hollow conductors with the inclusion of proximity effect,* IEEE Transactions on Power Delivery **27**, 2063 (2012).

[3] A. J. Urquhart and M. Thomson, *Series impedance of distribution cables with sector-shaped conductors,* IET Generation, Transmission & Distribution **9**, 2679 (2015).

[4] Y. Du and J. Burnett, *Experimental investigation into harmonic impedance of low-voltage cables,* IEE Proceedings - Generation, Transmission and Distribution **147**, 322 (2000).

[5] Z. Yuan and Y. Du, *Harmonic impedance of single-core armored cables,* 2003

IEEE PES Transmission and Distribution Conference and Exposition (IEEE Cat. No.03CH37495) **00**, 45 (2003).

[6] D. Shi, D. J. Tylavsky, K. M. Koellner, N. Logic, and D. E. Wheeler, *Transmission line parameter identification using PMU measurements,* European Transactions on Electrical Power **21**, 1574 (2011).

[7] D. Ritzmann, J. Rens, P. S. Wright, W. Holderbaum, and B. Potter, *A novel approach to noninvasive measurement of overhead line impedance parameters,* IEEE Transactions on Instrumentation and Measurement **66**, 1155 (2017).

[8] P. Ren and H. Lev-ari, *Tracking Three-Phase Untransposed Transmission Line Parameters Using Synchronized Measurements,* IEEE Transactions on Power Systems **33**, 4155 (2018).

[9] V. Milojevi, S. Calija, G. Rietveld, S. Member, and D. Colangelo, *Utilization of PMU Measurements for Three-Phase Line Parameter Estimation in Power Systems,* IEEE Transactions on Instrumentation and Measurement **67**, 2453 (2018).

[10] P. A. Pegoraro, K. Brady, P. Castello, C. Muscas, and A. V. Meier, *Line Impedance Estimation Based on Synchrophasor Measurements for Power Distribution Systems,* IEEE Transactions on Instrumentation and Measurement **68**, 1002 (2019).

[11] P. D. Welch, *The use of fast Fourier transform for the estimation of power spectra: A method based on time averaging over short, modified periodograms,* IEEE Transactions on Audio and Electroacoustics **15**, 70 (1967).

[12] D. Borkowski, A. Wetula, and A. Bien, *New method for noninvasive measurement of utility harmonic impedance,* IEEE Power and Energy Society General Meeting **1**, 2 (2012).

[13] JCGM 100:2008, *Evaluation of measurement data – Guide to the expression of uncertainty in measurement* (Joint Committee for Guides in Metrology, 2008).

5

MODELLING OF NON-LINEAR SOURCES

Accurate models of harmonic producing sources are essential for studying their impact on voltage distortion levels. The challenge in developing a model suitable for harmonic propagation studies in the distribution networks is to accurately represent the impact of background voltage distortion on harmonic current emission of a certain device. This challenge is governed by a trade-off between the complexity of a model and its level of details. Moreover, not only the modelling approach itself is important but also the convenience of practical applicability of the developed model in the commercially available simulation packages. To meet these requirements in this chapter a modelling methodology is investigated which makes use of a certain deterministic function derived from the reasonable amount of field measurements. The outcome of this modelling procedure represents the behavior of a harmonic source in the form of a compact algebraic equation. A strong advantage of such an approach is its ease of application in a simulation environment and reckoning on a large amount of simulation scenarios.

5.1. REVIEW OF THE EXISTING MODELLING TECHNIQUES

THE current modelling practice encompasses several approaches but among the most efficient and preferable is the Norton coupled frequency admittance matrices (FCM) [1]. This modelling method accounts on the sensitivity of harmonic currents to the angle and the magnitude of a background voltage distortion. Additionally, it allows to consider harmonic interaction between voltages and currents of different harmonic orders. A thorough attention to this method was given in [2] where coupled capacitor-smoothed bridge rectifiers were modelled as a coupled admittance. The authors of this study proved that harmonic current is influenced significantly by applied harmonic voltage amplitudes and phase angles. Moreover, complex deviations of model output vector from the measurements were used to evaluate accuracy of the investigated models. The results showed 10-20% average deviations for 50% quantiles of data.

In [3] the authors emphasized the importance of metrological requirements to the measurement system used for obtaining initial data for Norton models. They demonstrated that derivation of FCM depends strongly on the accuracy of such a system.

The properties of admittance elements with respect to the topology of power electronics equipment have been studied in [4] and [5]. The Fourier descriptors were proposed for estimating and analyzing FCM. It was found out that depending on the topology of power electronic device, specifically on the type of power factor correction (PFC) some equipment types can indicate wide linear range in the coupled Norton approach - a brilliant observation leading to the prediction of harmonic behavior of certain devices. Based on the measured values the authors of these papers proposed the quantification of linearity - a non-linearity harmonic current response index (NLI).

To conclude, the Norton frequency-coupled matrices is a powerful modelling approach, which de facto requires significant amount of accurate measurement sets and ample mathematical derivations. Its implementation in commercial simulation packages can be somewhat limited since an iterative harmonic load flow would require a large number of admittance matrices comprised in advance in order to take into consideration all scenarios of interest.

As an alternative to Norton FCM a component-based modelling of harmonic loads is capable of reproducing the instantaneous input current waveform of each individual power electronic device. Such models require the fundamental knowledge about topology of studied devices and numerical values of the components. In [6] a method for modelling residential aggregate loads for harmonic analysis was presented. Generic models based on the equivalent circuits of the power electronics-driven equipment have been developed. Based on the results authors of this paper concluded that proposed aggregate models were suitable for preserving full information on the electrical characteristics of the modelled load mix. This approach was further developed in [7]. The main contribution of this work is a combination of detailed component-based modelling approach with the Markov-chain Monte Carlo routine allowing to account on user-load interaction. The case study involved modelling of groups of compact fluorescent lighting (CFLs) and important observation concerned diversity factors to quantify harmonic cancellation effects between different groups.

A rigorous component-based modelling of modern switched-mode power supply, photovoltaic inverter (PV) and electric vehicle charger (EV) has been shown in [8]. In this work authors also introduced an influence of changing power operating mode on resulting harmonic emission levels as well as gave an important remark to test modern power electronics equipment in presence of non-sinusoidal supply voltage waveform. This modelling approach in combination with probabilistic methods was also applied in [9] for studies of the commercial load sector.

As it can be deduced from these works, the component-based models introduce high level of details and associated complexity into the simulation scenario but they, nevertheless, require knowledge on generic underlying equipment topology, type of the control system and values of the base components. Being able to accurately reproduce harmonic content of a certain device or a group of individual devices, they are bound to be used within specialized simulation software, for instance EMTP.

Finally, deterministic modelling methods are complemented by harmonic finger-

prints. This modelling process was firstly described in [10] where harmonic current injections were comprised in look-up table according to the applied individual voltage background harmonics. The phase and magnitude of each individual harmonic voltage were changed step-wise providing at the end of procedure full harmonic current spectrum of equipment under study. The measurement approach is quite similar to the one used for FCM models, yet the post-processing part does not require complex mathematical equations. The idea was further developed in [11] for aggregate models of photovoltaic inverters.

Next, stochastic aggregate harmonic load models form a distinct family of methods focusing on application in stochastic harmonic propagation studies. Among research works involving development of such probabilistic models are [12] and [13]. These methods are best suited for simulating an impact of large bulk of aggregate low-voltage load on medium-voltage networks with both composition and participation factor of loads usually modelled as random variables. As it was shown in these works, the accuracy of such models relies on the extent of measurement campaign typically lasting weeks at one particular location. On the other hand, the uncertainty of probabilistic models can be large if part of the measured data is substituted with historical or typical values.

Some work has been done in order to apply data-fitting routines to the measured sets of data. In [14] authors presented a method based on a linear least-square (LLS) estimator performed on the decoupled Norton admittances matrices of CFL. Due to the numerical instability of the algorithm it was not possible to obtain either accurate estimates of full Norton model or coupled admittance model. The results of this particular case study demonstrated reasonably good accuracy of the derived model in terms of current magnitudes but omitted angle derivation. The underlying reason in disregarding angle of harmonic is the nature of LLS, which requires modifications in order to resolve phase information.

In [15] an excellent method for modelling background harmonic voltage source has been presented. A non-linear least-square (NLSF) was applied to the sets of field data after statistical processing which involved smoothing and filtering the data with Gaussian distribution. While the output of this algorithm in the form of normal distribution deemed to be appropriate for representing current magnitudes of combined operation of many harmonic sources, a different approach is required to model a response of the certain harmonic load.

To conclude, despite the research aiming to derive algebraic equations associated with harmonic sources, there is currently a lack of harmonic models of that type.

5.2. FUNDAMENTALS OF CIRCULAR STATISTICS

IN this chapter, we propose a novel method for modelling individual harmonic producing sources based on the foundations of circular statistics. A measurement procedure attributed to the harmonic fingerprinting [10] is used for obtaining the initial sets of data for three modern power electronics devices: photovoltaic inverter, battery charger and a group of CFLs. After that, coefficients of the models are estimated with the application of circular regression algorithm. The output of the modeling process is compared with the measured data to check for satisfactory performance. The methodology is focused on the derivation of relationships between applied harmonic background voltage

angle and the phase angle response of the harmonic current emission of the device. The described modelling process brings an improvement over the fingerpint method [10].

In this chapter we prove that an accurate modelling of harmonic angles cannot be performed on the base of Gaussian distribution of linear data but rather needs to be tackled by approach of circular (directional) statistics. Naturally, circular statistics methods lay a foundation for explaining relationships between dependent and independent angular variables.

Owing its origins to Medicine and Astronomy and later finding applications in Biology, Geology and Meteorology, circular or directional statistic methods have been mostly untouched by power system engineers and researchers. In the latter, the basic electrical parameters - currents and voltages are represented fundamentally by magnitudes and angles, making the linear approximations in analysis of such data possible, but not sufficient for routine data processing.

Approximate linearity may serve its purpose in large variety of power system analysis cases, but specific fields - for instance analysis of harmonic distortions would require a different approach. This is merely due to the fact that harmonic-producing sources exhibit non-linear behavior and harmonic phase angles therefore can be analysed as two-dimensional orientations on a unit plane. Whilst partially based on the theoretical knowledge included in [16], this chapter emphasizes the applicability of the directional statistics methods to the power systems harmonic analysis.

5.2.1. FUNDAMENTAL PARAMETERS

The fundamental step in analyzing directional sets of data is identifying whether or not measured set contains certain modal (directional) group or, perhaps, several modes (multimodal data). One of the most important quantities is a mean direction of circular data given as:

$$cos\bar{\theta} = C/R, \quad sin\bar{\theta} = S/R \tag{5.1}$$

where

$$C = \sum_{i=1}^{n} cos\theta_i, \quad S = \sum_{i=1}^{n} sin\theta_i, \quad R^2 = C^2 + S^2 \tag{5.2}$$

and θ_i is individual angle measurement. Furthermore, the next descriptive quantity associated with the mean direction $\bar{\theta}$ is the mean resultant length $\bar{R}$ given by:

$$\bar{R} = R/n \tag{5.3}$$

where n is the number of samples and R is a sum of variables of representative data set defined on a cyclic interval $[0, 2\pi]$. Thus, the mean resultant length is the outcome of vectorial summation but not arithmetic. Its value lies in range (0,1) and $\bar{R} = 0$ can potentially but not necessarily imply uniform distribution of samples around the circle. On the other hand, values close to $\bar{R} = 1$ indicate rather large concentration of data points. In other words, $\bar{R}$ is an estimator measuring the concentration.

These two quantities form angular and amplitude components of the first trigonometric moment:

$$m_1{}' = \bar{C} + i\bar{S} = \bar{R}e^{i\bar{\theta}} \tag{5.4}$$

and trigonometric moment $m_1{}'$ is a basic population characteristic describing the underlying probability distribution function.

5.2.2. PROBABILITY DISTRIBUTION ON THE CIRCLE

From section 5.2.1 it follows that circular data cannot be described by Normal Gaussian distribution since all basic statistical parameters are presented in vectorial rather than scalar form. The most often used model is von Mises symmetric unimodal distribution for which dispersion equals to a concentration parameter k on contrary to the Normal distribution, where dispersion is represented by the variance σ^2. It is worth noting that increasing k value indicates rising concentration around reference direction and typically if $k \geqslant 2$ it is reasonable to fit measured data to von Mises distribution and apply corresponding statistical methods.

The probability density function is given as:

$$f(\theta) = [2\pi I_0(k)]^{-1} exp[kcos(\theta - \mu)] \\ 0 \leqslant \theta < 2\pi, \quad 0 \leqslant k < \infty \tag{5.5}$$

where k is a concentration parameter and μ is a mean direction and

$$I_0(k) = (2\pi)^{-1} \int_0^{2\pi} exp[kcos(\phi - \mu)]d\phi \tag{5.6}$$

is the Bessel function. Finally, the distribution function of von Mises distribution is represented by:

$$F(\theta) = [2\pi I_0(k)]^{-1} \int_0^{\theta} exp[kcos(\phi - \mu)]d\phi \tag{5.7}$$

If k approaches 0, the distribution converges to the uniform distribution whilst if $k = 1$, the distribution tends to the point distribution concentrated in the direction μ.

The evaluation of these equations requires working with Bessel functions and this can be conveniently executed by R software package allowing among others the analysis of circular data.

It is worth of noting that in some cases the von Mises distribution can be closely approximated by Wrapped Normal distribution which can be obtained by wrapping Normal distribution around the circle [16].

5.2.3. STATISTICAL TESTS

In order to decide whether or not the particular set of angular data can be fit to unimodal distribution a number of tests must be performed. Test of uniformness against a unimodal alternative or Rayleigh test is a suitable formal tool for that purpose. The Rayleigh test statistic is then given as:

$$\bar{R}_0 = \bar{R}cos(\bar{\theta} - \mu_0) \tag{5.8}$$

where $\bar{R}$ is a mean resultant length, θ is a mean direction and μ_0 is the mean direction of the alternative unimodal model. It is typical to reject the null hypothesis of uniformity if $\bar{R}_0$ is large and exceeds the significance probability of $\bar{R}_0$ defined as P_0 and calculated as:

$$P_0 = 1 - p_z + f_z[(3Z_0 - Z_0^3)/(16n) \\ + (15Z_0 + 305Z_0^3 - 125Z_0^5 + 9Z_0^7)/(4608n^2)] \tag{5.9}$$

5

where $Z_0 = (2n)^{\frac{1}{2}}\bar{R}_0$, n is a number of samples and $p_z = \Phi(Z_0)$ is table values which define percentiles of the Normal distribution.

Other tests exist to verify specific alternative assumptions, for instance Watson test aiming to check null hypothesis of randomness against von Mises distribution.

5.3. ANALYSIS OF THE MEASURED DATA

INJECTIONS of three distinct types of low-voltage power electronics equipment were modelled, namely 1 kW single-phase photovoltaic inverter, Li-Ion battery charger with rated input current of 16 A and a group of CFL lamps comprised of 36 pieces of different brands.

The measurements were performed according to [10] for every equipment type. Firstly, a harmonic source is connected to the undistorted voltage supply and the emission level at this condition is measured. Further, individual harmonics with magnitudes between 0.5% and 5% depending on the harmonic order are added one by one. Next, within each level of harmonic voltage magnitude a phase shift is being varied between 0 and 360 degrees with standard step of 30 degrees and the harmonic current response of equipment under test is recorded. Finally, all the obtained data are organized into convenient look-up tables.

In order to investigate the shape of distributions of measured values the harmonic currents were split into the magnitude and phase angle components. After that, harmonic phase angles were organized on a unit circle pane. Figure 5.1 presents measured harmonic current angles of PV inverter in response to voltage background angles varied as 0, 30, 60, 90, 120, 150, 180, 210, 240, 270, 300 and 330 degrees. The composition of these plots is typical for representing angular data by means of circular statistics. On the shown unit panes every black dot corresponds to the one specific value of an angle of emitted harmonic current. Whenever the phase of harmonic current falls within the same sector multiple times - the dots are plotted on a "stacked" manner. At the later stages this technique allows to assess the modes of distribution. The magnitude of voltages was kept at the same level. The recorded data are then analyzed with circular statistics methods.

5.3.1. EXPLORATORY ANALYSIS

At this stage, the purpose of the initial graphical analysis is to merely assess the fundamental harmonic behavior of equipment under test and to conclude if there are certain patterns in angle distribution. The black filled circles in Figure 5.1 designate directions of harmonic phase angles. The prevailing direction is clearly visible for 5th harmonic, where points falling under the same group are drawn in a stacked manner. Furthermore, the spread of angles is increased for 7th and 9th harmonic and becomes nearly evenly distributed for 13th harmonic component.

For visual evaluation of the presence of certain directional modes, another nonparametric statistical instrument is apllied. Figure 5.2 shows kernel density etimates of the measured data. In general, the influence of each data point is stretched over reasonably small arc containing this data point. Next, the final density estimate for prevailing direction is then represented as the sum of all the contributions of smoothed points. The

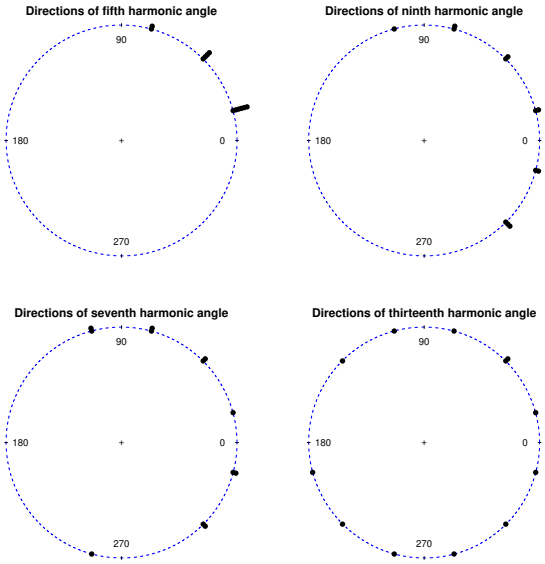

Figure 5.1: Fingerprint of measured current angles of PV inverter.

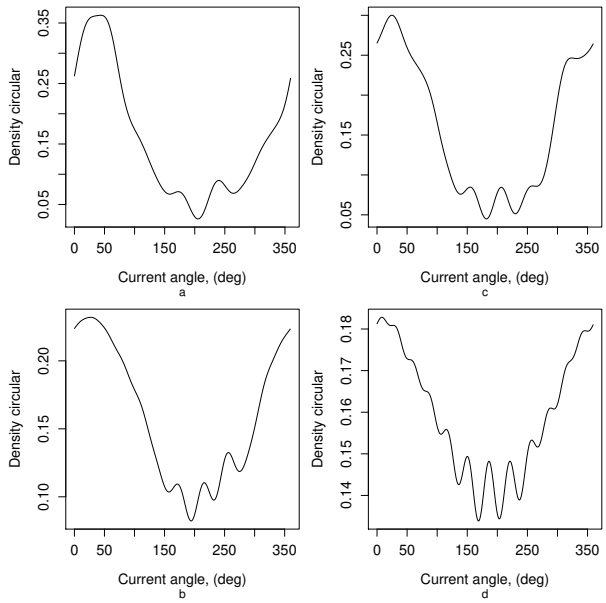

Figure 5.2: Kernel density estimate of PV inverter current angles. (**a**) Fifth harmonic; (**b**) seventh harmonic; (**c**) ninth harmonic; (**d**) thirteens harmonic.

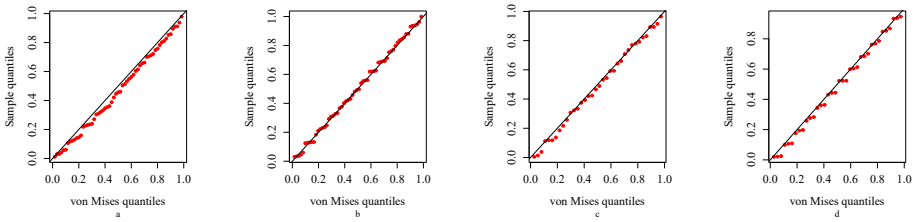

Figure 5.3: von Mises Q-Q plot for the PV inverter harmonic angles. (**a**) Fifth harmonic; (**b**) seventh harmonic; (**c**) ninth harmonic; (**d**) thirteens harmonic.

unimodal groups falling between 0 and 75 degrees are clearly observable in Figure 5.2a, Figure 5.2b and Figure 5.2c. Some irregularities in the form of additional bumps can be visible in Figure 5.2d corresponding to 13th harmonic order.

Based on this initial analysis it can be concluded there is an evidence of prevailing directions of harmonic phase angles as consequence of changing background voltage distortion angle.

Furthermore, once the presence of unimodal groups in measured data is established, a graphical assessment of goodness-of-fit for the von Mises model is performed. One way to check whether samples of data belong to a specified distribution is quanitle-quantile (Q-Q) plots. Along the y-axis the input data is plotted versus the x-axis which is a collection of theoretical values of expected distribution. In case when the resulting plot shows signs of linearity it can be concluded that the data sample comes from the sought distribution. Figure 5.3 demonstrates that studied circular distribution model is suitable for the representing measured set of data. There is little evidence of the departure from the model for 5th (Figure 5.3a) and 13th (Figure 5.3d) harmonic orders, however, Q-Q plots can be fluctuating and therefore formal statistical tests are required.

The exploratory phase of analysis was performed in a similar fashion for the other two equipment types and results are shown in Figures 5.4 through Figure 5.7. It is interesting to note the spread of harmonic current angles of the battery charger (Figure 5.4). From these directional plots it is observable that for 7th and 9th harmonic the angles are distributed visually evenly, and this is confirmed by Figure 5.5b and Figure 5.5d. The latter Kernel density estimate graphs demonstrate the presence of several modes of distribution. This in theory can point to the lesser goodness-of-fit, however, at this stage the data samples cannot be discarded based only on the visual analysis. It will be shown in the following section that formal mathematical tests identify the presence of one large mode. Moreover, the effect of even spread of the majority of current harmonic angles can possibly be referred to the notion of linearity studied in [1] and [4] and can be attributed to the underlying topology of power electronic equipment, to be more specific to the type of PFC.

On the other hand, a group of CFLs demonstrates highly nonlinear behavior with angles being concentrated strictly in certain quadrants (Figure 5.6). As it was mentioned before, a current angle response belonging to the same sector is being stacked on the response of previous test scenarios of changing voltage background angle with a step of 30 degrees. The fact is confirmed by kernel density plots (Figure 5.7) showing quite

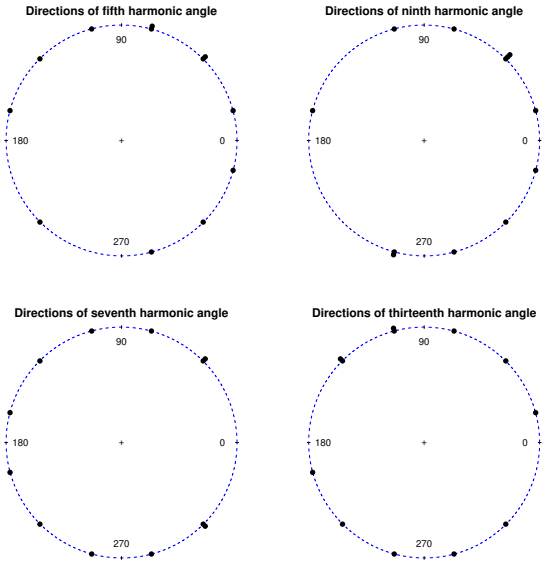

Figure 5.4: Fingerprint of measured current angles of battery charger.

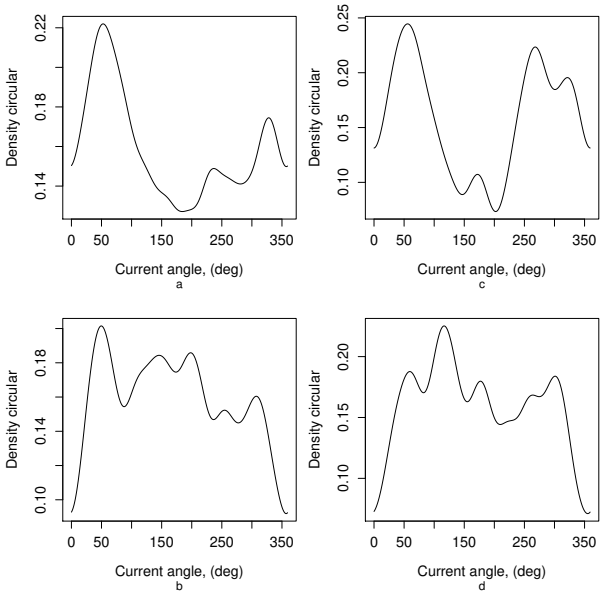

Figure 5.5: Kernel density estimate of battery charger current angles. (**a**) Fifth harmonic; (**b**) seventh harmonic; (**c**) ninth harmonic; (**d**) thirteens harmonic.

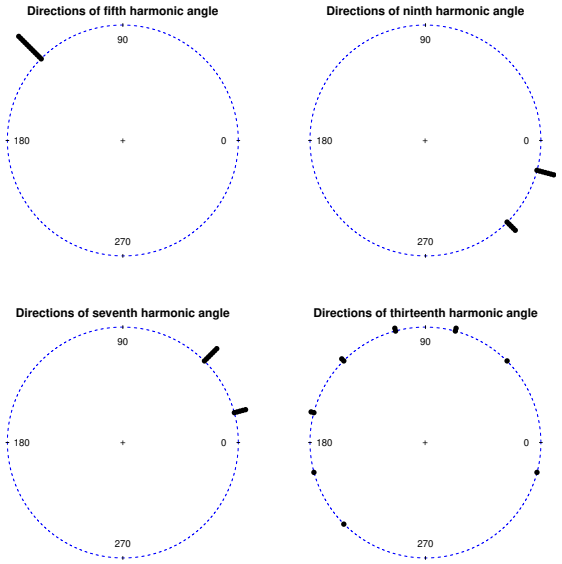

Figure 5.6: Fingerprint of measured current angles of CFLs.

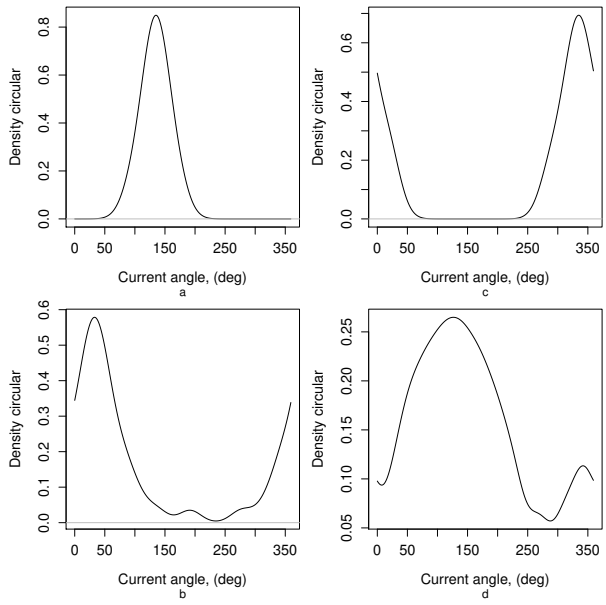

Figure 5.7: Kernel density estimate of CFLs current angles. (**a**) Fifth harmonic; (**b**) seventh harmonic; (**c**) ninth harmonic; (**d**) thirteens harmonic.

narrow modal groups for selective harmonics.

5.3.2. FORMAL TESTS

Having concluded graphical analysis of measured angular data it is reasonable to calculate all fundamental statistic values and perform tests of null hypothesis. In this section, the statistic quantities are calculated as it is explained in section 5.2 and Rayleigh tests are performed as per Section 5.2.3. The results for every studied device are summarized in Table 5.1.

The calculated statistical quantities are in a good agreement with theoretical information of section 5.2 stating that mean resultant vector length $\bar{R}$ close to 0 does not necessarily imply uniform distribution of phase angles. Looking at the rows related to battery charger in Table 5.1 it is visible that mean resultant lengths equal to 0.11 and 0.13 for 7th and 13th harmonic orders, respectively, correspond to large values of Rayleigh statistics. Moreover, the outcome of the Rayleigh test shows that significant probability values P_0 are exceeded by $\bar{R}_0$ by several orders of magnitudes for these harmonics. It can be concluded therefore that unimodal directional groups are indeed present in the measured set of data, however, initial graphical analysis can be insufficient for drawing this conclusion.

On the other hand, $\bar{R}$ = 0.11 of 13th harmonic PV current angles corresponds to $\bar{R}_0$ = 0.18 and is less than calculated significance probability P_0 = 0.29. This confirms the visual analysis presented in Figure 5.2d and can indicate ambiguity in determining prevailing phase angle directions.

Finally, the results presented for a group of CFL in Table 5.1 implicate high level of data concentration in relation to prevailing directions for every harmonic order.

Table 5.1: Calculated statistical quantities.

Equipment type	Harmonic order	$\bar{R}$	$\bar{\theta}$	$\bar{R}_0$	P_0
Battery charger	5	0.29	52.37	0.91	0.078
	7	0.11	173.09	3.02	0.3
	9	0.35	12.01	0.21	0.04
	13	0.13	134.55	2.35	0.26
PV inverter	5	0.94	35.1	0.61	0
	7	0.54	24.1	0.42	0.0036
	9	0.67	14.6	0.25	0.0002
	13	0.11	10.24	0.18	0.29
CFLs	5	0.99	134.16	2.34	0
	7	0.98	32.93	0.57	0
	9	0.98	-21	5.91	0
	13	0.50	123.02	2.15	0.0057

$\bar{R}$ - mean resultant length, $\bar{\theta}$ - mean direction (deg), $\bar{R}_0$ - Rayleigh statistic, P_0 - significance probability of $\bar{R}_0$.

5.4. CIRCULAR REGRESSION MODEL

THE analysis of measured data which was carried out in section 5.3 proves that current harmonic angles measured with fingerprint approach can be used as the input for circular modelling process. In fact, one of the advantages of treating data as a sample of von Mises distribution is the possibility to model a circular response variable with respect to the explanatory variable. In the case of harmonic modelling it means that within fixed background voltage magnitude level there will be a distinct response of equipment current angle to the change of applied voltage angle. In other words, a circular regression model can be derived which explains the systematic variability of harmonic current angles. This means that the response of estimated model for any input value of background voltage angle can be predicted.

A fundamental assumption in the modelling process is that all data points have been taken from von Mises distribution with specified prevailing mean direction. The general purpose of the model therefore is to estimate the mean direction with relation to the explanatory variables. In essence, the mean direction can be calculated as:

$$\mu_i = \mu + g(\beta' X_i) = \mu + g(\beta_1 X_1 + ...\beta_k X_k) \tag{5.10}$$

where X_i is the explanatory variable, $\beta = (\beta_1, ...\beta_k)$ is the vector of coefficients to be estimated and g is the link function, subject to selection in advance. This model explains the behavior of response variable when explanatory variables are in the form of linear covariates.

Given the case when both response and independent variables, u and v , are circular, the general regression model was modified by the authors of [17]. The following model was proposed:

$$E(e^{iv}|u) = \rho(u)e^{i\mu(u)} = g_1(u) + ig_2(u) \tag{5.11}$$

with $e^{iv} = cosv + isinv$ being the conditional expectation of estimated mean direction, $\mu(u)$ is the conditional mean direction of v with respect to u and $\rho(u)$ is the conditional concentration parameter for periodic functions $g_1(u)$ and $g_2(u)$. It is interesting to note that model proposed in [17] estimates not only mean direction but also the concentration parameter.

The predicted value of mean direction is derived as:

$$\begin{aligned} \mu(u) = \hat{v} &= \tan^{-1}\frac{g_2(u)}{g_1(u)} \\ &= \begin{cases} \tan^{-1}\frac{g_2(u)}{g_1(u)}, & if \quad g_1(u) > 0 \\ \pi + \tan^{-1}\frac{g_2(u)}{g_1(u)}, & if \quad g_1(u) \le 0 \\ undefined, & if \quad g_1(u) = g_2(u) = 0 \end{cases} \end{aligned} \tag{5.12}$$

The trigonometric polynominals are then utilized as the approximations of $g_1(u)$ and $g_2(u)$:

$$\begin{aligned} g_1(u) &\approx \sum_{k=0}^{m} (A_k \cos ku + B_k \sin ku) \\ g_2(u) &\approx \sum_{k=0}^{m} (C_k \cos ku + D_k \sin ku) \end{aligned} \tag{5.13}$$

where k is the trigonometric order and A_k, B_k, C_k, D_k are the parameters to be estimated.

Finally, the generalized least squares estimation algorithm is used for estimating parameters of (5.13). If $\varepsilon = (\varepsilon_1, \varepsilon_2)$ is the vector of random errors then the following is in order:

$$\begin{aligned} \cos v &= g_1(u) + \varepsilon_1 \\ \sin v &= g_2(u) + \varepsilon_2 \end{aligned} \tag{5.14}$$

As it can be deduced from the (5.14) the final circular regression model is represented by both cosine and sine terms. According to (5.12) the estimated mean direction is given as:

$$\hat{v} = \tan^{-1} \frac{\sin v}{\cos v} \tag{5.15}$$

This model is conveniently integrated in the "Circular" package of R software. The proposed algorithm is summarized in the flow chart of Figure 5.8.

5.4.1. MODEL OF PHOTOVOLTAIC INVERTER

Figure 5.9 shows the results of deriving circular regression model from the measured sets of data for selective harmonics produced by PV inverter. The presented scatter plots provide convenient way of visualizing the dependence of one variable on another, i.e. the response of harmonic current angle to the changes of background voltage phase angle. In Figure 5.9 the measured values (designated with colored bullet •) are plotted together with fitted data (designated with colored plus +).

The regression models are estimated separately for different levels of magnitudes of voltage background distortion. It can be seen that harmonic injection patterns are significantly different for every studied frequency. Additionally, at 5th harmonic the magnitude of the applied background voltage impacts to the great extent the pattern of harmonic current angle evolution.

On the other hand, nearly linear trend is observable for thirteens harmonic, with all points being quite close to each other regardless of the magnitude of voltage.

All in all, the fitted model demonstrates good agreement with measured data. Moreover, in certain cases of manifested linearity (thirteens harmonic) the estimated harmonic angles overlap the measured ones.

Figure 5.10 shows the residual analysis corresponding to the derived regression models, where fitted data are plotted against estimated residuals. Fifth harmonic plot (Figure 5.10a) suggests there are some outlying points corresponding to -40 and 40 degrees, but the majority of residuals is enclosed between -10 and 10 degrees. A similar behavior is observed for seventh (Figure 5.9b) and ninth (Figure 5.10c) harmonics. Figure 5.10d, on contrary, is characterized by the residuals mostly concentrated between -3 and 3 degrees indicating good performance of the regression model.

5.4.2. MODEL OF BATTERY CHARGER

Figure 5.11 and Figure 5.12 demonstrate the fitted data together with measured values and model residuals for the battery charger. It is observable that for every plotted har-

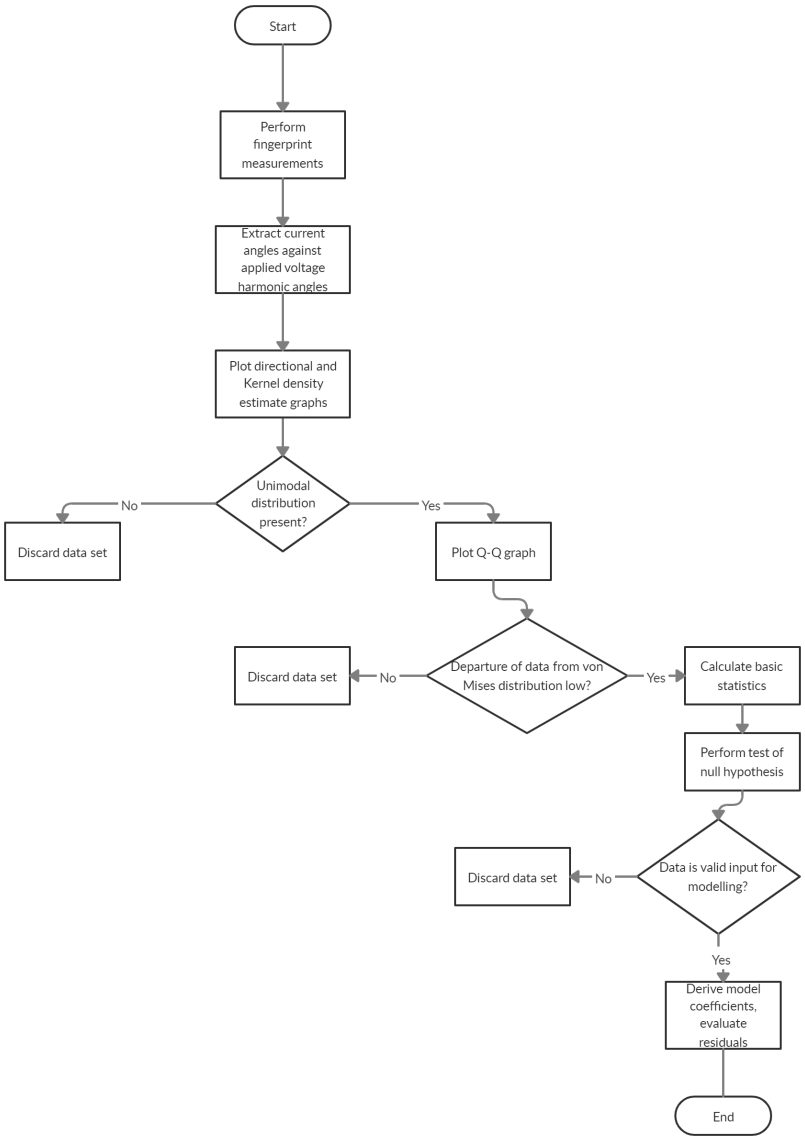

Figure 5.8: Modelling algorithm.

monic order the linear trends are explicit, with the exception of ninth harmonic. Furthermore, some outlier points are clearly present in the thirteens harmonic. Once again, the nearly linear behavior of harmonic current angle response is in agreement with the analysis presented in section 5.3.

The spread of residuals is mostly enclosed between -10 and 10 degrees with some outlier points visible in Figure 5.12d (13th harmonic).

5.4.3. MODEL OF CFL

The studied group of energy-efficient lights is characterized by strong nonlinear and asymmetric harmonic patterns. Figure 5.13 allows to conclude that for 5th and 7th harmonic order the current angle response alternates drastically under the influence of different harmonic voltage magnitudes. On the other hand, this is not the case for 9th and 13th harmonic components. For the former it can be observed that all data points are roughly concentrated within one prevailing direction regardless of the magnitude of applied voltage. Furthermore, in agreement with Fig. 5.7d the dispersion of the current angles for 13th harmonic order is larger than for other frequencies, nevertheless, different voltage magnitudes levels do not influence significantly the response of harmonic current phase angles.

An analysis of the residuals presented in Figure 5.14 shows that most of the points lie between -2.5 and 2.5 degrees suggesting that measured set of data is represented well by derived circular regression model. An exception to this is however, 13th harmonic with its residuals being enclosed between -10 and 10 degrees.

5.5. ADDITIONAL CONSIDERATIONS

ONE of the fundamental assumptions allowing to make progress in modelling method described in this chapter is that all measured values fit to the underlying von Mises distribution for circular data. While this distribution is a natural choice for many theoretical problems, it can be difficult to use in practise, in particular when concentration parameter k associated with measured data set is less or approaching the value of 2. However, since circular statistics includes vast varieties of methods and analysis capabilities, it can be reasonable to estimate confidence intervals associated with estimated prevailing direction of current harmonic angles and uncertainty of concentration parameter. For the specific case presented here, i.e. when the amount of samples in every data set is small, the so-called parametric bootstrap method is in order.

Furthermore, since proposed modelling method concerns derivation of algebraic equations with respect to the harmonic phase angles, a distinct procedure for handling harmonic current magnitudes must be applied. An influence of circular variable (voltage phase angle) on a linear variable (current magnitude) presents a separate class of a problem not falling under directional statistics methods. Based on the observations, this relationship for the most of cases demonstrates periodic trends. This allows to approximate current magnitude as a function of background voltage by simply applying interpolation or appropriate curve-fitting procedure. As an example, Figure 5.15 shows an evolution of fifth harmonic current magnitude with respect to the voltage angle as measured at the terminals of battery charger.

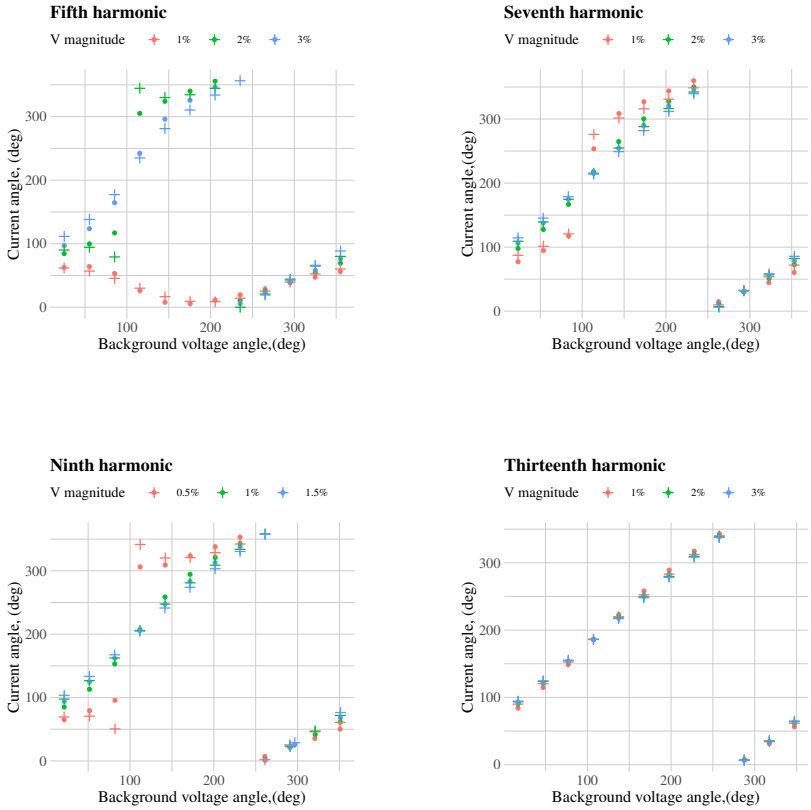

Figure 5.9: PV Inverter model. •Measured data +Fitted data

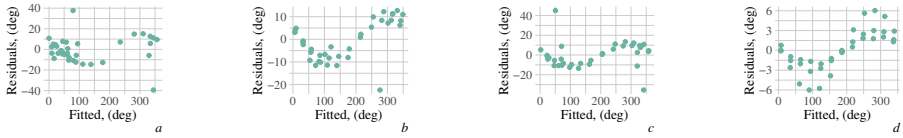

Figure 5.10: Model residuals of PV Inverter. (**a**)Fifth harmonic; (**b**)Seventh harmonic; (**c**)Ninth harmonic; (**d**)Thirteens harmonic.

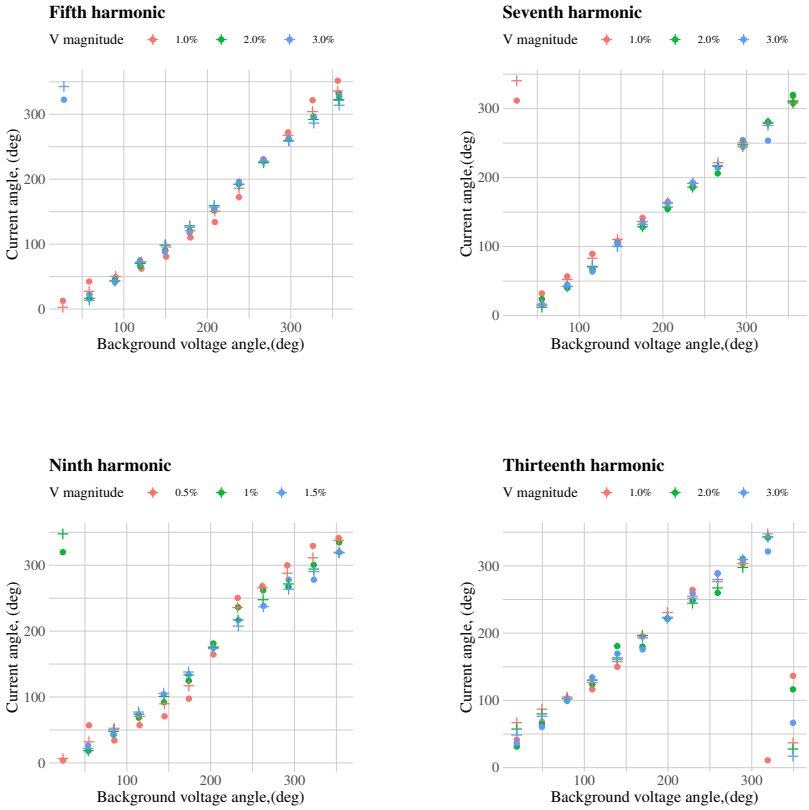

Figure 5.11: Battery charger model. •Measured data +Fitted data

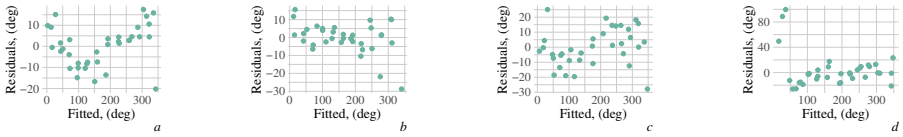

Figure 5.12: Model residuals of battery charger. (**a**)Fifth harmonic; (**b**)Seventh harmonic; (**c**)Ninth harmonic; (**d**)Thirteens harmonic.

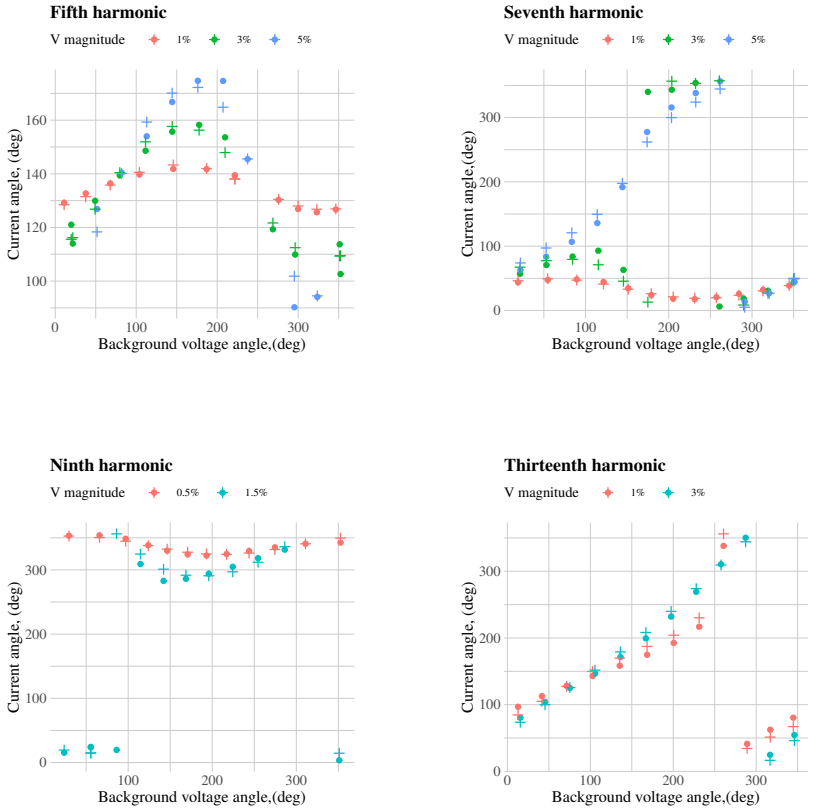

Figure 5.13: CFL model. •Measured data +Fitted data

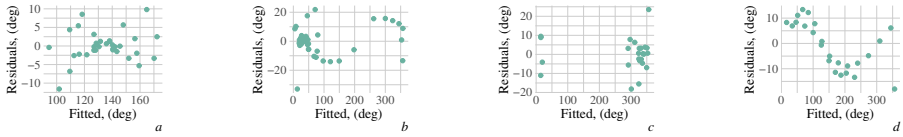

Figure 5.14: Model residuals of CFL. (**a**)Fifth harmonic; (**b**)Seventh harmonic; (**c**)Ninth harmonic; (**d**)Thirteens harmonic.

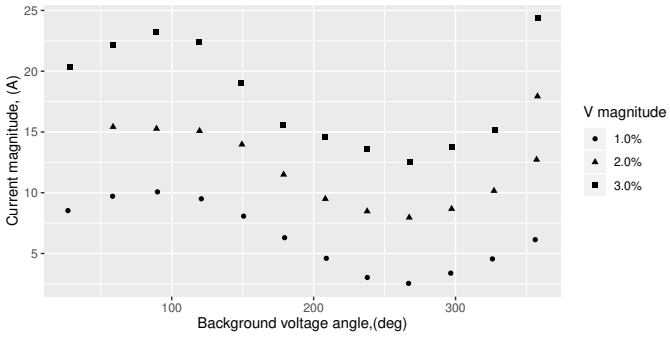

Figure 5.15: Battery charger fifth harmonic current magnitudes as a function of voltage phase angle.

5.6. CONCLUSION

SYSTEM studies which analyze large networks often require the use of a relatively large number of harmonic source models. Power-flow based calculation engines use iterations to reach a solution, which can be further complicated, and have their convergence jeopardized, in case of additional iterations of each source model due to e.g. frequency coupling [3]. For this reason an analytic relation between the supplied voltage and the injected harmonic current is a very useful simplification to use in studies on large networks.

The regression technique based on von Mises distribution provides algebraic relationship between explanatory variable - voltage phase angle and response variable - harmonic current angle. This relationship is valid within certain level of harmonic voltage magnitude to which regression technique is applied. The models derived from the described procedure are characterized by reduced level of complexity, yet providing stable output with regard to any input harmonic background voltage. It is, therefore, possible to reduce the models to an analytic dependency on the supplied voltage, which leads to the improvement of the iteration process in load-flow based solvers for harmonic analysis, as it avoids additional iterations in the simulations. This also allows to exclude possible convergence problems with the algorithm in case of large system studies with a significant number of sources present.

Generally, the accuracy of these models depends on how well theoretical von Mises distribution fits to the measured data. In most of the cases this is attributed to the underlying equipment topology which in turn affects harmonic behavior. The results in this chapter demonstrate that derived models are characterized by fair performance with residuals falling between -2.5 and 2.5 degrees in best case and between -10 and 10 degrees for the worst situation.

REFERENCES

[1] L. E. Gallego and J. Meyer, *Characterization of non-linear household loads for frequency domain modeling Caracterización de cargas residenciales no lineales para modelado en el dominio de la frecuencia,* **2015**, 65 (2015).

[2] A. S. Folting, J. M. A. Myrzik, T. Wiesner, and L. Jendernalik, *Practical implementation of the coupled norton approach for nonlinear harmonic models,* in *2014 Power Systems Computation Conference*, Vol. 1 (IEEE, 2014) pp. 1–7.

[3] D. Gallo, C. Landi, R. Langella, M. Luiso, A. Testa, and N. Watson, *On the Measurement of Power Electronic Devices' Frequency Coupling Admittance,* 2017 IEEE International Workshop on Applied Measurements for Power Systems (AMPS) , 1 (2017).

[4] J. E. Caicedo, A. A. Romero, H. C. Zini, R. Langella, J. Meyer, and N. R. Watson, *Impact of reference conditions on the frequency coupling matrix of a plug-in electric vehicle charger,* Proceedings of International Conference on Harmonics and Quality of Power, ICHQP , 1 (2018).

[5] R. Langella, A. Testa, J. E. Caicedo, A. A. Romero, H. C. Zini, J. Meyer, and N. R. Watson, *On the use of fourier descriptors for the assessment of frequency coupling matrices of power electronic devices,* Proceedings of International Conference on Harmonics and Quality of Power, ICHQP , 1 (2018).

[6] A. Collin, J. Acosta, B. Hayes, and S. Djokic, *Component-based aggregate load models for combined power flow and harmonic analysis,* , 171 (2011).

[7] A. J. Collin, G. Tsagarakis, A. E. Kiprakis, and S. Mclaughlin, *Simulating the Time-varying Harmonics of the Residential Load Sector,* 2014 16th International Conference on Harmonics and Quality of Power (ICHQP) , 768 (2014).

[8] X. Xiao, A. J. Collin, S. Z. Djokic, S. Yanchenko, F. Moller, J. Meyer, R. Langella, and A. Testa, *Analysis and Modelling of Power-Dependent Harmonic Characteristics of Modern PE Devices in LV Networks,* IEEE Transactions on Power Delivery **32**, 1014 (2017).

[9] A. J. Collin, R. Langella, and A. Testa, *Commercial Load Sector Models for Power Flow and Power Quality Analysis,* 2018 International Symposium on Power Electronics, Electrical Drives, Automation and Motion (SPEEDAM) , 183 (2018).

[10] J. Cobben, J.F.G., Kling, W.L., Myrzik, *The making and purpose of harmonic fingerprints,* in *CIRED 2007*, pp. 21–24.

[11] X. Xu, A. Collin, S. Djokic, S. Muller, J. Meyer, J. Myrzik, R. Langella, and A. Testa, *Aggregate harmonic fingerprint models of PV inverters. part 1: Operation at different powers,* in *2018 18th International Conference on Harmonics and Quality of Power (ICHQP)* (IEEE) pp. 1–6.

[12] M. T. Au and J. V. Milanović, *Development of stochastic aggregate harmonic load model based on field measurements,* IEEE Transactions on Power Delivery **22**, 323 (2007).

[13] S. R. Silva, E. G. Carrano, W. Uturbey, M. L. y. Gonzalez, and M. M. Silva, *Evaluating harmonic voltage distortion in load-variating unbalanced networks using Monte Carlo simulations,* IET Generation, Transmission & Distribution **9**, 855 (2015).

[14] A. Nassif, J. Yong, and W. Xu, *Measurement-based approach for constructing harmonic models of electronic home appliances,* IET Generation, Transmission & Distribution **4**, 363 (2010).

[15] S. Gao, X. Li, X. Ma, H. Hu, Z. He, and J. Yang, *Measurement-Based Compartmental Modeling of Harmonic Sources in Traction Power-Supply System,* IEEE Transactions on Power Delivery **32**, 900 (2017).

[16] N. Fisher, *Statistical analysis of circular data* (Cambridge University Press, Cambridge, England; New York, NY, USA, 1993) p. 277.

[17] S. Jammalamadaka and Y. Sarma, *Circular regression,* Statistical Science and Data Analysis , 109 (1993).

6

CASE STUDY: DISTRIBUTION SYSTEM MODELLING

The procedures for performing harmonic studies for medium-voltage distribution feeders have become relatively mature topic since early 1980s. The efforts of various electric power engineers and researchers were mainly focused on handling large harmonic nonlinear loads connected scarcely at several buses of medium-voltage feeders. In order to assess impact of these loads on voltage quality of distribution system, specific modeling and simulation strategies were proposed since then. These methodologies could deliver a reasonable estimation accuracy given the requirements of least computational efforts and reduced complexity. To uphold these requirements the certain analysis assumptions have been made which became de facto standards for establishing guidelines for harmonic analysis. These modelling practices were proven to be adequately effective for medium-voltage levels and laid the foundation for the harmonic modelling of low-voltage distribution systems. The changes that modern low-voltage networks had been facing recently, indicated that new modelling approaches overcoming previously made assumptions are required.

6.1. HARMONIC SIMULATIONS IN LOW-VOLTAGE SYSTEMS: AN OVERVIEW

As a general rule, harmonic simulations are typically executed for perfectly balanced system. More often than not for such a system the frequency-dependant impedance of various power system components is not modelled completely. In some cases for these components the detailed calculations of skin and proximity effects are not performed and resistance and reactance values are modeled based on the theoretical equations [1, 2]. The simplifications of the modelling routine have led to the commonly accepted practice of neglecting phase angle diversity effects [1–5]. This is mainly associated with developed load models which only in handful of cases are representing the complete harmonic behavior of the certain device as well as accounting on the harmonic

interaction between grid harmonic voltages and harmonic currents [6]. Currently, standard IEC 61000-3-14 suggests usage of summation coefficients which were introduced as a way to deal both with load fluctuations and the phase angle diversity. The suggested methodology includes set of approximate exponential coefficients for different harmonic orders. For medium-voltage systems having these assumptions in place for modelling and simulations in most cases does not result into significant deviation from true values [7].

However, harmonics in modern low-voltage distribution networks are characterized by high degree of variability and demonstrate sufficient diversity leading to certain level of cancellation effects [8]. What changed over the last several decades is clearly a massive increase in usage of residential electronic devices, recent and ongoing boom of electric vehicles and large-scale installing of distributed solar power. It is why the harmonic interaction, phase-angle diversity and uncertainty of system harmonic impedance shall be considered as the factors influencing performance and accuracy of harmonic load flow.

6.2. MODELLING AND SIMULATION APPROACH

THE harmonic models derived in chapter 5 bear remarkable quality — they describe a specific harmonic behavior of the certain device when exposed to different voltage harmonic magnitudes and angles. It is, therefore, feasible to create a quasi-static harmonic background voltage profile and use it as an input to the specific simulation scenarios. The load models' harmonic current injections in that case will always respond to the changes of supplied voltage. Commercial simulation package PowerFactory developed by DIgSILENT offers superior level of control over the simulation scenarios when paired to scripts written in Python. The simulation conditions including time-varying harmonic profiles give an opportunity to run harmonic calculations in a quasi-static way allowing to track evolution of frequency components in time. An example of the supplied 100 second-long background voltage distortion is demonstrated in Figure 6.1.

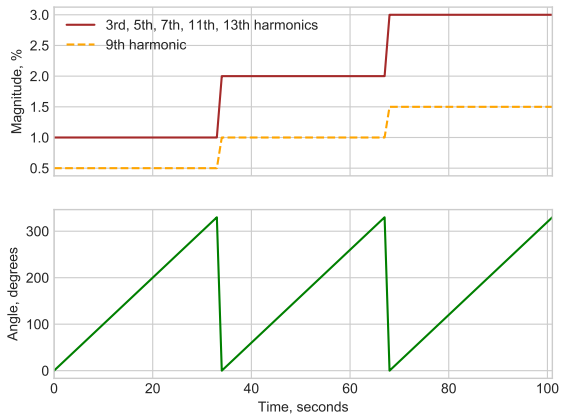

Figure 6.1: Background voltage distortion as continuous input for the simulation.

By utilizing technical data of practical low-voltage distribution feeder and taking into account its real configuration the following model depicted in Figure 6.2 was built in PowerFactory environment. The total length of the feeder is 500 m and its type is 4x150AL. The system is supplied by 400 kVA MV/LV transformer with u_k equal to 4%. Since in PowerFactory initial background distortion has to be entered at the medium-voltage level, the primary winding of transformer was changed to YN in order to be able to evaluate propagation of zero-sequence harmonic components. Furthermore, three separate connection points designated as H1, H2 and H3 were modelled as per initial layout at different distances. These connections are realized with EXVB 4x25 copper 3-phase cables approximately 10 m length each. The circular regression models of a photovoltaic inverter operating at constant power of 1 kW and single-phase battery charger were employed to simulate harmonic current source injections as described in chapter 5.

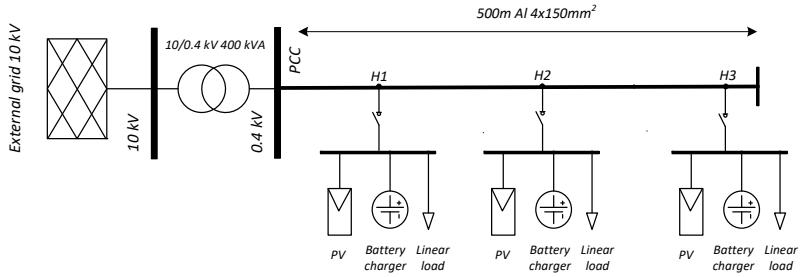

Figure 6.2: Network model.

To evaluate the performance of these loads in complete low-voltage distribution system we first look into their separate impact on the voltage quality. On figure 6.3 it is shown how each type of the studied device influences 7th harmonic voltage. The loads are connected towards the end of the feeder (point H3). The continuous simulation scenario of 100 seconds duration is based on the harmonic profile of Figure 6.1. For the PV inverter it is to mention that its impact is only observable at the end of the feeder with periodic fluctuations following the change of background harmonic voltage angle. The impact is more pronounced with the rising value of the magnitude of supplied 7th harmonic. On contrary, a sensitivity of current injections of a battery charger to the changes of harmonic phase angle at the terminals is significantly higher. The highest final values of harmonic voltage at the end of the feeder count about 4% with initial magnitude of 3%. The constantly sweeping phase angle can also lead to the cancellation between background voltage and harmonic distortion produced by the battery charger. For these periods of simulation time this resulted in the fact that harmonic voltage reduced to 2% at the end of the feeder while supplying 3%. Moreover, the moderate impact is also to observe at the location close to the PCC.

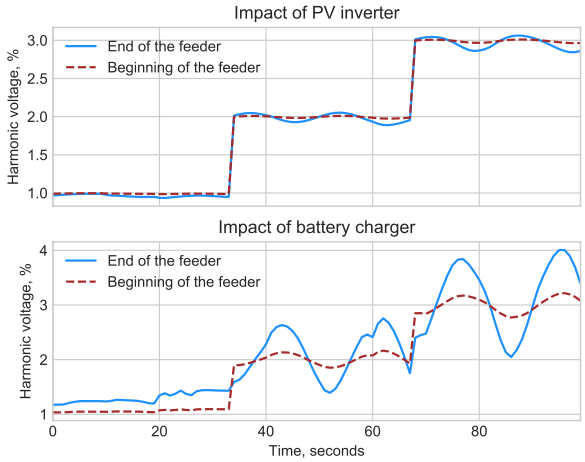

Figure 6.3: 7th harmonic voltages with respect to supplied background distortion.

6.2.1. BASE SIMULATION SCENARIO

To evaluate the simultaneous impact of distributed harmonic loads connected along the feeder, the simulation scenario is established with the configuration reflected in Table 6.1.

From Figure 6.4 we deduce that over the course of the simulation time both deterioration and improvement of the voltage quality towards the end of the feeder can take place. In essence, this is governed by the interaction of devices with the background distortion and in the first place dependent on voltage phase angle. The overall phenomena is, however, more complex due to the diversity of injected currents leading to cancellation or addition of the frequency components. To comprise more representative picture with regards this simulation case, we further calculate THD values. Figure 6.5 shows that worst case takes place at the end of the feeder with THD level close to 12%. At the same time 9% of total harmonic distortion is present at the beginning of the feeder. On the other hand, THD at the end of the feeder counts as low as 2.2% whilst at PCC we record 4.7% close to the end of simulation time.

PowerFactory executes harmonic power flow calculations taking into account standard theoretical values of frequency-dependent inductance of various power system com-

Table 6.1: Base simulation scenario.

Connection	Distance, m	PV, # units	Charger, # units	Linear load, kVA
H1	18	2	1	10
H2	200	3	2	0
H3	477	4	1	0

Linear load is 3-phase constant current with PF 0.9 (inductive).

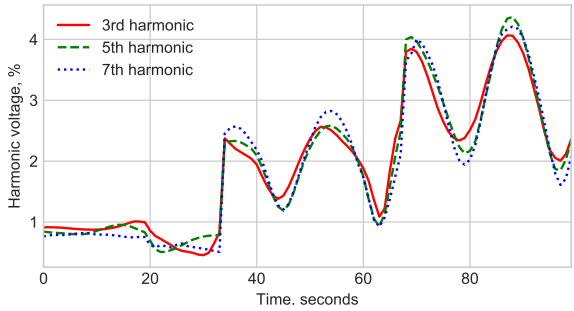

Figure 6.4: Harmonic voltages at the end of the feeder.

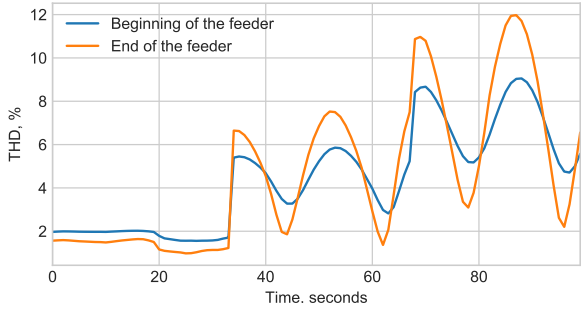

Figure 6.5: Total harmonic distortion.

ponents. As impedance of these components plays crucial role in impacting the voltage quality, their inaccurate estimates can compromise the outcome of power quality assessment. Therefore, it is important to adjust simulation conditions for accounting on this uncertainty.

6.2.2. IMPACT OF A FREQUENCY-DEPENDENT IMPEDANCE ON VOLTAGE QUALITY

The frequency-dependence of underground cables and power transformers impacts the levels of harmonic voltage distortion. When not considered in calculations and simulations it can cause a substantial deviation between measured and expected values, especially if there is a large chance of the resonance condition in studied network.

One of the methods to consider harmonic impedance of network components in simulations is to apply approximation functions, which are conveniently integrated into the PowerFactory environment. These functions together with coefficients for different types of components have been derived by authors of [9] and proven to be effective at frequencies below 5 kHz.

The following polynominal equations were proposed in [9]:

$$L(f) = (1-a) + a(\frac{f}{f_{nom}})^b \tag{6.1}$$

$$R(f) = 1 + a((\frac{f}{f_{nom}}) - 1)^b \tag{6.2}$$

Where (6.1) and (6.2) represent frequency-dependent inductance and resistance, respectively, and a and b are coefficients derived from measurements.

By introducing variations into the coefficients it is possible to simulate different scenarios with respect to frequency-dependent impedance. Table 6.2 comprises coefficients a and b used in harmonic load flow calculations. Whilst parameters of distribution transformer remained fixed, the frequency coefficients of main feeder were changed as per Table 6.2 for every subsequent case.

Table 6.2: Coefficients of approximation functions.

		$R(f)$		$L(f)$	
		a	b	a	b
Set 1	Transformer	0.2	1.5	1	-0.03
	Cable	0.1	0.9	1	-0.25
Set 2	Transformer	0.2	1.5	1	-0.03
	Cable	0.2	0.9	1	-0.35
Set 3	Transformer	0.2	1.5	1	-0.03
	Cable	0.3	0.9	1	-0.45
Set 4	Transformer	0.2	1.5	1	-0.03
	Cable	0.4	0.9	1	-0.55

The results of performed simulations in comparison with base case are presented in Figure 6.6 with respect to the end of the feeder.

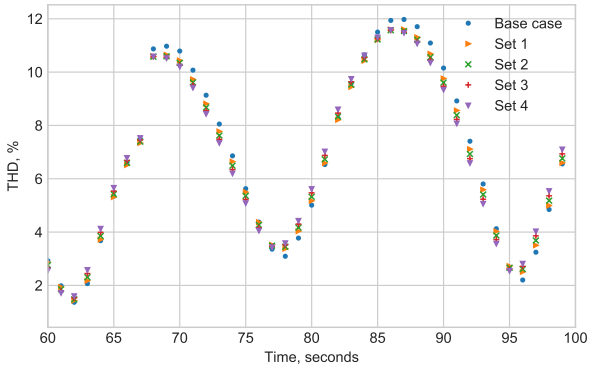

Figure 6.6: Impact of frequency-dependence of network components on THD_v.

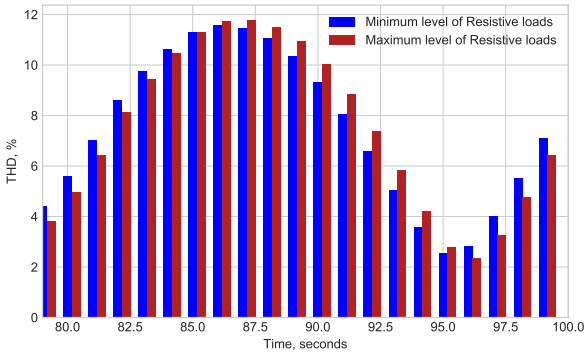

Figure 6.7: THD_v levels as a function of linear loads — end of the feeder.

By evaluating THD levels it is possible to conclude that even small changes in frequency coefficients can introduce a deviation in estimation of voltage harmonic distortion. At certain moments of time this difference counted 1%.

In addition to assigning frequency characteristics to network components and having taken into consideration skin and proximity effects, the next step is to evaluate an impact of linear loads on voltage quality. In harmonic studies, linear loads with high fraction of resistive loads are known for providing damping to the system.

Fig. 6.7 shows comparison of THD levels with low share of resistive loads (as per Table 6.1) and when additional 12 kVA and 14 kVA loads are connected to locations H2 and H3, respectively. Thus, the maximum level of resistive loads denoted in Fig. 6.7 corresponds to a total of 36 kVA of apparent power.

The outcome of the simulation shows that reduction of system harmonic impedance does not necessarily lead to the reduced levels of voltage distortion. Quite contrary, the THD exhibits increase at 85 seconds through 95 seconds.

6.2.3. UNIFORM VARIATION OF BACKGROUND VOLTAGES

In this simulation scenario voltage background magnitudes and angles are distributed randomly (uniformly) over 600 seconds period of time. This case allows to evaluate the general performance of the simulation model and voltage-dependent harmonic loads. Although, for practical studies a harmonic voltage background source is usually represented as a stochastic model with Gaussian distribution characterised by a prevailing angle [10, 11], in this section we input background voltages in accordance with statistical rules of random variation. This was deemed to be appropriate for the sake of methodology demonstration and for deducing certain statistical parameters.

Figure 6.8 shows histogram of THD levels at the end of the feeder. The simulation time is 10 minutes. In order to assess 95% probability values a cumulative distribution function has been plotted and is shown in Figure 6.9. For this random distribution THD level of less than 7.85% is recorded for the 95% values whilst maximum THD falls close to 9%.

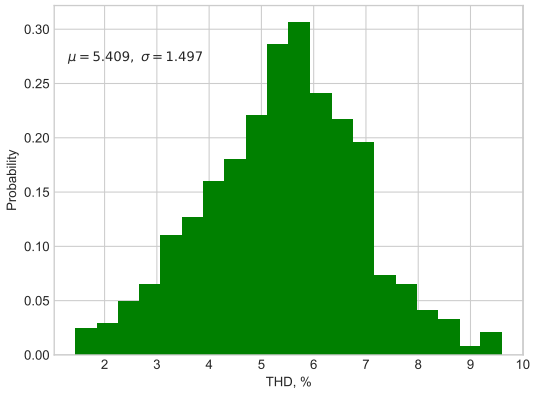

Figure 6.8: Distribution of harmonic voltages at the end of the feeder during 10 minutes.

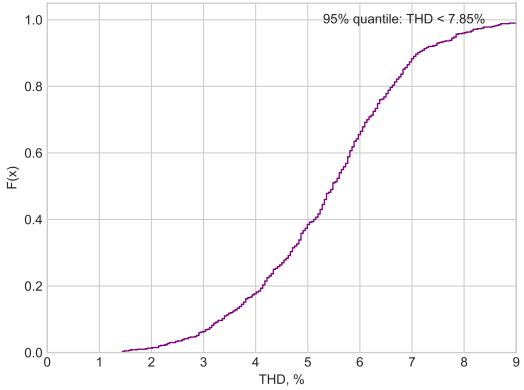

Figure 6.9: Cumulative distribution function.

6.2.4. COMPARISON WITH IEC-BASED SIMULATION SCENARIO

To compare the performance of the investigated phase-corrected modelling and simulation methodology with standard simulation option offered by PowerFactory functionality (IEC) we first choose 95% non-exceeding values for every harmonic order out of complete harmonic spectrum of the battery charger model. Based on these magnitude-angles pairs, respective background voltages causing the device to inject these harmonic currents are identified. In turn, these background harmonic voltages are also used to model the associated injections of PV inverter. After filling in all the required fields for voltage and current magnitudes the static harmonic load flow is run with a standard set of summation exponents as per IEC 61000-3-6.

Figure 6.10 and Figure 6.11 demonstrate results of the simulations for the PCC and end of the feeder, respectively.

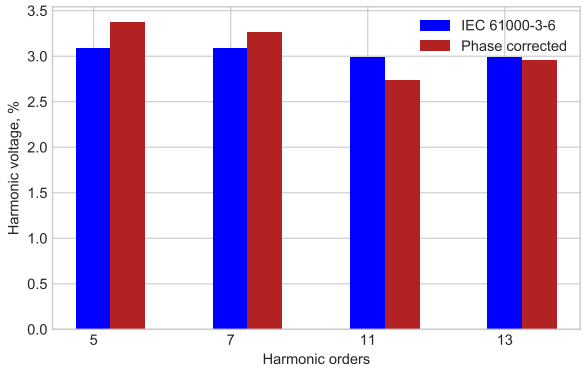

Figure 6.10: Harmonic voltages at the PCC.

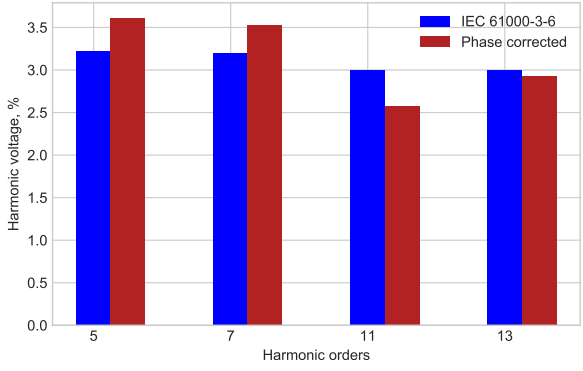

Figure 6.11: Harmonic voltages at the end of the feeder.

As it can be seen, at both locations the IEC-based simulations give results which are different from the phase-corrected scenario for all presented harmonic orders. Additionally, we observe that differences between two approaches are more pronounced towards the end of the simulated feeder.

6.3. CONCLUSION

IN order to complement harmonic analysis of the distribution systems the modelling approach resulting in realistic simulation scenarios and conditions shall be used. The transfer of harmonics can be estimated accurately when considering phase angle diversity of harmonic currents injected at various locations of a power network. These injections are of fluctuating nature, but nevertheless are predictable if simulation is equipped with harmonic load models derived as a function of harmonic voltage supplied at the terminals of these loads. Furthermore, as final indices describing voltage quality are dependent on the configuration of a network or in other words on impedance of power system components - simulations shall be executed in a way which allows to account for the associated uncertainty. In principle, this can be done by assigning accurate frequency characteristics to both inductance and resistance of network components or by estimating confidence intervals of the calculated harmonic voltages.

REFERENCES

[1] T. Hiyama, M. Hammam, and T. Ortmeyer, *Distribution system modeling with distributed harmonic sources,* IEEE Transactions on Power Delivery **4**, 1297 (1989).

[2] A. Bhowmik, A. Maitra, S. M. Halpin, and J. E. Schatz, *Determination of allowable penetration levels of distributed generation resources based on harmonic limit considerations,* IEEE Transactions on Power Delivery **18**, 619 (2003).

[3] Task Force on Harmonics Modeling and Simulation, *Modeling and simulation of the propagation of harmonics in electric power networks. I. Concepts, models, and simulation techniques,* IEEE Transactions on Power Delivery **11**, 452 (1996).

[4] M. McGranaghan, R. Dugan, J. King, and W. Jewell, *Distribution Feeder Harmonic Study Methodology,* IEEE Transactions on Power Apparatus and Systems **PAS-103**, 3663 (1984).

[5] A. Emanuel, J. Janczak, D. Pileggi, E. Gulachenski, C. Root, M. Breen, and T. Gentile, *Voltage distortion in distribution feeders with nonlinear loads,* IEEE Transactions on Power Delivery **9**, 79 (1994).

[6] S. Bhattacharyya, S. Cobben, P. Ribeiro, and W. Kling, *Harmonic emission limits and responsibilities at a point of connection,* IET Generation, Transmission & Distribution **6**, 256 (2012).

[7] S. Abdelrahman and J. V. Milanovic, *Practical Approaches to Assessment of Harmonics Along Radial Distribution Feeders,* IEEE Transactions on Power Delivery **34**, 1 (2019).

[8] V. Cuk, J. F. G. Cobben, W. L. Kling, and P. F. Ribeiro, *Analysis of harmonic current summation based on field measurements,* IET Generation, Transmission & Distribution **7**, 1391 (2013).

[9] G. Funk and H. Thomas, *Frequenzabhängigkeit der Betriebsmittel von Drehstromnetzen,* ETZ-Archiv **9**, 349 (1987).

[10] B. Peterson, J. Rens, and J. Desmet, *Harmonic emission assessment on a distribution network: The opportunity for the prevailing angle in harmonic phasors,* CIRED - Open Access Proceedings Journal **2017**, 668 (2017).

[11] B. Peterson, A. M. Blanco, J. Rens, J. Meyer, G. Botha, and J. Desmet, *Impact of Aggregation Interval on Harmonic Phase Angle Measurements,* 9th IEEE International Workshop on Applied Measurements for Power Systems, AMPS 2018 - Proceedings , 1 (2018).

7

WIDE-AREA HARMONIC MEASUREMENTS

This chapter is devoted to a practical analysis of voltage and current harmonics in the distribution grid. The phenomenon, widely known as harmonic distortion propagation, is studied based on the ample research of data acquired by time-synchronized distributed measurement system. Many factors are responsible for the propagation and fluctuating nature of the frequency components. In this case the following factors are studied and described: the impact of a background voltage distortion on the emission of harmonic-producing sources; the dynamic interaction between loads across the network and as a consequence harmonic cancellations caused by the diversity of their harmonic phase angles; the impact of the frequency-dependent network impedance. When these factors can be included in analyzing current and voltage distortion levels, the harmonic analysis yields rational results regarding quantification of transfer of waveform distortions and provides reasonable foundation for analytically-derived conclusions about origin of harmonic distortion and responsibilities of grid operators and or connected customers.

7.1. EXISTING STUDIES AND STATE-OF-THE-ART

THE sub-microsecond time synchronization accuracy is essential for resolving values of high-frequency components, as it was pointed out earlier in this book. Considering this requirement, the authors of [1] investigated the feasibility of assigning harmonic responsibilities based on data provided by distributed measurement system installed in a small test bench power network. In [2] a methodology for calculating synchronized harmonic phasors was proposed. This methodology aimed to accurately measure harmonic phase angles while reallocating samples between two subsequent pulse-per-second (PPS) edges. This allowed to take considerations with regards deviations in fundamental frequency.

Some studies investigated methodologies on determining individual harmonic cur-

rent contributions. In [3] the authors reported results of an experiment involving synchronized measurements at large industrial plant facilities. Furthermore, in [4] by utilizing GPS synchronized PQ recorders installed as part of a real HV network, the authors investigated the phenomena of dynamic interaction of harmonic sources with special attention given to the grid code compliance.

Large-scale harmonic measurements with provision of time-synchronized instruments were reported in [5]. The experiment was performed in a distribution system characterized by high penetration of distributed generation (DG). Values of harmonic amplitudes and intersite phase angles have been recorded and interpretation of results has been provided in comparison with the outcome of computer modeling. It is worth of noting that PQ measurement techniques based on synchronized sampling are currently being developed not only for distortion-related issues but also for other PQ events, for instance dips, swells and interruptions. An example of such a study was presented in [6] with focus on offshore wind farms.

As current state-of-the-art shows new measurement methods are vital for resolving challenges which are brought by the operation of modern power systems. These methods, depending on the PQ phenomena in question have to be linked to specific data processing algorithms, as requirements for these can vary substantially with respect to the final goal.

Still, the challenge in implementing such measurement systems for distortion evaluation lies to a large extent in the lack of commercially available instrumentation and the cost associated with customized solutions. On the other hand, as it was discussed above, stricter requirements on synchronization accuracy and specific signal processing algorithms (particularly for calculating harmonic phase angles) would be realized on these devices had these guidelines been reflected in the responsible standards, which is not the case at the current moment.

7.2. MEASUREMENT CAMPAIGN

To demonstrate the potential of a time-synchronized distributed measurement system and to investigate further in test scenarios the power network response to time-varying harmonic current injections we have established a wide-scale experiment in a MV/LV distribution grid.

7.2.1. DESCRIPTION OF THE TEST SETUP

Power Networks Demonstration Centre (PNDC) located in Cumbernauld, Scotland is a multi-functional power engineering facility. Among its purposes is a realistic technology testing and execution of the research projects aimed to facilitate development of smart grid sector. PNDC is in possession of a large power network, with substantial part of it having unprecedented levels of flexibility and control over the real time operation.

For the purpose of harmonic propagation study a part of the test network was configured. The diagram of this power network is shown in Figure 7.1. All in all three MV/LV distribution substations are connected to the main MV busbar (primary switchboard) via different impedance sections representing underground MV cables. There is a possibility to switch between sections A and B when energizing Substation G. Substation D on

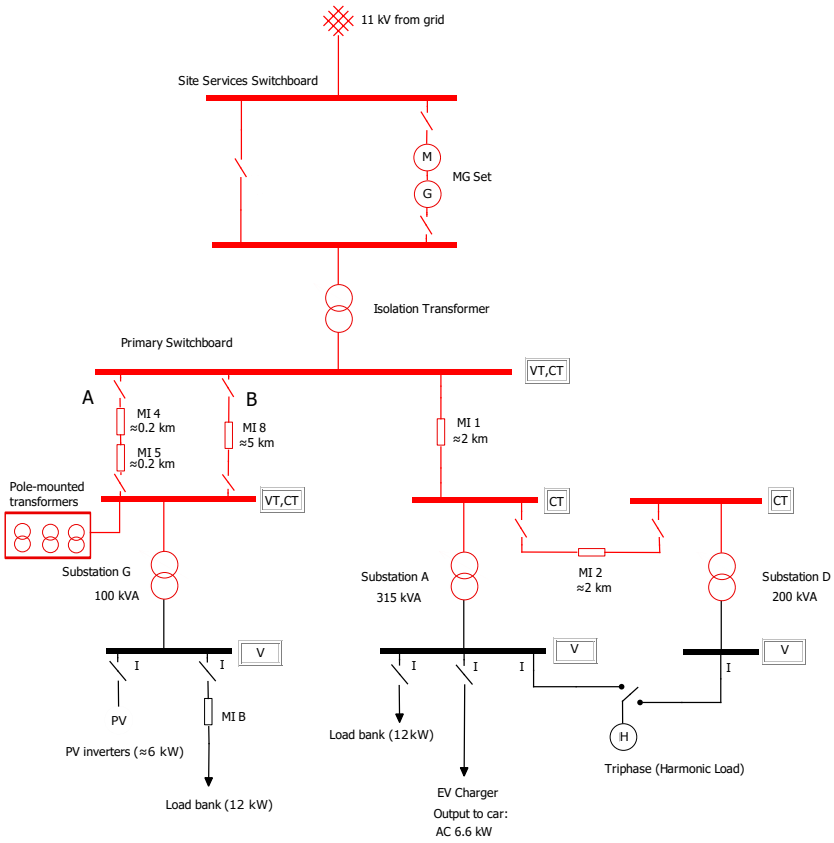

Figure 7.1: One-line diagram of test network.

the other hand can be connected on demand by means of two circuit breakers at both ends of impedance MI 2.

The setup offers a choice between two distinct power sources: the network can be energized by means of 11 kV public grid directly connected to Site Services Switchboard or alternatively via a motor-generator (MG) group providing stable 50 Hz output containing only fundamental frequency component. By engaging this power source it is possible to provide a low-distorted voltage at Primary Switchboard. At this fashion, we could make sure that fluctuating MV background voltage harmonics do not enter the setup after MG-set and minimum deviations of fundamental frequency could be secured.

Though, as it was explained above, while background voltage harmonics are not to enter the test network from the upstream MV grid when MG-set is employed, another source of voltage distortion was present in this network. The distortion originated from the series of pole-mounted MV/LV transformers connected to the MV busbar of Substation G. These transformers produced magnetizing current while being energized via

impedance section A. Alternatively, when bypassing connection via impedance section B, the primary windings of the pole-mounted transformers become disconnected from the rest of the network. The impact of this harmonic distortion will be mentioned later in corresponding test cases.

Several specific loads were configured and used for this study:

1. 3-phase 10 kVA solar inverter SMA Sunny Tripower;
2. EV charger with Nissan Leaf car capable of operating at 1-phase AC 6 kW;
3. Programmable converter Triphase in current source mode with programmed industrial harmonic profile (30 A fundamental current);
4. Banks of linear loads operating at unity power factor.

The control of the most of the devices can be performed through SCADA-software, however, in some cases manual switching actions and subsequent check procedures were required.

7.2.2. MEASUREMENT SYSTEM

The acquisition system is built on Beckhoff voltage and current sampling cards and is configured to 5 kHz sampling frequency. Voltage acquisition cards feature an oversampling principle with 16 bit resolution and measurement error not higher than 0.5 % relative to full scale value specified for frequencies up to 5 kHz. Current analogue acquisition cards are characterized by differential input and 16 bit resolution with measurement error less than 0.3 % relative to full scale. This accuracy is likewise applicable for the 5 kHz range. The monitoring and acquisition of the data is done through TwinCAT software.

On the MV side there are two voltage measurement points wired to VTs of Substation G and Primary Switchboard (Isolation Transformer). MV currents are measured through every substation as well as through Isolation Transformer. The accuracy class of these CTs is 0.2S providing superior performance at fundamental frequency. Since MV current transducers are typically not characterized for harmonic frequencies a higher phase shift can be expected at the output. In this study we do not use harmonic phase angles of MV side currents. At the LV side three voltage channels for every busbar are connected directly to the three phases at 250 V. Individual currents of every load are measured by means of Fluke i1000s AC Current Probes providing four-channel current input to sampling cards. The range selector of these current clamps was switched to 10 mV/A sensitivity with minimum measured current of 100 mA and maximum of 100 A. The basic accuracy at this range is 2 % of reading for the frequencies up to 5 kHz with a phase shift of no more than 10 degrees. Within the reported frequency range the linearity of measurements is ensured. On site all the utilized measurement equipment had valid calibration certificates.

As it can be seen this measurement system is characterized by modular architecture and capable of recording synchronously voltage and current waveforms. The distributed clock principle with local clock on slave controllers and a master clock ensure the synchronization of all components of the system via unique EtherCAT technology. Additionally, this system is synchronized to the higher-level absolute time making use of external

reference based on IEEE1588 PTP. This technique allows all the distributed clocks to be adjusted to a constant offset. By combining these two distinct synchronization routines it was possible to achieve the distributed clock precision of better than 1 μs.

7.2.3. TEST CASES

The harmonic propagation study includes two distinct packages. In Package A, an MG set is used to energize the network with ideal sinusoidal voltage supply. Every harmonic load is connected separately at its designated position. The individual current waveforms and synchronized voltage waveforms are measured at various points of the network. This test concludes with putting all the loads into the operation simultaneously and recording all the electrical parameters synchronously.

In test package B, the network is energized by the public grid and at the first stages the same scenarios as in package A are tested. Furthermore, an equal share of resistive load banks is connected to the substations G and A. At the next stage, the topology of the network was changed at the MV level by bypassing the impedance section A through section B. Finally, the last change in the configuration involved replacement of the Triphase-emulated harmonic load from Substation A to Substation D. The test mapping with change variables is shown in Table 7.1.

Table 7.1: Experimental scenarios.

Sequence	Supply	PV Setpoint	EV Charger	Triphase	Load Banks	Topology
A.1	MG	7.5 A	off	off	off	A
A.2	MG	off	32 A	off	off	A
A.3	MG	off	off	Sub A	off	A
A.4	MG	7.5 A	32 A	Sub A	off	A
B.1	Grid	7.5 A	off	off	off	A
B.2	Grid	off	32 A	off	off	A
B.3	Grid	off	off	Sub A	off	A
B.4	Grid	7.5 A	32 A	Sub A	off	A
B.5	Grid	7.5 A	32 A	Sub A	24 kW	A
B.6	Grid	7.5 A	32 A	Sub A	24 kW	B
B.7	Grid	7.5 A	32 A	Sub D	24 kW	B

Topology A—mock impedances MI 4 and MI 5; topology B—mock impedance MI 8.

7.3. ANALYSIS AND INTERPRETATION

THE amount of measurement data as the outcome of this experiment is significant, giving measurement windows of 10 min for every test sequence within package B and in an average of 2 min to 3 min for testing scenarios of package A. Typically, around 30 synchronized channels of raw waveforms were recorded for each test. For representing results of this work, we chose to process only one phase (A) for every measurement in question. The signal processing method of choice is FFT with 10 cycles rectangular window. For package A, only one selected window was used for the graphical representation of the results. As it was stated above when energizing the network with MG-set, a non-distorted voltage at the terminals of Isolation Transformer is ensured. This allows

for focusing on the harmonic processes originating from the downstream network on the customer side since background voltage harmonics cannot penetrate from MV upstream network via MG-set. It was therefore concluded that one 10-cycle window can be sufficient for analyzing harmonic distortion when no fluctuating background voltage harmonics are present in the test grid.

On the contrary, with grid power supply, it was important to demonstrate time evolution of the harmonics. For this purpose, every 10 min waveform was fully processed and 10-cycle RMS magnitudes were collected into coherent plots with 600 s duration time. This technique allowed for evaluating harmonic trends being a function of fluctuating voltage background distortion. For one specific test case B.4, we introduced additionally a numerical analysis based on the estimated synchronized harmonic phasors.

7.3.1. IMPACT OF SINGLE OPERATION OF THE EV CHARGER

The analysis begins by examining EV charger current emission and by assessing respective voltage distortion under sinusoidal power supply conditions. Figure 7.2 shows that current spectral components of the EV charger for this case are characterized by significant values of harmonics at 1150 Hz and 1250 Hz, which are 0.71 A and 1.24 A, respectively. Moreover, 150 Hz and 250 Hz spectral components exhibit 0.35 A while a 350 Hz harmonic component counts some 0.42 A. Finally, lesser levels can be observed for frequencies between 450 Hz and 1050 Hz.

By analyzing synchronized voltage spectral components presented in Figure 7.2, one can notice a coherent picture, where at 1150 Hz and at 1250 Hz harmonic magnitudes are 1.90 V and 2.80 V, respectively. For the rest, only harmonics at 250 Hz, 350 Hz, and 650 Hz are clearly visible with RMS magnitudes of 0.67 V, 1.22 V, and 0.65 V, respectively.

On the other hand, by energizing test networks by means of a public grid, a clear change of the harmonic profiles can be observed in Figure 7.3. An increase of 350 Hz and 550 Hz current components up to 0.51 A and 0.246 A, respectively, coincided with the rise of voltage at 350 Hz up to 1.64 V and substantial decrease of 650 Hz voltage harmonic which counted 0.284 V.

A value drop at 1150 Hz and 1250 Hz is quite remarkable with voltage and current levels at these frequencies being negligible. One of the underlying reasons explaining this sudden reduction of the aforementioned voltage frequency components is the different values of short-circuit power between cases A.2 and B.2. The power supply via public grid was characterized by 23.4 MVA short-circuit power whilst MG set's short-circuit power was equal to 8.3 MVA. On the contrary, a major difference can be noticed for 250 Hz with voltage magnitude as high as 1.68 V but in comparison with Figure 7.2 significantly smaller current of 0.14 A.

Furthermore, for test scenario A.2 (MG set supply), a set of synchronous voltage measurements at MV and LV sides of Substation G was processed and results are shown in Figure 7.4. At MV busbar, we recorded 15 V and 32 V at 250 Hz and at 350 Hz, respectively, and 16 V at 650 Hz. Moreover, the largest voltage harmonic distortion values were observed at 1150 Hz and 1250 Hz with 37 V and 63 V, respectively. Looking at the voltage harmonic values at LV test bay of Substation G, it is interesting to note differences in values at frequencies 1150 Hz and 1250 Hz when comparing to these from Figure 7.2. The levels of voltage distortion at these frequencies are lesser and equal to 1.60 V and 2.26 V

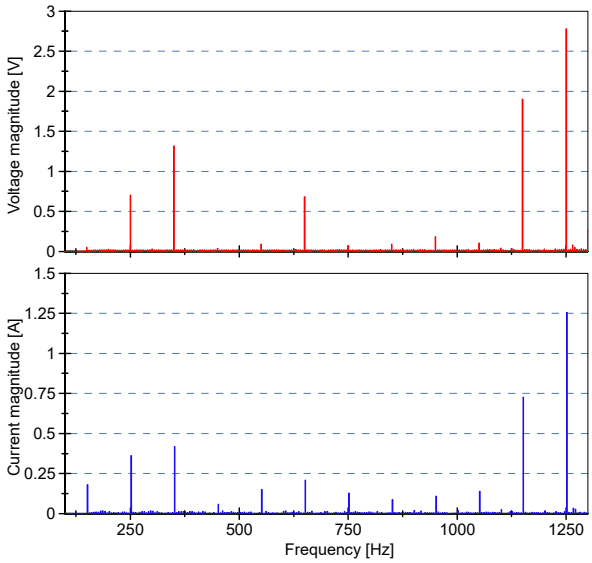

Figure 7.2: EV charger harmonic currents and voltages on the LV side of Substation A. Test sequence A.2 — MG set supply.

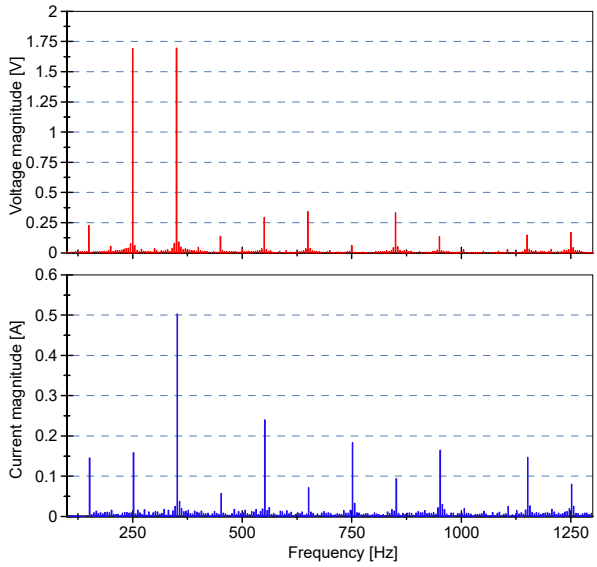

Figure 7.3: EV charger harmonic currents and voltages at LV side of Substation A. Test sequence B.2 — public grid supply.

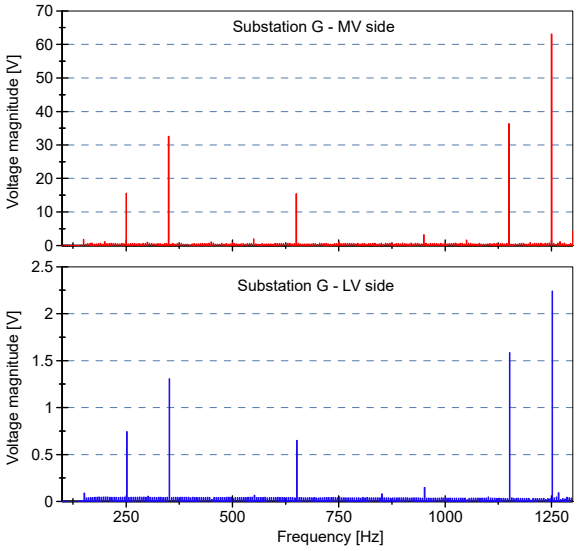

Figure 7.4: Harmonic voltages at MV and LV sides of Substation G. Test sequence A.2 — MG set supply.

for 1150 Hz and 1250 Hz, respectively.

As it can be deduced from the presented results, there exist visible differences in harmonic current emissions of an EV charger when exposed to different levels of background voltage distortion (cases A.2 and B.2). As it was proven in chapter 5 and shown with provision of circular regression models the emissions of the power electronics based loads are dependent on applied background harmonic voltage. To be able to interpret results, it was decided to measure harmonic current injections of this device by connecting it directly to a programmable power source. By supplying ideal sinusoidal voltage waveform to the input terminals of the EV charger, its load current waveform was recorded and processed with an FFT algorithm. This procedure is similar to the one usually performed during factory testing of power electronic interfaced equipment when the final THD value of the device under testing is then included in technical specifications. Figure 7.5 shows the FFT output of EV charger harmonic current emissions. When comparing to values from Figure 7.2, it can be concluded that the major differences are to be observed at 650 Hz, 1150 Hz, and 1250 Hz. At these frequencies, the natural emissions of this device are negligible, which brings the conclusion about harmonic interaction between already existing in the test network voltage distortion and harmonic current injections of EV charger. The measurement process with regard to this phenomena and some implications are best described in [7–9]. Moreover, the same phenomena are observed for frequency components at 250 Hz and 350 Hz—however, with current injections at these frequencies slightly higher when connected to the test grid.

Thus, a direct comparison of Figures 7.2, 7.4, and 7.5 allows for inferring that voltage distortion recorded at different points could not be caused by the EV charger itself but rather propagated from the path magnetizing circuit-MV side Substation G-MV side

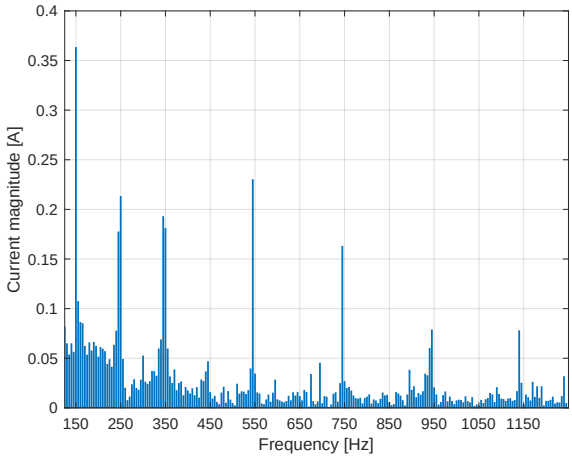

Figure 7.5: Harmonic emission of EV charger under ideal sinusoidal supply conditions.

Substation A. This conclusion can be supported by measuring synchronized spectra of magnetizing current produced by pole-mounted transformers versus spectra of the MV current through Substation A. This graph is shown in Figure 7.6. Based on this graph, it can be inferred that harmonic components of magnetizing current had a dominant influence on the voltage distortion in the system. Therefore, this current impacted MV voltage at Substation G and propagated down to its LV side, where reflected MV distortion patterns are clearly visible. Additionally, the synchronized data allow for drawing interesting conclusions with respect to Substation A. At frequencies 1150 Hz and 1250 Hz, we can notice that voltages at LV side are substantially higher in comparison with ones at Substation G. This is not only related to a larger system harmonic impedance with underground cable MI 1 being 5 times longer than MV cable connecting Substation G (in total 400 m), but also to a fact that, at these frequencies, an EV charger's emissions were relatively high, which resulted in larger harmonic voltage drop over impedance at these frequencies (as Figure 7.6 supports).

Furthermore, after analyzing the results presented in Figure 7.3, a conclusion can be drawn about the influence of harmonic voltage propagated from the upstream grid. A notable observation is a dissolution of voltage harmonics at 1150 Hz and 1250 Hz which again provoked change of harmonic currents at these frequencies. On the other hand, an increase of voltages at 250 Hz and at 350 Hz coincided with the change of EV charger current at these frequencies. While, as it was mentioned before, higher frequency order harmonic voltages reduced because of the higher short-circuit power capacity of the public grid, the change of spectral components at 250 Hz and 350 Hz was provoked by propagated background distortion interacting with the operation of the studied harmonic sources.

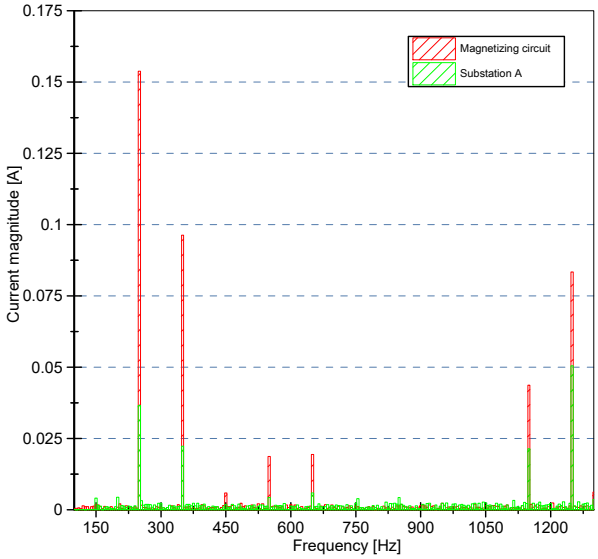

Figure 7.6: Comparison of magnetizing current spectra versus MV current through Substation A. Test sequence A.2 — MG set supply.

7.3.2. MULTIPLE HARMONIC SOURCES ENERGIZED BY MOTOR-GENERATOR GROUP

The simultaneous operation of devices injecting harmonics into grid is analyzed in this section. The loads studied in this test case are PV inverter, EV charger, and synthetic harmonic load emulated by Triphase. The system is energized by MG power supply set (sequence A.4). In Figure 7.7, synchronized voltage spectral components extracted from all points available for voltage measurements are shown. This plot contains components which were otherwise not present in previous cases. The drastic increase of voltages up to 30 V at 850 Hz and up to 22 V 950 Hz at MV side is clearly visible. Additionally, at 550 Hz, the recorded harmonic voltage value was approximately 11 V. It is obvious to note that no substantial difference was observed between voltages at Primary Switchboard (Isolation Transformer) and MV side of Substation G. The reason for this is relatively small electrical distance between these two points.

In order to gain insight into the reasons behind such harmonic response of the studied network, the synchronized substation currents were processed and results are demonstrated in Figure 7.8. The currents through Substation A are significantly higher than through Substation G for every frequency except 1150 Hz and 1250 Hz harmonic components. By looking at individual currents of every connected harmonics source, more details can be revealed. In Figure 7.9, the synchronized current spectra of PV inverter and EV charger are presented. Whilst the emissions of PV are blurred with significant amount of subharmonics, the harmonic currents of EV charger coincide with measured voltages.

Furthermore, the Triphase connected to substation A was programmed as a substan-

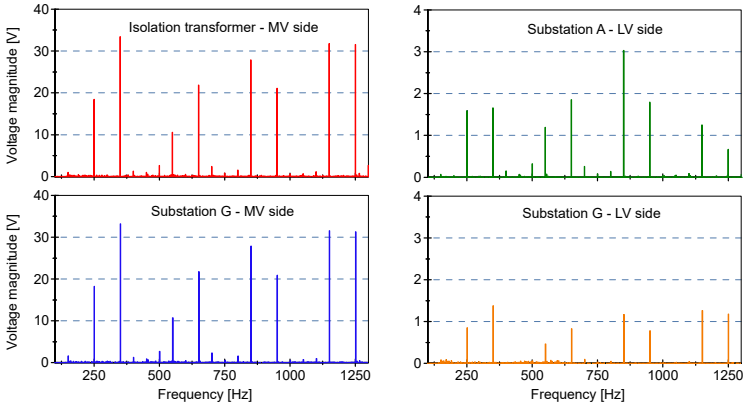

Figure 7.7: Harmonic voltages at multiple points. Test sequence A.4—MG set supply.

tially large source of harmonic current injections with a purpose of acting as reference device with fixed harmonic emissions. The values of harmonic currents for this load are presented in Table 7.2 for frequencies 150 Hz to 1050 Hz. It is worth noting that harmonic phase angles for every order were set to 0.

Table 7.2: Currents of emulated harmonic source (in A).

3rd	5th	7th	9th	11th	13th	15th	17th	19th	21st
1.055	6.07	2.312	0.225	2.167	2.805	0.588	3.324	1.644	0.091

Next, the measured harmonic currents of this device are shown in Figure 7.10. In comparison with Figure 7.7, the conclusions can be drawn that this emulated load acted as dominant source of harmonics provoking large harmonic voltage drops at 550 Hz, 850 Hz, and 950 Hz on the LV side of Substation A. This distortion in turn propagated towards the MV system and down to the LV side of Substation G. Moreover, while the 5th harmonic current injected by Triphase is substantial (6.07 A), it did not cause a significant voltage drop at this frequency at a medium voltage level. The reason for this is relatively small low-voltage impedance at this frequency which resulted on average in some 0.5 V of harmonic voltage drop at an LV level. Propagating further upstream, the resulting harmonic current phasor interacting with impedance angle at this particular frequency produced additionally about 3 V.

It is interesting to observe that this complex interaction between harmonic current phasors and system impedances provoked a significant decrease of voltage at 1250 Hz from 63 V (case A.2) to about 32 V. Since the emulated harmonic load was not programmed to inject current at this frequency, we shall look again at Figures 7.8 and 7.9 in order to evaluate harmonic current emissions of PV and EV chargers. While currents through Substation G are slightly higher, Figure 7.9 suggests that both PV inverters and EV chargers can be deemed to be responsible for the fraction of emissions at 1250 Hz. A notable observation is related to 1250 Hz current component of Triphase visible in Figure

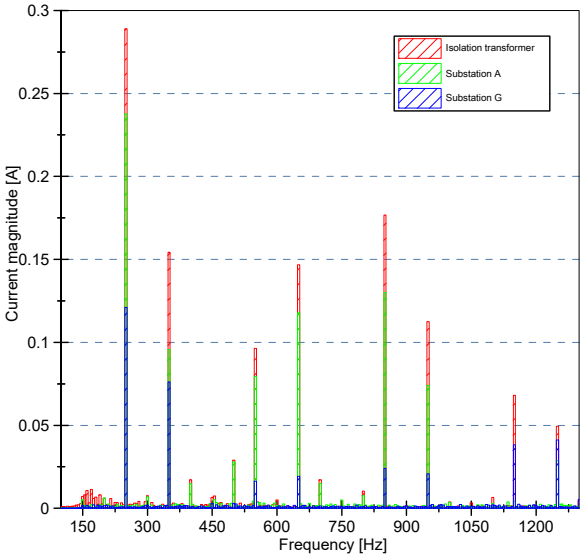

Figure 7.8: MV harmonic currents through transformers. Test sequence A.4—MG set supply.

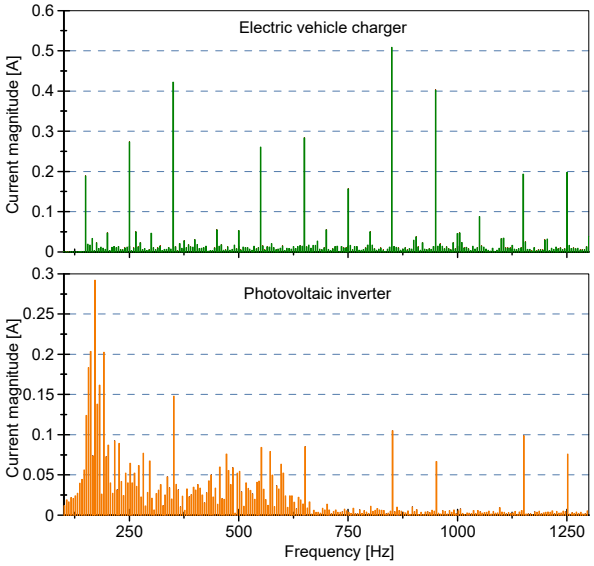

Figure 7.9: Individual harmonic currents of PV and EV chargers. Test sequence A.4—MG set supply.

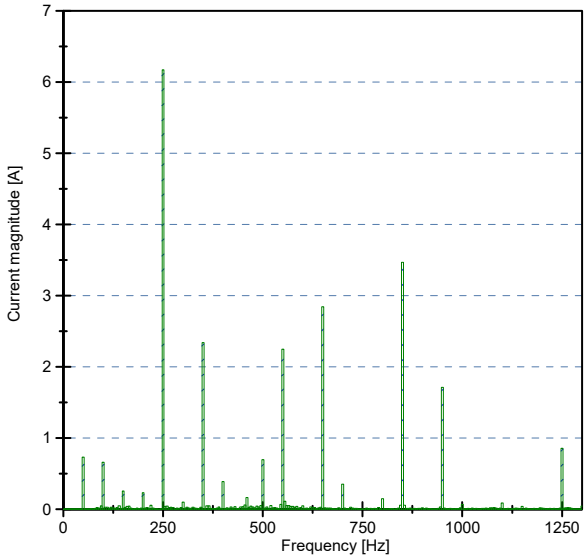

Figure 7.10: Currents of emulated harmonic source.

7.10. Since no injection was set at this frequency, we can conclude that this component resulted from the absorption of harmonics by the filter at the output stage of this device.

Finally, in Figure 7.7, we observe that propagated voltage distortion at LV side of Substation G settles to lower values when compared to the LV side of Substation A. As it was discussed before, the fundamental reason for this is lesser system impedance governed by short underground cable connection. An exception here is voltage harmonic at 1250 Hz recorded on the LV side of Substation G.

7.3.3. MULTIPLE HARMONIC SOURCES ENERGIZED BY PUBLIC GRID

The operation of the public grid is characterized by the presence of time-varying background harmonic voltages. This alters the harmonic behavior of the loads studied in this work and influences the final values of voltage distortion. To illustrate this case, the outcome of FFT analysis for selective harmonics collected in the form of synchronized time series is presented in Figure 7.11. A highly fluctuating behavior of voltages at 250 Hz and 350 Hz can be observed with some periodic patterns visible at frequencies 550 Hz and 650 Hz.

Furthermore, in Figures 7.12, and 7.13, synchronized time series of harmonic currents through distribution transformers are shown. It can be noted that these currents exhibit also time-varying behavior with levels of some of the harmonics changed in comparison with case A.4.

Looking at the harmonic voltages at low-voltage test bays (Figures 7.14 and 7.15), we observe a remarkable difference between these two points. With harmonic voltage at 250 Hz at Substation A as high as 3.7 V against a maximum of 2.7 V at Substation G and significantly higher values of voltages at 550 Hz and 650 Hz.

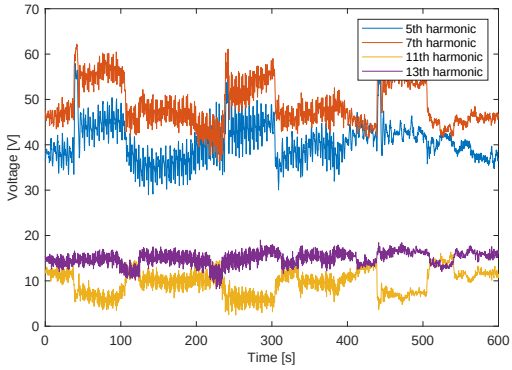

Figure 7.11: Isolation transformer harmonic voltages. Test sequence B.4—public grid supply.

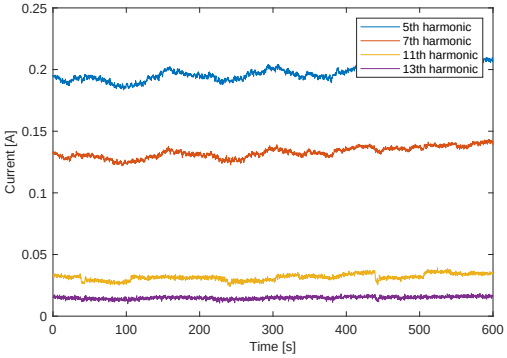

Figure 7.12: Harmonic currents through Substation G. Test sequence B.4—public grid supply.

Moreover, the final value of voltage distortion at MV level is the complex sum of background distortion transferred from upstream network and voltage drop produced by combined harmonic current phasor flowing through harmonic system impedance. A direct comparison between cases represented by Figures 7.8, 7.12 and 7.13 can lead to inconsistent conclusions about the nature of harmonic processes occurring in the grid; therefore, a quantitative method to evaluate the undergoing phenomena is required.

Synchronized harmonic phasors present a powerful tool for analyzing harmonic data. Here, an example is given on how to estimate LV harmonic contributions based on the Voltage Harmonic Vector Method [10]. For the sake of clarity, only harmonic components at 250 Hz and 350 Hz were considered in the calculations.

The calculations according to the Voltage Harmonic Vector Method require employment of utility harmonic impedance. In this work, we assume the MV/LV transformers as components dominating the system LV harmonic impedance. Based on the datasheets, the fundamental frequency reactance was estimated to 0.05 Ω and 0.0179 Ω for Substation G and Substation A, respectively. The harmonic impedances at 250 Hz and 350 Hz

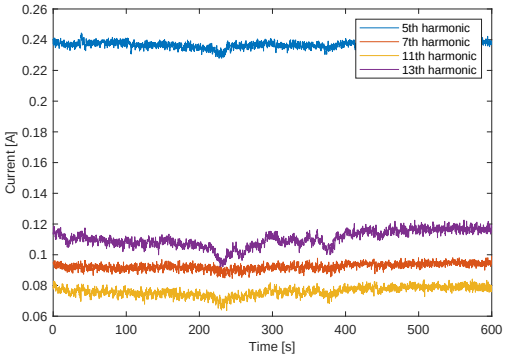

Figure 7.13: Harmonic currents through Substation A. Test sequence B.4—public grid supply.

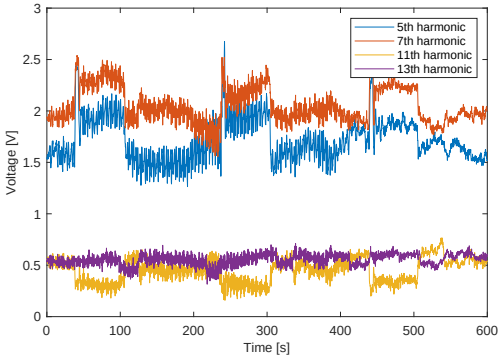

Figure 7.14: Harmonic voltages at LV side of Substation G. Test sequence B.4—public grid supply.

were then recalculated based on simple theoretical derivations providing proportional linear approximations for the frequency-dependent inductance. According to the Voltage Harmonic Vector Method, the following applies:

$$\underline{U}_{U-h} = \underline{U}_{\mathrm{PCC}-h} - \underline{I}_{\mathrm{PCC}-h} \cdot \underline{Z}_{U-h} \tag{7.1}$$

where $\underline{U}_{U-h}$ is utility voltage representing background harmonic voltage source, $\underline{U}_{\mathrm{PCC}-h}$ is harmonic voltage measured at LV side of respective substation, $\underline{I}_{\mathrm{PCC}-h}$ vectorial sum of individual injection currents, and $\underline{Z}_{U-h}$ is utility harmonic impedance. The harmonic impedance of transformer can be calculated as:

$$\underline{Z}_{U-h} = h \cdot X_f \tag{7.2}$$

where h is a harmonic order and X_f is a transformer reactance at fundamental frequency.

Therefore, based on the Equation (7.1), the following holds:

$$\underline{U}_{\mathrm{emission}} = \underline{U}_{\mathrm{PCC}-h} - \underline{U}_{U-h} \tag{7.3}$$

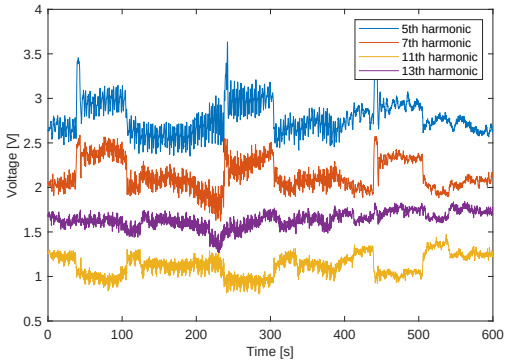

Figure 7.15: Harmonic voltages at LV side of Substation A. Test sequence B.4—public grid supply.

Figures 7.16 and 7.17 demonstrate estimated voltage harmonic phasors at Substation A for background distortion and voltage emission, respectively. The individual phasors of harmonic currents of equipment connected to the Substation A are shown in Figures 7.18 and 7.19.

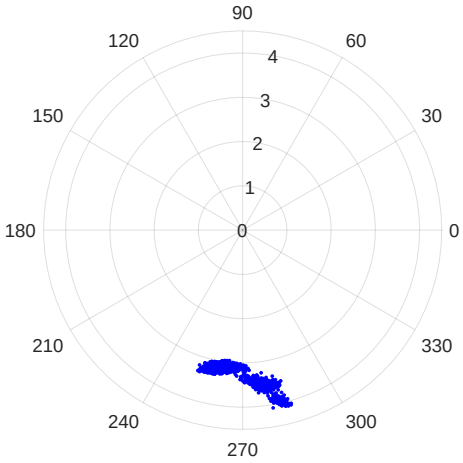

Figure 7.16: 5th harmonic background voltage phasors at LV side of Substation A (in volts). Test sequence B.4—public grid supply.

Figure 7.20 shows the result of harmonic current vectorial summation at LV side of substation A. It can be observed that, in that case, emulated harmonic load acts as the dominant source of harmonic current at 250 Hz. The harmonic voltage drop produced by this harmonic current (Figure 7.17) ensures a certain level of harmonic cancellation when added to the estimated voltage background phasors (Figure 7.16) with final measured values settled below the initial background levels (Figure 7.21).

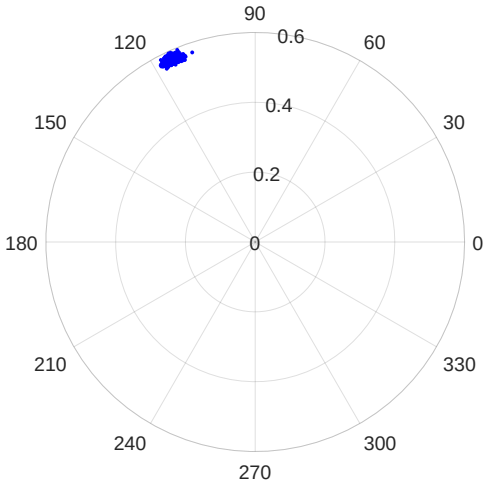

Figure 7.17: 5th harmonic voltage emission phasors at LV side of Substation A (in volts). Test sequence B.4—public grid supply.

Furthermore, an example of harmonic processes taking place synchronously for 350 Hz harmonic at Substation G is shown in Figures 7.22 and 7.23. Despite the dynamic nature of PV power, it is to observe that harmonic voltage emissions phasors at 350 Hz are localized at the 1st quadrant of unity pane. Given the phasors of voltage background distortion located at the 4th quadrant, the conclusions that a small harmonic cancellation took place within this specific substation can be made.

Finally, a small selection of average quantitative results derived by means of synchronized phasors and Voltage Harmonic Vector Method is collected in Table 7.3.

Furthermore, it is interesting to observe the time-evolving harmonic current behavior of EV charger demonstrated in Figure 7.24. The harmonic injections of this type of power-electronic devices are highly sensitive to the changes of applied harmonic background voltage, both in terms of magnitude and phase angles. This effect is attributed to the underlying topology of the equipment, namely to the type of power factor correction circuit [7, 9]. As it can be seen from synchronized harmonic trends, for every studied frequency, the current injections of EV charger exhibit nearly linear behavior in response to the background voltage distortion. This phenomenon renders such multi-point harmonic measurements to be important in an attempt to identify sources of disturbances and to quantify harmonic emissions.

Table 7.3: Average RMS magnitude of harmonic voltage emissions per substation.

Harmonic Frequency, Hz	Emission Voltage Sub A, V	Emission Voltage Sub G, V
250	0.574	0.043
350	0.232	0.054

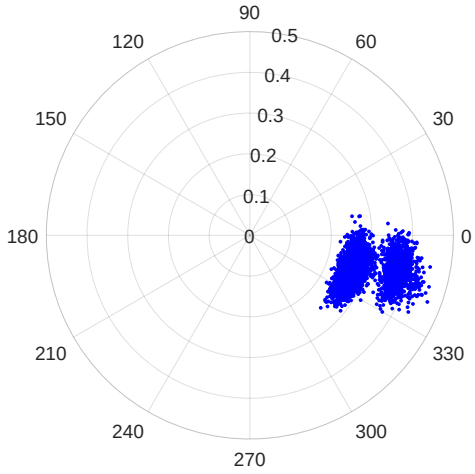

Figure 7.18: 5th harmonic current phasors of EV at Substation A (in amperes). Test sequence B.4—public grid supply.

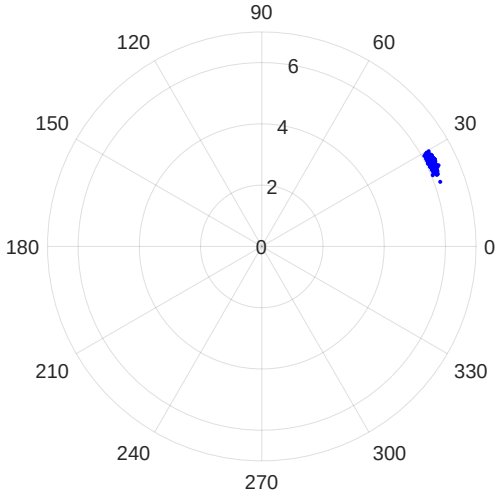

Figure 7.19: 5th harmonic current phasors of Triphase at Substation A (in amperes). Test sequence B.4—public grid supply.

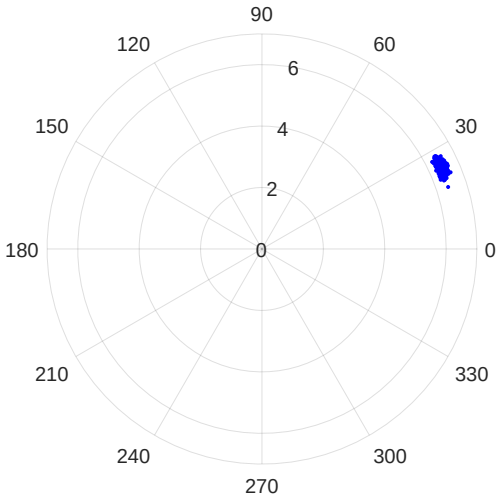

Figure 7.20: 5th harmonic current phasors (vectorial sum) at Substation A (in amperes). Test sequence B.4—public grid supply.

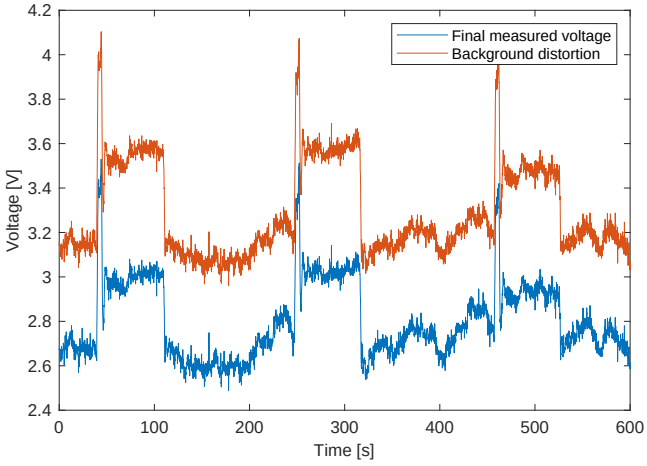

Figure 7.21: 5th harmonic voltages (RMS) at Substation A. Test sequence B.4—public grid supply.

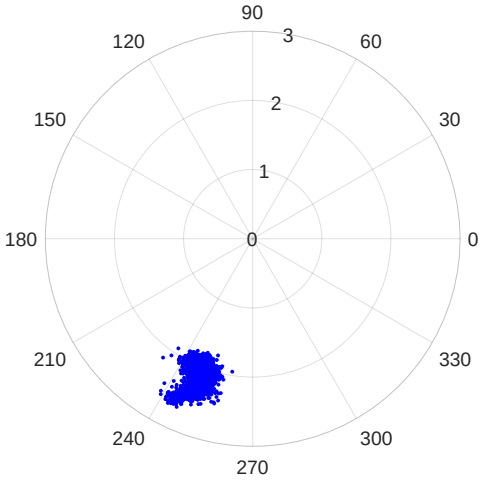

Figure 7.22: 7th harmonic background voltage phasors at LV side of Substation G (in volts). Test sequence B.4—public grid supply.

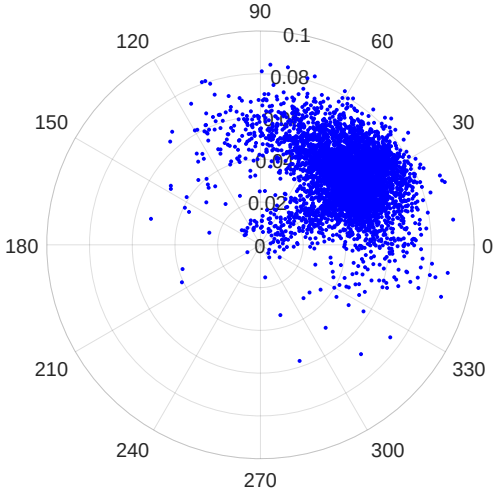

Figure 7.23: 7th harmonic voltage emission phasors at LV side of Substation G (in volts). Test sequence B.4—public grid supply.

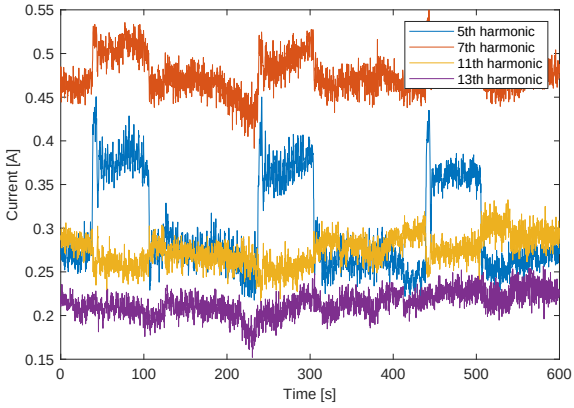

Figure 7.24: EV charger harmonic currents. Test sequence B.4—public grid supply.

7.3.4. IMPACT OF HARMONIC IMPEDANCE ON VOLTAGE DISTORTION LEVELS

In conventional power quality analysis, it is a common practice to omit influence of linear loads operating at nearly unity power factor. Such loads, however, by means of resistive nature act as a shunt impedance connected to the LV side of distribution substation. This shunt impedance in turn decreases proportionally the system impedance. It is important to differentiate scenarios when these loads can provide a harmonic damping to the system. The harmonic damping leads to the decrease of THD levels only when resistive behavior is ensured towards selective harmonics [11].

The performed experiments demonstrate that not in every case the reduce of harmonic content takes place. In this test sequence (B.5), we connected 24 kW of resistive loads equally divided between both distributed substations and evaluated THD at LV test bays both before and after this operation has been performed. In Figure 7.25, the results of this experiment are shown in the representative form of box plots rendered over the whole duration of the signals. As it can be seen for both substations, the median levels (red horizontal line) of THD are actually higher after connecting the linear load banks. Here, it is important to note that, while conventional power quality studies and computer simulations (mainly because of the nature of used models of harmonic loads) rely exclusively on calculations based on magnitudes of currents and voltages, the harmonic processes in real grid scenarios are more complex. Depending on the phase angles of harmonic current and voltage phasor (given that we did not have any control over background distortion) and new value of impedance, this interaction in some cases can lead to the rising levels of final THD values, even when expected otherwise.

Next, a dynamically changing topology at MV levels is considered to be a known issue for harmonic analysis. The reconfiguration of the network occurring at any given time can significantly alter the voltage distortion values and if not considered properly in subsequent simulations can lead to the erroneous outcome. As per test scenario B.6, we dropped the short cable connecting Primary Switchboard to Substation G and engaged cable B with equivalent electrical distance of about 5 km (see Figure 7.1). After

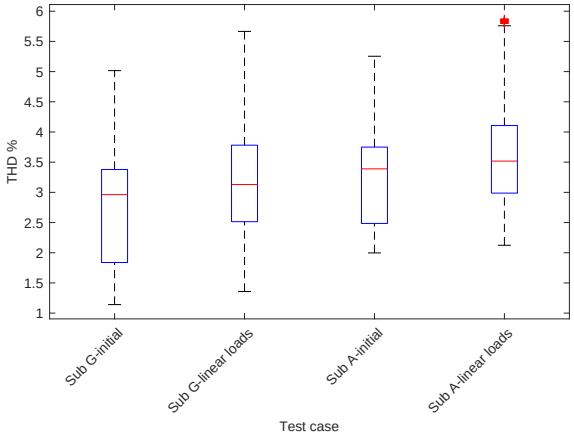

Figure 7.25: Influence of linear load banks on LV-side THD levels. Test sequence B.5—public grid supply.

recording synchronized voltage waveforms at MV busbars of both Substation G and Primary Switchboard (Isolation Transformer), the THD values were collected in the form of box plot and these are presented in Figure 7.26. While the spread of THD values became larger, we can clearly observe the increase of median values and, in this case, increased harmonic impedance at the MV level contributed to larger values of voltage distortion.

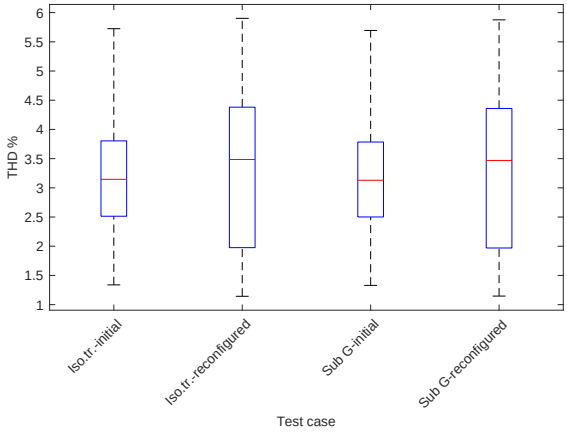

Figure 7.26: Impact of topology change on MV-side THD levels. Test sequence B.6—public grid supply.

7.3.5. LOAD SEPARATION

The final case studied in this chapter concerns a harmonic response of the system with an additional distribution transformer. To evaluate the differences, we energized Substation D by means of an underground cable with its sending end connected to the bus-

bar of Substation A (see Figure 7.1). The estimated length of this cable connection is about 2 km. Next, a reference Triphase harmonic load was moved from Substation A to Substation D. In Figure 7.27, we only present results for 5th harmonic voltage measured synchronously at all three LV test bays.

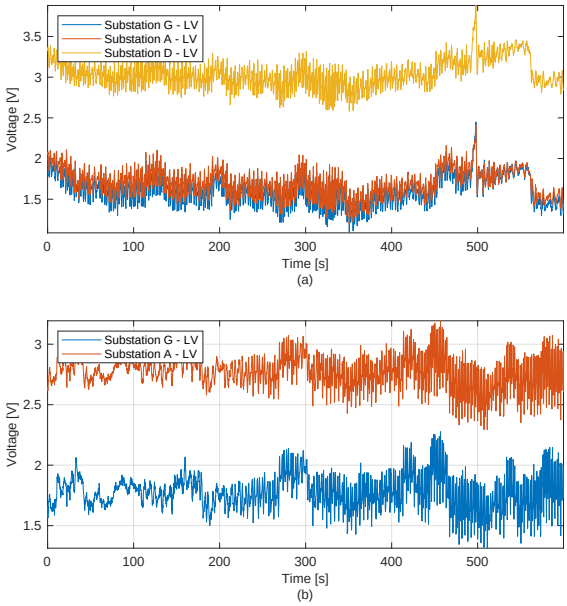

Figure 7.27: Change of 5th harmonic voltages as result of load separation. Test sequence B.7—public grid supply. (**a**) triphase-emulated harmonic load connected to Substation D; (**b**) triphase-emulated harmonic load connected to Substation A.

Whilst harmonic voltage at Substation A dropped after removing dominant injection source, we observe that 250 Hz harmonic trend measured at Substation D is visually higher in comparison with local harmonic voltage values when a disturbance source was connected to the distribution Substation A. Naturally, background harmonic levels also evolved in time, but, certainly, the additional impedance of 2 km cable equivalent boosted harmonic voltages at this substation. Furthermore, the transformer of Substation D is characterized by 0.0295 Ω fundamental frequency impedance.

7.4. CONCLUSION

THE global synchronization of current and voltage samples is efficient for evaluating various issues associated with voltage and current harmonic distortions in distribution networks. Bearing in mind that accuracy of time-synchronized waveform recorders is determining for the quality of harmonic analysis, the fundamental transfer mechanisms of harmonic components can be analyzed. The diversity of harmonic currents emitted by various devices and subsequent harmonic cancellation, the harmonic interaction and attenuation and the impact of system impedance are among factors whose

evaluation benefits from the application of distributed measurement system. In addition, the impacts on harmonic distortion can be recreated by calculation, even with network simplifications — for that purpose harmonic synchrophasors estimated from synchronized waveforms is an effective instrument. Altogether, it has been proven in this chapter that complete harmonic observability is advantageous for forming conclusions about dominant sources of the fluctuating distortion in power grids by assessing the path of frequency components' propagation.

REFERENCES

[1] C. Muscas, L. Peretto, S. Sulis, and R. Tinarelli, *Investigation on Multipoint Measurement Techniques for PQ Monitoring,* IEEE Transactions on Instrumentation and Measurement **55**, 1684 (2006).

[2] a. Carta, N. Locci, and C. Muscas, *GPS-based System for the Measurement of Synchronized Harmonic Phasors,* 2007 IEEE Instrumentation & Measurement Technology Conference IMTC 2007 **58**, 1 (2007).

[3] O. Unsar, O. Salor, I. Cadirci, and M. Ermis, *Identification of harmonic current contributions of iron and steel plants based on time-synchronized field measurements - Part I: At PCC,* IEEE Transactions on Industry Applications **50**, 4336 (2014).

[4] B. Peterson, J. Rens, J. Meyer, G. Botha, and J. Desmet, *Evaluation of Harmonic Distortion from Multiple Renewable Sources at a Distribution Substation,* IEEE International Workshop on Applied Measurements for Power Systems (AMPS) Proceedings , 37 (2017).

[5] P. S. Wright, A. E. Christensen, P. N. Davis, and T. Lippert, *Multiple-site amplitude and phase measurements of harmonics for analysis of harmonic propagation on bornholm island,* IEEE Transactions on Instrumentation and Measurement **66**, 1176 (2017).

[6] R. Ferdinand, M. Cupelli, and A. Monti, *Multipoint Synchronized Recordings in Offshore Power Quality Meters,* IEEE Transactions on Instrumentation and Measurement **67**, 2785 (2018).

[7] J. E. Caicedo, A. A. Romero, H. C. Zini, R. Langella, J. Meyer, and N. R. Watson, *Impact of reference conditions on the frequency coupling matrix of a plug-in electric vehicle charger,* Proceedings of International Conference on Harmonics and Quality of Power, ICHQP , 1 (2018).

[8] J. Cobben, J.F.G., Kling, W.L., Myrzik, *The making and purpose of harmonic fingerprints,* in *CIRED 2007*, pp. 21–24.

[9] L. E. Gallego and J. Meyer, *Characterization of non-linear household loads for frequency domain modeling Caracterización de cargas residenciales no lineales para modelado en el dominio de la frecuencia,* **2015**, 65 (2015).

[10] I. Papic, D. Matvoz, A. Spelko, W. Xu, Y. Wang, D. Mueller, C. Miller, P. F. Ribeiro, R. Langella, and A. Testa, *A Benchmark Test System to Evaluate Methods of Harmonic Contribution Determination,* IEEE Transactions on Power Delivery **34**, 23 (2019).

[11] T. Vandoorn, B. Meersman, J. De Kooning, and L. Vandevelde, *Controllable Harmonic Current Sharing in Islanded Microgrids: DG Units With Programmable Resistive Behavior Toward Harmonics,* IEEE Transactions on Power Delivery **27**, 831 (2012).

8

CONCLUSIONS AND RECOMMENDATIONS

Learn the basics of science before attempting to climb it.
Never take on the next step without mastering the previous one.
Never try to cover up the shortcomings of your knowledge,
even with the most daring guesses and hypotheses.

I.P. Pavlov

As steadily more measurement devices featuring synchronization to the time precision source become available at the market, the amount of pilot and research projects with new time synchronized measurement infrastructure is gradually increasing worldwide. Without any doubts, this pattern demonstrates that modern and future power systems have an explicit demand for improved observability and control. In a handful of cases system operators have already opted for advantages of the synchronized distributed monitoring, mainly built on phasor measurement units providing more insight into power system real time processes. Fault detection, improved diagnostics of cables and lines, parameter estimation and evaluation of power system stability are among functions already integrated at the transmission system level. The cost of these devices and corresponding infrastructure is high and justification of their installation at the distribution system level must be solid. In the presence of high penetration of distributed generation and increasing amount of power electronics interfaced loads the results of this work indicate that there will be a potential in establishing new multi point time synchronized measurement infrastructures in distribution systems for the purpose of harmonic distortion monitoring. To reveal this potential we have studied the performance of distributed measurement systems from the metrological point of view and from the standpoint of methods and algorithms which can be applied to the sets of synchronized data.

Whether a measurement system consists of waveform recorders or phasor measurements units, the harmonic distortion analysis can be only conclusive and meaningful

if a time synchronization accuracy is higher than it is required by the synchrophasor standard for the quality of phasors used for the analysis at power frequency. Our experimental results demonstrate that the time error of ± 500 ns between measurement devices is sufficient to ensure a strong correlation of magnitude and phase angle components for frequency harmonics up to the 40th order. On contrary, accepting an error of sub-millisecond range leads to the loss of representative harmonic phase angle information whilst further impairment is followed by drastic asynchronization of harmonic magnitudes. In medium voltage systems in addition to the synchronization accuracy, harmonic measurements are significantly impacted by current and voltage transducers. The results of the field experiment indicate that ratio and phase angle biases associated with current transducers are substantial even for low harmonic orders. Therefore, just when a highly accurate acquisition system is used, the values of estimated harmonic components become already erroneous due to the influence of the instrumentation transformer. An elegant solution in this case can be the estimation of correction coefficients serving as an indication of the uncertainty associated with transducers. As a representative example it appears that current value at 550 Hz may be corrected by 80% bias in magnitude and 16 degrees in phase. The algorithm for estimating these coefficients is generalized to the case where one of the two current transducers installed at two ends of the cable has the highest possible accuracy class.

As power system components have determining impact on the total harmonic distortion levels, it is important to have instruments and knowledge on quantifying this impact and in certain cases on controlling it. For medium voltage and low voltage systems we have elaborated in details on the most common components - underground cables. Upon bringing the discussion on uncertainty for harmonic assessment associated with simple π model of medium voltage underground cable, it is shown that synchronized voltage and current harmonic phasors are well suited for the recalculation of missing current measurements through model based equations. However, as the results indicate, the limiting factor in it is the uncertainty of the cable model which at low frequencies counts almost 10% and will increase at higher harmonic orders. For low voltage level where cable parameters at harmonic frequencies might be not known we developed a non-invasive harmonic impedance estimation method. With the provision of two time synchronized waveform recorders and by employing in the estimation procedure natural injections of a large harmonic source in laboratory conditions we demonstrated that values of cable resistance and reactance at harmonic frequencies can deviate significantly from the theoretical derivations. For this experiment we have performed complete metrological characterization of the instrumentation chain. It was emphasized that while recording data with highly accurate system is beneficial, the more important fact is to be aware of the final levels of uncertainty and to be capable of assigning correct confidence intervals to final impedance values. With proposed algorithm filtering out noise and uncorrelated components in laboratory environment it appears that standard uncertainty of magnitudes of harmonic impedance decrease with higher excitation currents. For instance, for the specific studied case at 150 Hz the standard uncertainty of impedance equaled to 3.8 mΩ whilst at 650 Hz it counted 82.3 mΩ for estimated impedance magnitudes of 0.102 Ω and 0.237 Ω, respectively. As for the method itself, while it contributes to the understanding of harmonic behavior of low

voltage feeder, it is limited to balanced operation conditions since it makes use of single phase measurements.

As it was emphasized in this work several harmonic processes can be thoroughly studied through application of synchronized measurements. Among considered are: the complex interactions between background voltage distortion and fluctuating harmonic currents and the cancellation phenomena between diverse sources of distortion. To test this hypothesis we first needed to develop an understanding of the nature of these processes through modelling and simulations. As an initial step novel harmonic models of low voltage power electronics devices were proposed. These models are derived from accurate fingerprint measurements which are used as an input to circular regression equations. The model explains the relationships between independent and response variables - supplied voltage harmonic phase angle and phase of the injected harmonic current. An advantage of this model is that it can be conveniently integrated into the commercial simulation packages while retaining the simplicity of frequency-domain models. As results demonstrate the performance of the models shows good compliance with actual measurements. Whilst these models can be adapted to any simulation scenario, the limiting factor may nevertheless be an accurate estimation of current magnitude since these models explain at first place the behavior of angular components. As the next step, the developed models of a photovoltaic inverter and a battery charger were used for harmonic simulations in commercial simulation software. The modelling of a low voltage feeder and simulation conditions were intent on overcoming a number of typical assumptions imposed on low voltage harmonic analysis. Such assumptions as perfectly balanced systems, simplified representation of frequency dependent impedance and employment of summation coefficients, as the results of the performed simulations indicate, need to be reconsidered for the sake of accurate outputs of a harmonic load flow routine. On comparing results between phase corrected harmonic load flow and the one executed according to IEC 61000-3-6 we indicated the differences between final harmonic voltages calculated by applying each of the methods.

Finally, the results of the wide area measurement campaign indicate that synchronized harmonic measurements will be a powerful instrument in evaluating complex harmonic processes in distribution systems. If waveform acquisition is performed, this opens up a possibility to apply any suitable signal processing method including the ones presented in this work - Welch averaged periodogram and wavelet transforms. Additionally, the correlation techniques as it was proved can serve various purposes from the impedance estimation to harmonic source localization. After recording voltage and current waveforms synchronously at different points of low voltage and medium voltage parts of the test network we derived conclusions on harmonic interactions, cancellation phenomena and path of the distortion propagation also in case of topological changes in the grid. Moreover, with provision of harmonic synchrophasors we separated contributions of nonlinear loads from the background voltage distortion.

To facilitate applications of synchronized measurement infrastructure a number of recommendations for future research and experiments can be given. A characterization of current and voltage transducers at harmonic frequencies is required before investing into synchronized measurement infrastructure for medium voltage electrical networks. In certain cases estimation and application of correction factors can be an option, how-

ever, it is recommended to elaborate on the estimation methodology. One of the plausible ways is to find function global minimum or maximum via applicable optimization techniques. Further investigations on uncertainty of the medium voltage cable model are required. These shall involve more complex cable models, for instance the equivalent π model with hyperbolic corrections. As for the estimation of low voltage cable harmonic impedance, it is advised to test the proposed methodology in field involving part of the real distribution system. For circular regression models of harmonic producing sources more equipment types need to be included with ultimate goal of comprising a database which can be used for extensive simulations. Finally, in the light of ongoing research on supraharmonic distortion it seems reasonable to investigate how synchronized measurement infrastructure may contribute to the analysis of supraharmonics.

LIST OF PUBLICATIONS

1. Babaev, S, Cuk, V and Cobben, JFG 2020, 'Application of Wavelets for Study of Harmonic Propagation in Distribution Networks', ICHQP 2020 - 19th International Conference on Harmonics and Quality of Power. vol. 2020-July, IEEE Computer Society, pp. 1-6, Dubai, United Arab Emirates.

2. Babaev, S, Singh, RS, Cobben, JFGS, Cuk, V and Desmet, J 2020, 'Circular regression models of modern harmonic producing sources', IET Generation, Transmission & Distribution, vol. 14, no. 18, pp. 3826 – 3836.

3. Babaev, S, Singh, RS, Cobben, S, Cuk, V and Downie, A 2020, 'Multi-point time-synchronized waveform recording for the analysis of wide-area harmonic propagation', Applied Sciences (Switzerland), vol. 10, no. 11, 3869.

4. Babaev, S, Cobben, S, Cuk, V and van den Brom, H 2020, 'Online estimation of cable harmonic impedance in low-voltage distribution systems', IEEE Transactions on Instrumentation and Measurement, vol. 69, no. 6, 8755269, pp. 2779-2789.

5. Singh, RS, van den Brom, H, Babaev, S, Cobben, S and Cuk, V 2019, 'Estimation of impedance and susceptance parameters of a 3-phase cable system using PMU data', Energies, vol. 12, no. 23, 4573.

6. Singh, RS, Babaev, S, Cuk, V, Cobben, S and van den Brom, H 2019, 'Line parameters estimation in presence of uncalibrated instrument transformers', 2nd International Colloquium on Smart Grid Metrology, SMAGRIMET 2019 - Proceedings, 8720376, Institute of Electrical and Electronics Engineers, Split, Croatia.

7. Babaev, S, Cobben, JFG, Cuk, V, Singh, RS and van den Brom, HE 2018, 'Considerations on the performance of multi-point synchronized harmonic measurement system', 9th IEEE International Workshop on Applied Measurements for Power Systems, AMPS 2018 - Proceedings, 8494894, Institute of Electrical and Electronics Engineers, Piscataway, Bologna, Italy.

8. Babaev, S, Cuk, V, Cobben, JFG and van den Brom, HE 2018, 'Harmonic source location in the distribution grid using time-synchronized measurements', Renewable Energy & Power Quality Journal, vol. 2018, no. 16, pp. 276-280.

9. Babaev, S, Cuk, V, Cobben, JFG, van den Brom, H, Rietveld, G and Jongepier, A 2018, 'On the limitations of harmonic modeling with measured inputs — a case study', ICHQP 2018 - 18th International Conference on Harmonics and Quality of Power. vol. 2018-May, IEEE Computer Society, pp. 1-5, Ljubljana, Slovenia.

CURRICULUM VITÆ

Stanislav Babaev was born in Russia. He received the M.Sc. (tech.) degree in electrical engineering focused on Smart Grids from Tampere University of Technology, Tampere, Finland, in 2016. From 2010 to 2014 he held engineering positions in several energy companies where his main task was reconstruction and modernization of electrical substations. In 2016 he joined Electrical Energy Systems Group in Eindhoven University of Technology as a Ph.D. candidate. His research interests include power quality, power system analysis and metrology for Smart Grids.

Printed by: Ipskamp Enschede

Cover design: Levi Kaladse (levi200127@gmail.com)

A catalogue record is available from the
Eindhoven University of Technology Library
ISBN: 978-90-386-5166-8